NASA CONTRACTOR REPORT

NASA CR-62078

Farfield Structure of an Aircraft Trailing Vortex, Including Effects of Mass Injection

by William Henry Mason
and James Franklin Marchman, III

Prepared for
NATIONAL AERONAUTICS AND SPACE ADMINISTRATION
under Grant No. NGL 47-004-067

April 1972

Prepared by
Department of Aerospace Engineering
Blacksburg, Virginia 24061
for Wallops Island

College of Engineering
Virginia Polytechnic Institute
and State University

NASA CONTRACTOR
REPORT

NASA CR-62078

FARFIELD STRUCTURE OF AN AIRCRAFT TRAILING VORTEX, INCLUDING EFFECTS OF MASS INJECTION

by William Henry Mason
and James Franklin Marchman, III

Prepared for
NATIONAL AERONAUTICS AND SPACE ADMINISTRATION
under Grant No. NGL 47-004-067

APRIL 1972

Prepared by
Virginia Polytechnic Institute
and State University
College of Engineering
Department of Aerospace Engineering
Blacksburg, Virginia 24061
for Wallops Island

FARFIELD STRUCTURE OF AN AIRCRAFT TRAILING VORTEX, INCLUDING EFFECTS OF MASS INJECTION

by

William Henry Mason
James F. Marchman, III

ABSTRACT

With the introduction of the "Jumbo Jet" class of aircraft it has become important to predict the aircraft wake turbulence due to the tip trailing vortex accurately. A yawhead pressure probe has been used in the Virginia Tech 6-Foot Subsonic Tunnel to obtain detailed mean flow measurements at stations up to thirty chordlengths downstream in an aircraft trailing vortex. Mass injection at the wingtip has been shown to hasten the decay of the trailing vortex. A theoretical method has been given to show the effect of the circulation distribution on the wing on the structure of the outer portion of the vortex, and excellent agreement with experiment has been shown. Experimental results indicate a much slower decay and higher tangential velocities than previously expected.

TABLE OF CONTENTS

LIST OF TABLES

LIST OF FIGURES

List of Figures (Cont'd) Page

NOMENCLATURE

A_c	core radius, ft.
A_n	coefficients of series representing wing circulation
a_o	2-D lift curve slope
a	constant in solution of Batchelor, radius of probe
b_l	wingspan, ft.
b'	impulsive wingspan, ft.
c	wing chord, ft.
$\bar{c}$	mean wing chord, ft.
C_o	root chord, ft.
C_L	wing lift coefficient
C_{L_o}	midspan section lift coefficient
D_i	induced drag
E_i	inner vortex energy
E_o	outer vortex energy
ei(ζ)	exponential integral
F	force between vortex and probe
f(ζ)	Batchelor's function
J_o	momement of inertia with respect to centerline
$J_{\bar{y}_l}$	moment of inertia with respect to center of gravity
FP	flow pitch, degrees
FY	flow yaw, degrees
K_p	probe coefficient
K_i	hole coefficient

$\dot{m}$	mass flow rate, slugs/sec
p	pressure
p_o	total pressure
p_{st}	static pressure
p_{st_∞}	freestream static pressure
p_i	probe hole defined pressure
Q, g	dynamic pressure
R_{e_t}	swirl Reynolds number
t	time, sec.
$\overline{u'v'}$	Reynold's stresses
u	axial velocity
U_∞	freestream velocity
V	freestream velocity
V_x, V_y, V_z	cartesian coordinate velocities
V_r, V_θ, V_z	cylindrical coordinate velocities
$V_{\theta_{cor}}$	corrected tangential velocity
W	Batchelor's freestream velocity
y_1	center of gravity of vortex
x, y, z	coordinate directions
α	angle of attack
α_o	zero lift angle of attack
δ	strength of undeveloped discontinuity behind wing
Γ	circulation
Γ_{AC}	circulation at core radius
Γ_o	circulation at root of wing
θ	coordinate direction, transformation angle, vortex roll angle

PRECEDING PAGE BLANK NOT FILMED

μ	viscosity
ν	kinematic viscosity
ν_T	effective kinematic viscosity
ρ	mass density
ω	solid body rotation speed
ζ	similarity

INTRODUCTION

The prediction of the turbulence trail of an aircraft has become extremely important with the introduction of "Jumbo Jet" class aircraft into high density terminal areas. The FAA has initiated holding times after Jumbo Jet operations that nullify the advantages of the large aircraft. In addition the next generation of avionics will allow aircraft to land and take off with virtually no interval necessary between aircraft. In order to minimize the wait time of aircraft on the ground and in the air, with its accompanying noise and chemical pollution, the wake turbulence must be predicted accurately, and reduced or eliminated if possible, allowing the most efficient use of present airport facilities.

It has been shown[1] that the wake turbulence is due to the tip trailing vortex and this has led to increased publicity and pilot education efforts regarding the behavior and dangers of the trailing vortex. Increased theoretical and experimental research efforts are being employed and two recent specialists meetings[2,3] have been held. The meetings pointed out that although a detailed set of measurements is sorely needed at distances far downstream of the wing, the vortex is extremely difficult to measure with a probe since the vortex reacts to the placement of any object in the vortex core. The least understood aspects were found to be the axial flow far downstream, and the possible existence of secondary vortices rolling around the primary vortex. Flow visualization methods were strongly recommended as a means of study, but because of the difficulty of obtaining

quantitative information by flow visualization techniques and the need for such information for comparison with theory, the present work explores the possibility of making measurements in the vortex core with a probe. A detailed set of measurements are presented using this method.

Aircraft wake turbulence and trailing vortices have been the subject of many studies in the past, but interest has centered on the effects near the aircraft, such as the effects of the vortex and wake on the tail and control surfaces of the aircraft and on the following blade in helicopter rotor blade interaction studies. The trailing vortex, as pictured in Figure 1, is a result of the circulatory lifting flow on the aircraft wing. The classic Joukowsky Theorem gives the relation between circulation and lift. Hence the large gross weights of the new aircraft can be expected to generate much larger circulation and thus larger, more intense trailing vortices. According to the Prandtl lifting line theory, the circulation occurs as a bound vortex about the wing, and since the vortex cannot "end" in the fluid, it turns at the wing tip and proceeds downstream behind the wing. Any wing shape can be simulated by a superposition of these "horseshoe vortices". Much work has been done on the way in which the distributed vortices tend to roll up into an single vortex flowing downstream behind each wing tip. Indeed a figure of this phenomena was given by Lanchester in 1907, and is reproduced in Figure 1. Good descriptions of vortex rollup have been given by Sprieter and Sacks[4], and Hackett and Evans[5]. Roughly, the structure of this resulting vortex can be described as an outer inviscid vortex, and an inner viscous core that exhibits a rotation similar to that of a solid body. The present work examines the nature of these trailing vortices and shows the dependence of the outer inviscid vortex on the

initial conditions, i.e., distribution of the circulation on the wing.

Of the many investigations of the downwash behind the wing, only three studies have been made at several chordlengths downstream in the fully developed trailing vortex. Fage and Simmons[6] (1925) conducted tests at up to 13 chordlengths downstream using a hot wire anemometer. A comparison of the hot wire method and a pressure probe method showed that for the axial velocity distribution u/U_∞ = 1 for the pressure probe, and u/U_∞ = 1 for the hot wire anemometer. Mowforth[7] has conducted experiments at up to 10 chordlengths downstream, and attempted to make static pressure measurements. No velocity profiles are presented, and the measurements were made with an extremely small wind tunnel and probe. Perhaps the experiment most similar to the present work was conducted by Gasparek[8]. Measurements were made at chordlengths up to 3.7/c, beyond which Gasparek found it impossible to keep the probe in the vortex. In this experiment the static pressure was assumed constant across the vortex.

Recent work using a larger model and freestream velocity has been done by Chigier and Corsiglia[9] using a hot wire probe, but only at distances up to four chordlengths downstream. The results show a velocity overshoot in the vortex core. It is interesting to note that the work done using hot wire probes shows a velocity overshoot, while workers using pressure probes predict a velocity defect. Several investigations recently conducted have used a split sheet for the simulation of the trailing vortex. This method uses two sheets which connect with equal and opposite angles of attack and produce a stream, stable vortex that travels straight downstream. It is not clear if the vortex cores will be of equal with

a vortex produced by a single airfoil. This technique, originated by Hoffman and Joubert[10], is being used by Donaldson[11], and has been used in recently reported work by Poppleton[12] which included the effects of mass injection. Another recent investigation including the effects of mass injection at the tip was conducted at VPI&SU[13] using a tuft grid at distances up to thirty chordlengths downstream of the wing. These experiments are summarized in Table 1.

Vortices have been a classical part of the study of fluid mechanics, but the difficulties of describing free viscous vortex flows and the apparent lack of applications have resulted in relatively few theoretical investigations of these flows. Hall[14] has given a thorough discussion of such flows. An important recent contribution to the stability theory of trailing vortices has been given by Crow[15] and is not discussed here, since the present vortex observed experimentally was stable and well behaved, and interest lies in the simple viscous decay of the vortex. Batchelor[16] has shown for laminar flows that in cases where the velocity excess or deficit in the core is small compared to the freestream velocity, the circumferential velocity distribution is identical to the solution given by Lamb[17] for the impulsively generated planar vortex by use of the simple transformation $Z/U_\infty = t$.

The theory of turbulent vortex cores is at best primitive, despite the fact that the trailing vortex is turbulent as is almost every real vortex. The simplest method of dealing with turbulent flows has been to employ the concept of an eddy viscosity in which the turbulent diffusivity is supposed to be directly proportional to the molecular viscosity. With

this assumption the governing equations are reduced to the laminar case and methods used for laminar flows can be applied to the turbulent case. Squire[18] gave the first solution using this concept, making the eddy viscosity proportional to the circulation at the plane of symmetry of the wing.

Further improvement on the theory can be achieved by using a different viscosity model for the flow in the axial direction. This approach has been used by Fernandez and Lubard[19] in an integral approach, with the results showing that adjustments of the initial conditions could cause singularities in the solution. These singularities are supposed to indicate conditions that would correspond to vortex breakdown. This is the theoretical justification for varying the initial conditions experimentally through mass injection. All of these theoretical and experimental efforts seem to indicate that vortex decay due to simple diffusion is one of the least rapid diffusion processes that occurs in free turbulent flows, hence the necessity to predict it accurately.

Until recently, it has been supposed that the vortex exhibits a 1/r "potential" type behavior immediately outside the vortex core. Donaldson[20] recently reviewed an early study by Betz[21] which shows that this is not the case, and that the outer inviscid vortex depends on the cirulation distribution about the wing. Betz performed his calculations for the elliptic wing case, and Donaldson was able to show that this theory describes the outer portion of the vortex much better than any theory which included viscosity effects. The present work extends this theory to include any wing planform that can be described using lifting line theory, showing the importance of the various parameters for the outer portion of the vortex.

EXPERIMENTAL INVESTIGATION

The experimental study was conducted in the VPI&SU 6-Foot Subsonic Wind Tunnel, which has a test section 28 feet long. An NACA 0012 rectangular wing was placed at the test section front, allowing measuring stations of up to 30 chord lengths downstream. This wing was also modified to allow mass injection at the wing tip. The vortex was investigated by use of small 5-hole yawhead and static pressure probes. Pressures were measured on three inclined manometers and the probe orientations were measured by potentiometers, with readings recorded on a digital voltmeter. The details of the apparatus, test procedure, and data reduction are given in the following paragraphs.

The VPI&SU 6-Foot Subsonic Wind Tunnel is a continuous, single-return, closed test section tunnel with a 6 x 6 foot square test section. The tunnel turbulence level is very low due to seven anti-turbulence screens upstream of the test section. Preliminary calibration of the wind tunnel was conducted using a large yawhead probe, mounted on a mechanism to traverse the entire tunnel width. Horizontal traverses were made at the test section midpoint, halfway between the floor and ceiling of the tunnel. A vertical traverse was made at the point corresponding to the leading edge of the wing. Results show low flow angularity and total velocity variation at the test section midpoint, and an acceptable variation in properties at the wing station. Figure 2 shows the results of the preliminary calibration.

Tunnel speed is controlled by coarse and fine rheostats. The operator used a Merriam Micro-Manometer attached to a pitot-static tube placed in

an area free from the wing disturbance in order to control the freestream speed. Attached to the same pitot-static tube was a pressure transducer used in conjunction with a Barocell electric manometer. This manometer was placed on the table with the special test instrumentation, allowing operators to monitor the tunnel speed while performing the tests. Free-stream temperature was monitored by a temperature probe at the wall of the test section and recorded on a Digitemp temperature gauge. The pressure in the wind tunnel test section is identical to that of the control room since the room is in a large pressure-sealed building. The static pressure was measured on a Kahlsico Precision Aneroid Barometer Mk 2.

An NACA 0012 straight square-tipped wing was mounted vertically from the center of the tunnel roof one foot from the front of the test section. The mounting allowed the wing to be set at variable angles of attack, and placed the free wing tip near the center of the wind tunnel. The mounted wing is shown in Figure 3. This mounting allowed placement of the traversing mechanism at up to 30 chord lengths behind the wing before the flow reached the diffuser section of the tunnel. Complete specification's of the wing are given in Table 2. The present tests were made using a wing angle of attack of 7½° to produce a strong vortex.

In order to include mass injection at the wing tip, the wing model was modified to carry a copper tube ¼ inch in outside diameter along the leading edge and tip as shown in Figure 4. Mass injection was obtained by metering air from an available high pressure supply using a simple orifice metering system constructed according to the specifications given in the ASME Fluid Meters book[22]. Jet operating conditions for the tests

are given in Table 2. The wing was tested on the mechanical balance system for comparison of the wing lift and drag coefficients with and without mass injection and the results are shown in Figure 5.

The traversing mechanism used in this study consisted of an existing traverse that provided one translation movement (vertical in this test) of 4 feet. The basic traverse is shown in Figure 3. Added to this assembly was an adapter unit that allowed a probe to rotate in pitch and yaw around its point. The general layout of the adapter unit is shown in Figure 6. It was designed so as to be rigid in intensely swirling flows while presenting minimum disturbance to the flowfield at the point of the probe. Throughout the tests no vibration of any probe could be detected visually, insuring accurate pressure measurements. Rotation in pitch is accomplished by a machined steel arc and track. A flat rack gear was silver-soldered to the arc, creating a curved gear of 28 inches pitch diameter. This allowed a rotation of 34° at the probe point. The rack gear was driven by a 1-rpm Hurst motor, spring mounted for constant tension on the curved rack gear. The motor gear was of one-inch pitch diameter, and produced a rotation speed of 0.2 degrees per second, which was sufficiently slow to insure positive control of the pitch position, measured by a Bournes ten-turn potentiometer. This was connected to the motor shaft, and a constant 5 volt power supply was then connected to the potentiometer, with the voltage position reading then made on a Doric digital voltmeter. Rotation in yaw is accomplished by design of any probe attached to the system such that the point of the probe is above its shaft, as shown in the detail Figure 7, so that it is free to rotate about its

shaft. The probe is then rotated by another 1-rpm Hurst motor mounted on the traverse arm through a series of linkages. Its position was then monitored by a 1-turn Bournes potentiometer mounted directly behind the probe as shown in the figure. The position was measured using the same electric system that was used to obtain pitch positions. The range for the yaw was about 70 degrees and the speed of rotation was 0.4 degrees per second.

The 1/8 inch outside diameter yawhead probe used in the investigation was custom built for the experiment by United Sensor Corporation. It had 5 holes, with one hole in the middle, of the point, and opposite holes in the vertical and horizontal planes. The entire probe is shown in Figure 8. By measuring pressure differences between opposite holes in the same plane the angle of flow can be determined. The probe showed a linear response over a range of ± 10°, and the small holes and long pressure leads caused the pressure difference read on the manometers to be very slow in coming to an equilibrium state. The 1/16th inch O.D. static probe used in the experiment was also made by United Sensor Corporation. This probe, as shown in Figure 8, has a much smaller area than the yawhead probe. The entire test installation inside the tunnel is shown in Figure 3.

Three inclined manometers were used for the test. All manometers used a red manometer oil with a specific gravity of .826. The total pressure was measured on a Dwyer manometer that was incremented in intervals of 0.02 inches of water. The total pressure measured was referenced to the freestream static pressure. Pressure differences in the horizontal plane were measured on a Dwyer manometer also graduated in 0.02 inches of water,

and the manometer had an operating range of ± 1.1 inches of water. Vertical plane flow angularity was measured on a manometer constructed in the Aerospace Engineering Laboratory, and was graduated at intervals of .01 inches of water. All manometers were operated using the pitot-static tube that was the standard for the test, and no deviation between these manometers and the reading on the Merriam Micromanometer was found. Additional lighting was placed on the manometers and readings were taken with a magnifying glass. All pressure lines were standard thick wall plastic pressure tubing. As a test for leaks, a cover was placed over the 5-hole pressure probe tip with readings on the manometers out of their equilibrium position and left overnight. No change was found in the readings over a twelve hour period, and it was concluded that there were no leaks in the system.

The special instrumentation used for the test was grouped as shown in Figure 9. Notice that the control box for the adapter unit contains a voltmeter to monitor the constant 5 volt power supply, and the electric manometer is below the digital voltmeter, allowing a constant monitor of the freestream dynamic pressure.

After the calibration of the tunnel a tuft grid study behind the wing was made as described in Reference 13. The yawhead probe was then calibrated for the linearity of the potentiometers in yaw and pitch. In pitch the zero angle was defined as the angle in which the probe was parallel with the base. In yaw the zero angle was defined as the point where the probe was perpendicular to the plane of the front of the base. The probe was then examined to assure probe tip rotation about a stationary

point. Through several hundred cycles of the equipment during calibration the zero angles did not vary. With the mechanical characteristics of the traverse defined, the characteristics of the probe were examined. Calibration tests were conducted at freestream dynamic pressures of 1, 2, and 5 inches of water, with both pitch and yaw sensitivity recorded. The probe was tested in both upright and inverted positions in order to determine the probe error. The results showed that the probe had no error to the accuracy of the experiment. Calibration curves for probe position and flow angularity are given in Figures 10 and 11. The flow angularity curves were repeatable for a large range of values of dynamic pressures over the range of interest.

The change of indicated dynamic pressure with yaw angle was also of interest for the yawhead probe and is given in Figure 12. The static pressure probe was calibrated for the reduction of static reading with yaw angle increase, and is given in Figure 14.

The procedure used for the investigation of the trailing vortex was straight forward. All the information necessary from the yawhead probe was obtained, and then the same series of tests was conducted using the static probe. The parameter study conducted is outlined in Table 3. Initially at each station the vortex center was found by raising the probe until the yaw angle of the flow was found to be zero, and then the traverse was moved laterally in the test section until the pitch angle was found to be zero. Because of symmetry, the vortex center will occur where both the pitch and yaw angles are zero. Once the vortex center was found, a vertical traverse was made starting from the center and going 4 inches above the center (approximately 8 core radii), and then returning to the

center and travelling 4 inches below the vortex center. Originally it was planned to allign the probe so that there was no flow angularity relative to the flow. It was found however that moving the probe in the vortex caused the vortex to move. For example, a movement in the yaw direction could cause the flow angularity in pitch to change drastically, indicating that the probe was no longer directly above the vortex center where the pitch angle was nearly zero. Because of the importance of knowing the relative position of the vortex center and probe in order to reduce the pressure data into velocity profiles and accurately find the core radius, it was decided not to move the probe in yaw or pitch while traversing the vortex. Thus the disturbance of the vortex was minimized. Another related problem was that the static pressure measurement had to be made with the probe alligned with the local flow direction. Therefore the static probe was much smaller in projected side area than the yawhead probe, and it was assumed that the disturbance of the vortex due to the static probe moving in yaw was negligible. It was found possible to make the static pressure measurements using the static probe only in the case of mass injection, due to the low flow angles and gradients involved in the mass injection case. For the normal trailing vortex it was found that the static probe could not be aligned in the flow with adequate confidence and centerline total head minus freestream static measurements could not be adequately duplicated at the same positions. Thus a method for determining static pressure from the yawhead probe was used. This method was described by Winternitz[23], and involves several additional calibration curves (Figure 13). Use of this method showed consistent results with the pressure predicted from inviscid considerations and high repeatability,

and the results from this method in the area of the centerline were used to key the inviscid theory for static pressure distribution.

Data reduction was accomplished in a manner that allowed for easy comparison of data reduction performed for various assumptions. Several general assumptions were made; the most basic of these was the assumption of incompressible flow since the Mach Number was never greater than .1 for any test. It was also assumed that the vortex path was parallel to the free-stream path. This is consistent with earlier work[13] showing that after a distance of a few chordlengths downstream of the wing the vortex travels parallel to the freestream. This study does not make any conclusions as to the path of the vortex due to the effects of the tunnel walls. However in the analysis of flow properties at particular stations, it is assumed that the wall has no effect. This seems justified since the vortex core is at least 24 core diameters from the nearest wall. Any pressure gradient in the freestream direction would have an effect on the vortex, but the VPI 6-Foot Tunnel has a negligible pressure gradient throughout the entire test section.

The experimental information was obtained in the form of pressure measurements from the yawhead and static probes; and probe position measurements for vertical height, pitch and yaw rotation angles. From this information, the angularity of the flow and the local static and dynamic pressures could be determined using the calibration curves and sign conventions given in Figures 10 through 15. Because of the importance of minimizing the vortex disturbance due to the presence of the probe, preliminary work indicated that the most accurate method of traversing the vortex with the yawhead probe was to keep the probe

stationary in yaw and pitch, while moving vertically through the vortex center. The total head reading error was then corrected due to the large flow angularity by use of the calibration curve (Figure 12). Initial results assuming a constant static pressure distribution showed very high circumferential velocities. Examination of the radial momentum equation,

$$\frac{1}{\rho}\frac{\partial P}{\partial r} = V_\theta^2/r \qquad (1)$$

shows that if V_θ is large then $\partial P/\partial r$ cannot be negligible. Because the yawhead probe was calibrated in a uniform stream for $\Delta P/Q$ indicated, it was difficult to decide what the proper indicated dynamic pressure for initial data reduction should be. Preliminary work indicated that there was a slight axial velocity excess in the core and thus it was assumed that the dynamic pressure to use initially was that of the freestream. Using this dynamic pressure the initial flow angularities were calculated. Using these angularities the static pressure probe traverse was made. Then using the correct static pressure distribution the final dynamic pressure and flow angularities could be calculated. This was possible because inspection of the static probe calibration shows negligible error for misalignment angles less than ten degrees, and none of the corrected angles were more than ten degrees different than the initial angle.

The various axis system and sign conventions for determining the velocity profiles are shown in Figure 16. Note that from Bernoulli's incompressible equation

$$P_o = \tfrac{1}{2}\rho V^2 + P_{st} \qquad (2)$$

the total velocity V, can be calculated from

$$V = \sqrt{\frac{2[(P_o - P_{st_\infty}) - (P_{st} - P_{st_\infty})]}{\rho}} \quad . \tag{3}$$

The velocity components V_x, V_y, and V_z are then known at any point in the flowfield. For this study the vortex is assumed symmetrical and the velocity components of interest are V_r, V_θ, V_z, which are obtained by the transformation

$$\begin{aligned} V_r &= V_x \cos\theta + V_y \sin\theta \\ V_\theta &= -V_x \sin\theta + V_y \cos\theta \\ V_z &= V_z \end{aligned} \tag{4}$$

where

$$\begin{aligned} V_x &= V \sin (FP) \\ V_y &= V \cos (FP) \sin (FY) \\ V_z &= V \cos (FP) \cos (FY), \end{aligned} \tag{5}$$

and FP and FY are the total flow pitch and yaw angles respectively.

In the present case traverses were made parallel to the wing trailing edge, and hence $\theta = 0°$, and the above relation (4) simplifies to

$$\begin{aligned} V_r &= V_x \\ V_\theta &= V_y \\ V_z &= V_z \quad . \end{aligned} \tag{6}$$

With V_θ known, the circulation Γ, can be calculated from

$$\Gamma = 2\pi V_\theta r \ , \qquad (7)$$

where r is the distance from the vortex center defined as the location of $V_\theta = 0$.

As stated previously, for the mass injection case the measured static pressures were used in all calculations. In the cases without mass injection a method of obtaining static pressures from the yawhead was used. Data points were not obtained for every point originally investigated when the data was found to fit the theoretical pressure distribution described in the Theoretical Considerations section. Thus the data was reduced based on static pressures from the theory, where the theory was keyed to the experimental data at the centerline of the vortex.

In order to obtain the static pressure from the yawhead several additional calibrations based on a uniform stream must be used[23]. Initially the yaw angle Ψ is found from the calibration probe constant

$$K_p = \frac{(P_3-P_4)}{(P_5-P_2)}$$

at each point. Using the defined calibration curves

$$K_i(\Psi) = \frac{P_i-P_{st}}{q} \ , \ P_i = P_{st} - qK_i$$

where q is the dynamic pressure, we can write

$$q = \frac{(P_5 - P_{st\infty}) - (P_4 - P_{st\infty})}{k_5 - K_4}$$

and hence

$$(P_{st} - P_{st\infty}) = (P_4 - P_{st\infty}) - qK_4 \ .$$

Combining the above relations an expression for the static pressure can be obtained where ψ is known from K_p.

$$(P_{st} - P_{st\infty}) = \frac{K_5(P_4 - P_{st\infty}) - K_4(P_5 - P_{st\infty})}{K_5 - K_4} \qquad (8)$$

Using the above results on the centerline the data and theory were matched. On the axis the pressure is

$$(P_{st\infty} - P_{st}) = \frac{\rho\Gamma^2}{4\pi^2 A_c^2} \ .$$

From the observation that A_c, the core radius, seemed to be independent of the method of data reduction it could be assumed known for each case. The data and theory were then keyed by solving for Γ,

$$\Gamma = 2\pi A_c \sqrt{\frac{(P_{st\infty} - P_{st})_{r=0}}{\rho}} \qquad (9)$$

The pressure distribution from theory was then used across the vortex.

THEORETICAL CONSIDERATIONS AND INVESTIGATION

Although the present work is mainly experimental, it is important to understand the theoretical aspects of the problem in order to interpret the results intelligently. A description of the generalization of a method due to Betz to include arbitrary wings will be given in some detail to clarify some points of confusion in recent literature due to several sign errors in the translation of the original work. Viscous theories will then be discussed in order to examine the correlation between theory and experiment.

It is planned to study the effect of wing plan forms and other wing parameters on the inviscid portion of the trailing vortex, and therefore obtain information on the desired wing for minimizing the trailing vortex disturbance. In order to use the method of Betz it is necessary to know the spanwise circulation distribution of the wing, $\Gamma(y)$, and also its derivative, $d\Gamma/dy$. Many methods for finding these properties have been proposed, but for initial work the method of Glauert is simple and satisfactory. It is felt that a brief description of Glauert's method must be given before the method of Betz can be described.

The monoplane equation is used to solve for the unknown coefficients of a Fourier series representing the circulation distribution. Its derivation can be found in any aerodynamics text[24]. It is written here in the form

$$\mu(\theta)\,\alpha(\theta) = \sum_{i=1}^{\infty} A_n \sin n\theta \left(1 + \frac{n\mu(\theta)}{\sin\theta}\right) \qquad (10)$$

where

$$\mu(\theta) = \frac{a_o[y(\theta)]c[y(\theta)]}{8S}$$

and

$$\alpha(\theta) = \alpha(\theta) - \alpha_o(\theta)$$

s = semi-span

a_o = lift curve slope for 2-D airfoil

c = chord

α = geometric angle of attack

α_o = zero lift angle of attack

y = $s\cos\theta$ - transformation between y and θ

By knowing the wing shape, Eqn. (10) can be solved for the coefficients desired, A_n, and the circulation distribution for a given wing can then be written

$$\Gamma = 4sV \sum_{i=1}^{\infty} A_n \sin n\theta \qquad (11)$$

where V = freestream velocity.

We can also compute

$$\frac{d\Gamma}{dy} = \frac{d\Gamma}{d\theta}\frac{d\theta}{dy}$$

where

$$\frac{d\Gamma}{d\theta} = 4sV \sum_{i=1}^{\infty} nA_n \cos n\theta \qquad (12)$$

and

$$\frac{d\Gamma}{dy} = (-\ 4V \sum_{1}^{\infty} nAn \cos n\theta)/\sin\theta \qquad (13)$$

It is noted that for symmetric loadings $A_n = 0$ for n even.

As an example the coefficients A_n have been computed for the wind tunnel model and the coefficients are found to diminish rapidly. The $\Gamma(y)$ distribution is given in Figure 17.

Betz[21], in 1932, gave some theorems on the "Behavior of Vortex Systems". These can be applied to trailing vortices and Betz applied them to an elliptically loaded wing. Donaldson[20] recently rediscovered this work and states the needed theorems from Betz's work as:

1. All the vorticity shed by each half of the wing is found rolled up in the trailing vortex behind the appropriate half of the wing;

2. The "center of gravity" of the vorticity distribution remains at a constant distance from the plane of lateral symmetry;

3. The "moment of inertia" of the vorticity shed by each half of the wing about its "center of gravity" is a constant.

For the present work these theorems can be expressed as:

$$\int_{o}^{b/2} \frac{d\Gamma}{dy}\, dy = \text{const.} = \Gamma_o = \int_{o}^{b/2} \frac{d\Gamma}{dr}\, dr$$

$$\int_{o}^{b/2} y \frac{d\Gamma}{dy}\, dy = \text{const} = \bar{y}\,\Gamma_o ,$$

$$\int_{o}^{b/2} (y-\bar{y})^2 \frac{d\Gamma}{dy}\, dy = \text{const} = \int_{o}^{b/2} r^2 \frac{d\Gamma}{dr}\, dr .$$

In order to show the method of calculating circulation distribution in the vortex, the discussion of Betz is presented with some added clarifications. First examine the undeveloped area of discontinuity behind the wing. (See Figure 18). The total circulation of one group of the undeveloped area of discontinuity from y_1 to s is

$$\Gamma(y_1) = \int_{y_1}^{s} \frac{\partial \Gamma}{\partial y}\, dy \ . \tag{14}$$

The distance of the center of gravity of this group can be computed as follows: (See Figure 18)

$$\overline{y}_1 = \frac{\int_{y_1}^{s} y\,dA}{\int_{y_1}^{s} dA} \ . \tag{15}$$

From Figure 18, we see that

$$dA = \gamma(\eta)\, d\eta \ , \tag{16}$$

where we let $\gamma(\eta)$ denote the strength of the trailing vortex sheet per unit length along y.

It is important to realize that the strength of the trailing vortex sheet per unit length is equal to the change of the circulation per unit length at some y_1 since this gives the amount of vorticity that must be shed by the wing at this point. Since the circulation is maximum at $y = 0$ in most cases, and decreases to zero at the tip, the strength of the trailing vortex sheet per unit length γ, must be related to the

circulation Γ by

$$\gamma(y) = \frac{-d\Gamma(y)}{dy} \quad , \tag{17}$$

and hence

$$dA = \frac{-d\Gamma(y)}{dy}\, dy, \text{ and (15)} \tag{18}$$

becomes $$\bar{y}_1 = \frac{\int_{y_1}^{s} y\left(\frac{-d\Gamma(y)}{dy}\, dy\right)}{\int_{y_1}^{s} \frac{-d\Gamma}{dy}\, dy} \quad ,$$

and the expression for $\bar{y}_1$ is finally

$$\bar{y}_1 = \frac{-1}{\Gamma(y_1)} \int_{y_1}^{s} y\, \frac{d\Gamma(y)}{dy}\, dy \quad . \tag{19}$$

Here we note that using the Glauert method we will find convenient the transformation

$$y = s\cos\theta, \text{ or } \cos\theta = y/s, \sin\theta = \sqrt{1-(y/s)^2}$$

$$\text{and } dy = -s\sin\theta d\theta \quad . \tag{20}$$

Using (20) we can transform (19) and obtain

$$\bar{y}_1 = -\frac{1}{\Gamma(y_1)} \int_{y_1}^{s} s\cos\theta \left(\frac{d\Gamma}{d\theta}\right)\left(-\frac{1}{s\sin\theta}\right)(-s\sin\theta)d\theta$$

combining terms and reversing the new limits obtained

$$\bar{y}_1 = \frac{s}{\Gamma(y_1)} \int_0^{\theta_1} \cos\theta \, \frac{d\Gamma}{d\theta} \, d\theta \quad . \tag{21}$$

Similarly we can compute the moment of inertia of the group with respect to the center of the area of discontinuity (y=0), which is

$$J_o = \int_{y_1}^{s} y^2 \, dA \tag{22}$$

from the previous definition of dA we have

$$J_o = - \int_{y_1}^{s} y^2 \frac{d\Gamma}{dy} \, dy \quad . \tag{23}$$

Using (20) we can transform (23) to

$$J_o(y_1) = s^2 \int_0^{\theta_1} \cos^2\theta \, \frac{d\Gamma}{d\theta} \, d\theta \, . \tag{24}$$

The inertia moment of this group with respect to its center of gravity ($\bar{y}_1$) is

$$J_{y_1} = J_{o_{y_1}} - \Gamma_{y_1} \bar{y}_1^{\,2} \, . \tag{25}$$

This moment of inertia must exist after the discontinuity has rolled-up into a trailing vortex.

Now, from Betz, we see that the coiled up group can be assumed to be circular (the effect of one tip vortex on the structure of the other

is assumed negligible) so that circulation can be given as $\Gamma = f(r)$ only. The vortex group from y_1 to s is coiled up into a spir... which fills the circle with radius r. Then the circulation of Γ_r must be equal to the original vortex group.

$$\Gamma_{r_1} = \Gamma_{y_1} , \tag{26}$$

and likewise, the inertia moment of the vortices coiled up in this circle must be equal to the original inertia moment of the vortex group

$$J_r = \int_0^r \frac{\partial \Gamma}{\partial r} r^2 dr = J_y . \tag{27}$$

Permitting r to increase by dr, then y decreases by dy and θ increases by $d\theta$ under these premises. The result is an increase in circulation of

$$\frac{\partial \Gamma_r}{\partial r} dr = \frac{\partial \Gamma_y}{\partial \theta} d\theta \tag{28}$$

and in inertia moment of

$$\frac{\partial \Gamma_r}{\partial r} r^2 dr = \frac{\partial J_y}{\partial \theta} d\theta. \tag{29}$$

Then the differentiation of (25) gives

$$\frac{\partial J_{y_1}}{\partial \theta} = \frac{\partial J_o}{\partial \theta} - \frac{\partial \Gamma_{y_1}}{\partial \theta} \bar{y}_1^2 - 2\,\Gamma_{y_1} \bar{y}_1 \frac{\partial \bar{y}_1}{\partial \theta} \,. \tag{30}$$

Substituting for $\partial Jy/\partial\theta$ into (29) and rewrite

$$\frac{\partial \Gamma r}{\partial r}\, dr = \frac{1}{r^2}\left[\frac{\partial J_y}{\partial \theta}\right] d\theta = \frac{1}{r^2}\left[\frac{\partial J_o}{\partial \theta} - \frac{\partial \Gamma_{y_1}}{\partial \theta} \bar{y}_1^2 - 2\Gamma_{y_1}\bar{y}_1 \frac{\partial \bar{y}_1}{\partial \theta}\right] d\theta \tag{31}$$

and from (28)

$$\frac{1}{r^2} \frac{\partial J_y}{\partial \theta}\, d\theta = \frac{\partial \Gamma_y}{\partial \theta}\, d\theta$$

and thus

$$r^2 = \frac{\dfrac{\partial J_y}{\partial \theta}}{\dfrac{\partial \Gamma_y}{\partial \theta}} \,. \tag{32}$$

This can be written in final computational form

$$r = \sqrt{\frac{\partial J_o/\partial\theta - (\partial \Gamma_y/\partial\theta)\bar{y}_1^{\,2} - 2\Gamma_{y_1}\,\bar{y}_1\,(\partial \bar{y}_1/\partial\theta}{\partial \Gamma_{y_1}/\partial\theta}} \,. \tag{33}$$

The relation between y_1 and r is known and all that remains is to calculate

$$r_1 = r(y_1) \,,$$

and $\Gamma(r_1)$ will be known from 26. Then

$$V_\theta = \frac{\Gamma(r)}{2\pi r} \quad . \tag{34}$$

The computational details can be derived using the method of Glauert and recalling the transformation (20). With the coefficients A_n known for a specific wing, the quantities $\bar{y}_1$, $\partial\bar{y}_1/\partial\theta$, J_o, $\partial J_o/\partial\theta$, can be readily evaluated.

First the computational formula for $\bar{y}_1$ is obtained.

Recall that

$$\bar{y}_1 = \frac{s}{\Gamma(y_1)} \int_o^{\theta_1} \cos\theta \, \frac{d\Gamma}{d\theta} \, d\theta$$

$$= \frac{s}{4sV \sum_{i=1}^{\infty} A_n \sin n\theta_1} \left[\int_o^{\theta_1} A_1 \cos^2\theta d\theta + \int_o^{\theta_1} \sum_{i=3}^{\infty} nA_n \cos\theta \cos n\theta d\theta \right]$$

and finally

$$\bar{y}_1 = \frac{s}{\sum_{i=1}^{\infty} A_n \sin n\theta_1} \left[\frac{A_1\theta_i}{2} + \frac{A_1 \sin 2\theta_1}{4} + \sum_{i=3}^{\infty} nA_n \left(\frac{\sin(1-n)\theta_1}{2(1-n)} + \frac{\sin(1+n)\theta_1}{2(1+n)} \right) \right]. \tag{35}$$

Now calculate $\partial\bar{y}_1/\partial\theta$.

Let $$\frac{\partial y_1}{\partial \theta} = \frac{\partial (fg)}{\partial \theta}$$

where $$f = \frac{s}{\sum_{i=1}^{\infty} A_n \sin n\theta} ,$$

$$g = \frac{A_1 \theta}{2} + \frac{A_1}{4} \sin 2\theta + \sum_{i=3}^{\infty} nA_n \left(\frac{\sin(1-n)\theta}{2(1-n)} + \frac{\sin(1+n)\theta}{2(1+n)}\right) ,$$

$$\frac{\partial f}{\partial \theta} = \frac{-s \sum_{i=1}^{\infty} nA_n \cos n\theta}{\left(\sum_{i=1}^{\infty} A_n \sin n\theta\right)^2} ,$$

$$\frac{\partial g}{\partial \theta} = \frac{A_1}{2} + \frac{A_1 \cos 2\theta}{2} + \frac{\partial}{\partial \theta} \left[\sum_{i=3}^{\infty} nA_n \left(\frac{\sin(1-n)\theta}{2(1-n)} + \frac{\sin(1+n)\theta}{2(1+n)}\right) \right]$$

$$= \frac{1}{2} \left[A_1 + A_1 \cos 2\theta + \sum_{i=3}^{\infty} nA_n \left(\cos(1-n)\theta + \cos (1+n)\theta\right) \right] ,$$

and the result can be stated:

$$\frac{\partial y_1}{\partial \theta} = \left(\frac{-s \sum_{i=1}^{\infty} nA_n \cos n\theta_1}{\left(\sum_{1}^{\infty} A_n \sin n\theta_1\right)^2} \right) \left(\frac{A_1\theta_1}{2} + \frac{A_1}{4} \sin 2\theta + \sum_{i=3}^{\infty} nA_n \left(\frac{\sin(1-n)\theta}{2(1-n)} + \frac{\sin(1+n)\theta}{2(1+n)}\right)\right)$$

$$+ \frac{s[A_1 + A_1 \cos 2\theta + \sum_{1=3}^{\infty} nA_n (\cos(1-n)\theta + \cos(1+n)\theta)]}{2 \sum_{i=3}^{\infty} A_n \sin n\theta} , \qquad (36)$$

Next we calculate J_o, where

$$J_o(y_1) = s^2 \int_o^{\theta 1} \cos^2 \theta \frac{d\Gamma}{d\theta} \, d\theta$$

so that

$$J_o(y_1) = 4s^3 V \int_o^{\theta 1} \sum_{i=1}^{\infty} nA_n \cos^2 \theta \cos n\theta \, d\theta$$

$$= 4s^3 V \int_o^{\theta 1} \sum_{i=1}^{\infty} nA_n \left(\frac{1}{2} + \frac{\cos 2\theta}{2}\right) \cos n\theta \, d\theta ,$$

$$J_{(y_1)} = s^3 V \left[\sum_{i=1}^{\infty} 2A_n \sin n\theta + \sum_{i=1}^{\infty} nA_n \left(\frac{\sin(n-2)\theta}{(n-2)} + \frac{\sin(n+2)\theta}{(n+2)}\right)\right]$$

(37)

and we obtain $\partial J_o/\partial\theta$ by differentiating (37)

$$\frac{\partial J_o}{\partial \theta} = s^3 V \left[\sum_{i=1}^{\infty} 2A_n \, n \cos n\theta + \sum_{i=1}^{\infty} nA_n \left(\cos(n-2)\theta + \cos(n+2)\theta\right)\right]. \quad (38)$$

Wings of several types were investigated. An example for the case of Betz and the wind tunnel model is shown in Figure 19.

With the outer portion of the vortex described excellently with the present theory, it proves instructive to re-examine the method used by Prandtl[25] to calculate the core radius and maximum velocity. Energy considerations are used, assuming that the vortex cores are circular and rotating as solid bodies. The energy of the inner and outer region of the vortex must equal the induced drag of the wing,

$$D_i = E = E_o + E_i . \quad (39)$$

D_i can be given in terms of the coefficients A_n by

$$D_i = 2\rho s^2 V^2 \pi \sum_{i=1}^{\infty} nA_n^2 . \quad (40)$$

The solid body rotation energy is given by

$$E_i = 2\left(\frac{\rho}{2}\right)\int_o^{A_c} \left(\frac{\Gamma}{2\pi A_c}\right)^2 \left(\frac{r}{A_c}\right)^2 2\pi r dr$$

$$= \frac{\rho \Gamma^2}{8\pi} . \quad (41)$$

Here Γ is the value of Γ at the core radius A_c.

For the outer core, the energy will be given by,

$$E_o = \int_{-}^{+} \int_{\infty}^{\infty} \frac{\rho q^2}{2} \, dy \, dz$$

where $$q = V_T = \frac{\Gamma}{2\pi r}$$

and we can calculate this in terms of r,

$$E_o = \int_{o}^{2\pi} \int_{A_c}^{\infty} \frac{\rho \Gamma^2}{(2\pi)^2 r^2} \, r dr d\theta$$

$$= \int_{A_c}^{\infty} \frac{\rho \Gamma^2}{(2\pi)^2 r^2} \, 2\pi r dr$$

$$= \int_{A_c}^{\infty} \frac{\rho \Gamma^2}{2\pi r} \, dr,$$

and here we follow the work of Prandtl and integrate to b',

$$E_o = \frac{\rho}{2\pi} \int_{Ac}^{b'} \frac{\Gamma^2}{r} \, dr \, . \qquad (42)$$

Note that $\Gamma = \Gamma(r)$ for $0<r<r(y/s=0)$

$$E_o = \frac{\rho}{2\pi} \left[\int_{-A_c}^{-r(y/s=0)} \frac{\Gamma^2}{r} \, dr + \int_{r(y/s=0)}^{b'} \frac{\Gamma^2}{r} \, dr \right] .$$

For our purposes it is sufficient to use the elliptic wing case and the approximation for $\Gamma(r)$ used by Donaldson, i.e.,

$$\Gamma = \Gamma_o \left[6 \left(\frac{r}{b}\right) - 9 \left(\frac{r}{b}\right)^{2}\right]^{\frac{1}{2}} \qquad 0 \leq r/b < 1/3$$

$$\Gamma = \Gamma_o \qquad r/b > 1/3$$

where b = wing span.

We note that if we use the assumption of Prandtl,

$$\Gamma = \Gamma_o \text{ for } r/b > \frac{Ac}{b} ,$$

we obtain $$\frac{Ac}{b} \cong .086.$$

Also, the energy is infinite if $A_c \to 0$. It is well known that A_c/b is an order of magnitude too big. However, in our case it is seen that

$$\lim_{\frac{r}{b} \to 0} \Gamma = 0$$

and we realize that the energy associated with the term E_o is finite as $A_c \to 0$.

With these observations, it is possible to proceed with the calculation of

$$\frac{A_c}{b} ,$$

$$D_i = E_o + E_i \ ,$$

$$D_i = \frac{\rho\Gamma^2}{8\pi} + \frac{\rho}{2\pi} \left[\int_{A_c}^{r(y/s=0)} \frac{\Gamma^2}{r}\, dr + \int_{r(y/s=0)}^{b'} \frac{\Gamma^2}{r}\, dr \right] ,$$

and for the elliptic wing

$$\frac{2\pi}{\rho} D_i = \frac{\Gamma_o^2\pi^2}{4} \ , \ \frac{b'}{b} = \frac{\pi}{4}$$

or

$$\frac{\Gamma_o^2\pi^2}{4} = \frac{\Gamma_o^2}{4} \left[6\,(r/b) - 9(r/b)^2\right] + \int_{\frac{A_c}{b}}^{1/3} \frac{\Gamma^2}{(r/b)}\, d(r/b) + \Gamma_o^2 \int_{1/3}^{b'/b} \frac{d(r/b)}{(r/b)}$$

which results in a quadratic for A_c,

$$\left(\frac{A_c}{b}\right)^2 - 2\,\frac{A_c}{b} - .04784 = 0$$

or

$$\frac{A_c}{b} = -.024,\ 2.024 \ . \qquad (43)$$

The above calculation shows that with the proper description of $\Gamma(r)$ it is <u>not</u> possible to calculate the core radius A_c from consideration of the kinetic energy due to swirl without including the effects of viscosity. Since the core is a viscous effect, it is certainly comforting to realize that the concept put forth by Prandtl does not predict

a plausible answer when the correct value of $\Gamma(r)$ is used. Thus the energy of the viscous core must be included in calculations for core size.

Since the approximation

$$\Gamma_{APR}\ (r) \geq \Gamma_{ACT}\ (r)$$

over the range of the wing, it is seen that if the core radius cannot be predicted for the approximation it will not provide a correct prediction for the actual circulation distribution.

Acknowledging the need to predict A_c from viscous considerations, it is instructive to inspect the variation of static pressure through the vortex. It is well known that pressure gradients are calculated from inviscid flowfields. Examples are the assumption of constant pressure across boundary layers and many free turbulent flows. Therefore we will investigate the pressure variation by inviscid considerations. The variation will be calculated using the Rankine vortex or uniformly distributed vorticity model.

In the vortex core solid body rotation is assumed, i.e.

$$V_\theta = \omega r$$

where ω is the angular velocity

$$\Gamma = 2\pi r V_\theta = 2\pi r\, \omega r = 2\pi r^2 \omega$$

and the circulation at A_c must be

$$\Gamma = 2\pi A_c^2 \omega$$

and we can solve for ω.

$$\omega = \frac{\Gamma}{2\pi A_c^2}$$

and $$V_\theta = \frac{\Gamma}{2\pi A_c^2} r \qquad \text{for } r < A_c$$

where Γ is the value at A_c and in the outer vortex

$$V_\theta = \frac{\Gamma}{2\pi r} \qquad r \geq A_c .$$

By noticing from preliminary experimental work that in the outer portion of the vortex the axial velocity is very nearly the same as the freestream velocity, Bernoulli's Equation can be written

$$P_o = P + \tfrac{1}{2}\rho V^2 = P + \tfrac{1}{2}\rho (V_z^2 + V_\theta^2) .$$

As $r \to \infty$, $V_\theta \to 0$ and

$$P_o = P_\infty + \tfrac{1}{2}\rho V_\infty^2 ,$$

so that

$$P_\infty + \tfrac{1}{2}\rho V_\infty^2 = P + \tfrac{1}{2}\rho (V^2+V_\theta^2)$$

and $$P_\infty - P = \tfrac{1}{2}\rho (V^2 - V_\infty^2) + \tfrac{1}{2}\rho V_\theta^2 ,$$

if $$V = V_\infty ,$$

$$P_\infty - P = \tfrac{1}{2}\rho V_\theta^2 ,$$

substituting for V_θ

$$P_\infty - P = \frac{\rho \Gamma^2}{8\pi^2 r^2} \qquad \text{for } r > A_c \qquad (44)$$

where Γ is the value at $r = A_c$ and is determined from experimental work.

In the vortex core the flow is not irrotational and Bernoulli's Eqn. is not valid in its simple form.

The governing equation can be written

$$\frac{\partial p}{\partial r} = \rho \frac{V_\theta^2}{r}$$

and

$$V_\theta = \frac{\Gamma}{2\pi A_c^2} r .$$

Therefore,

$$p = \int \rho \frac{\Gamma^2}{(2\pi)^2 A_c^4} r dr ,$$

$$p = \frac{\rho\Gamma^2}{8\pi^2 A_c^4} r^2 + \text{const.}$$

and the pressure must match at $r = A_c$; i.e.,

$$P = \frac{\rho\Gamma^2}{8\pi^2 A_c^2} + \text{const.} = P_\infty - \frac{\rho\Gamma^2}{8\pi^2 A_c^2},$$

$$\text{const.} = P_\infty - \frac{\rho\Gamma^2}{4\pi^2 A_c^2},$$

and

$$P = \frac{\rho\Gamma^2}{8\pi^2 A_c^4} r^2 + P_\infty - \frac{\rho\Gamma^2}{4\pi^2 A_c^2}$$

and

$$P_\infty - P = \frac{\rho\Gamma^2}{4\pi^2 A_c^2}\left(1 - \frac{r^2}{2A_c^2}\right) \qquad \text{for } r < A_c. \qquad (45)$$

In order to predict the decay of the trailing vortex it is necessary to consider the effects of viscosity. No contribution is made to the theory, but a brief outline of results is necessary in order to intelligently analyze the data. For a discussion of the governing equations Hall[14] should be consulted.

As stated previously the solution for the case of small axial velocity excess or defect, the tangential velocity can be described by the expression for the impulsively started vortex,

$$V_\theta = \frac{\Gamma_o}{2\pi r}\,(1 - e^{-\zeta}) \tag{46}$$

where $\zeta = \dfrac{Wr^2}{4\nu z}$,

which is the similarity variable for laminar motions. The axial velocity can be given by

$$w = W - \left(\frac{\Gamma_o^2}{(2\pi)^2 \nu z}\,\log\frac{Wz}{\nu}\right) e^{-\zeta} + \frac{\Gamma_o^2}{(2\pi)^2 8\nu z}\, f(\zeta)$$

$$- \frac{aW^2}{8\nu z}\, e^{-\zeta}$$

where a is a constant fixed by the upstream conditions, and

$$f(\zeta) = e^{-\zeta}\,(\log\zeta + \mathrm{ei}(\zeta) - .807) + 2\,\mathrm{ei}(\zeta) - 2\,\mathrm{ei}(2\zeta)$$

where $\mathrm{ei}(\zeta)$ = the exponential integral.

Finally the pressure can be obtained by

$$\frac{P-p}{\rho} = \frac{\Gamma_o^2}{(2\pi)^2}\,\frac{W}{8\nu z}\left[-\frac{(1-e^{-\zeta})^2}{\zeta} + 2\,\mathrm{ei}(\zeta) - 2\mathrm{ei}(2\zeta)\right].$$

The above results were derived by Batchelor[16]. In order to include the effects of turbulence it is usually assumed that

$$\overline{u'v'} = -\nu_T\left(\frac{\partial v}{\partial r} - v/r\right) .$$

The most successful model for ν_T has previously[19] been found to be

$$\frac{\nu_T}{\nu} = 0.185 \left(\frac{\Gamma_o}{2\pi\nu}\right)^{2/3} ,$$

given by Ise and Eschenroeder[26].

Another parameter often used in swirling flows is the swirl Reynolds Number,

$$R_{e_t} = \frac{V_{\theta max} A_c}{\nu} = \frac{\Gamma(A_c)}{2\pi\nu} .$$

It is possible to solve for A_c and $V_{\theta max}$ from (46), and examine the behavior of these properties with downstream distance z.

$$V_{\theta max} = .0507 \Gamma_o \sqrt{\frac{V_\infty}{z}} \cdot \frac{1}{\sqrt{\nu}} \qquad (47)$$

and

$$A_c = \sqrt{\frac{1.26(4\nu z)}{V_\infty}} \qquad (48)$$

Any substitution for ν can be made as long as it is not a function of r. By applying the experimental values of $V_{\theta max}$ and A_c, it is possible to estimate the ratio of turbulent to laminar viscosity. If this "standard" viscous theory is correct, then the results at a particular point should produce the same ν_T/ν for both (47) and (48).

Notice that the behavior downstream for cases where $\nu_T \neq f(z)$ is predicted to be

$$V_{\theta max} \sim \frac{1}{\sqrt{z}}$$

$$A_c \sim \sqrt{z} .$$

RESULTS AND DISCUSSION

The theoretical and experimental results obtained produced an interesting and unified picture of the farfield structure of an aircraft trailing vortex. An experimental vortex was obtained which was shown to agree well with theoretical considerations for the outer vortex and with an empirical equation derived from investigations of full scale aircraft trailing vortices.

The results of the theoretical investigation for several types of wings are shown in Figures 20, 21, 22, and 23. The conclusion to be drawn is that the vortex will become more intense as the circulation is concentrated on the outer portion of the wing. This provides theoretical verification of several experimental observations. Garodz[1] has concluded that the vortex is much less intense when originated by a wing configuration in which flaps are deflected. Smith[27] has also shown that the vortex is much less intense if a porous wingtip is used. It is certain that in such cases the circulation is concentrated near the wing root. Therefore it appears that any configuration that generates the major portion of the lift near the wing root will minimize the trailing vortex disturbance. For the wind tunnel case the agreement between experiment and theory is shown in Figure 24. These results can also be compared to the experimental work of Grow[28], who concluded that the core size seemed to remain independent of aspect ratio and become

larger as the taper ratio increased, while the maximum tangential velocity increases with both aspect ratio and taper. This is entirely consistent with the theoretical results of Figures 20 and 22, which show increases in the predicted inviscid circulation in the area of the vortex center. This comparison with experimental results also seems to warrant the general conclusion that even though the inviscid theory does not predict a maximum tangential velocity, it does seem to imply that for a fixed root circulation Γ_o, the maximum tangential velocity will become larger as the major portion of the vorticity is shed near the wing tip. Finally, it seems that Garodz's observation that some smaller aircraft (e.g. DC-9) with very "clean" wing configurations produce very intense vortices is also compatable with the theoretical predictions. Therefore, the effects of the T-tail on the vortices from such aircraft is probably of secondary importance.

The complete experimental results are tabulated in Appendix B. It should be noted that although runs were made for the modified wing with no blowing at each station, the differences between these results and the results of runs with the clean wing at the same station were considerably smaller than the expected experimental error. Thus, the results of these runs are not given. It is obviously not necessary to present all of this data graphically. The results of principal interest are the tangential and axial velocities and the static pressure and circulation distributions. It is well known that the radial velocity is a second order term and is more subject to experimental error since, if the traverse is not made perfectly, the radial velocity will contain contributions from the other velocity components which will be of the same order as the radial velocity.

Therefore, the radial velocity has been tabulated but is not plotted.

The tangential velocity profiles are plotted for each case in the conventional manner in which the cylindrical coordinate velocities are shown in a way similiar to the typical plots of downwash distribution behind a wing. Each figure contains the inviscid prediction based on the present work, and an empirical prediction proposed by McCormick[29] and based on an analysis of flight test data. The latter is written as

$$\frac{V_\theta}{V_{\theta max}} = \frac{1 + \ln(r/A_c)}{r/A_c} ,$$

where

$$V_{\theta max} = .68\ C_L\ V_\infty\ (1+.00063\ \frac{z}{\bar{c}C_L})^{-1/2}$$

and

$$A_c = .02\ C_o C_{l_o}\ (1+.00063\ \frac{z}{\bar{c}C_L})^{1/2} ,$$

with

C_o = midspan chord of wing

$\bar{c}$ = mean chord of aircraft

C_L = wing lift coefficient

C_{L_o} = midspan section lift coefficient.

While it appears that the expression for $V_{\theta max}$ and A_c are purely empirical, the expression for $V_\theta(r)$ is based on the analysis of Hoffman and Joubert[10]. They predict that the circulation distribution should be

proportional to ln r. This will fail as $r \to o$ and as $r \to \infty$ the circulation will not converge to some constant value. Thus this relation can be expected to be valid over a limited range, as Hoffman and Joubert have shown experimentally. Since the results agree fairly well with McCormick's empirical theory it proves instructive to plot the distribution of circulation for the present work. It can be seen in Figure 40 that the present theory is also a linear function of ln r in the region around A_c. From this figure it is not clear whether this result is general or happens to coincide with the Hoffman and Joubert result only for the rectangular wing case. In general the inviscid predictions of the present work will not be linear functions of ln r, but in order to examine this around A_c, the value of A_c must be known from experiment.

Examination of vortex tangential velocity profiles shows good agreement with the inviscid theory and adequate correlation with the flight test derived empirical equation. It is seen that as the vortex moves downstream there is very little decay. The change of $V_{\theta max}$ and A_c with z/c are given in Figures 42 and 43. It is seen that the decay is much less than the standard prediction of $(z/c)^{-\frac{1}{2}}$ for $V_{\theta max}$ and $(z/c)^{\frac{1}{2}}$ for A_c. Note that as the vortex moves downstream the outer portion of the vortex "widens". This must be the initial effect of viscous decay.

The effect of mass injection for three downstream stations at $V_\infty = 70$ fps is shown on the appropriate figures. Examination of these figures shows the drastic effect of mass injection on the tangential velocity. It is important to notice that the profiles converge to the zero mass injection case for the outer portion of the vortex, showing that the total amount of

circulation in the vortex has not been changed but that the vorticity has been distributed over a larger area. The trend of larger core radius and low tangential velocities seems to be continuing as the vortex moves downstream. Figure 45 shows the effect of mass injection on the characteristic core parameters $V_{\theta max}$ and A_c at z/c = 30. This result is in agreement with the work of Rinehart[30], who predicted these effects from analytical considerations.

These results seem to indicate that mass injection is much more effective than the experimental results of Poppleton indicated. The difference could be due to the fact that Poppleton used a split wing and injected directly in the axial direction, while in the present case a simple wing was used with the injection parallel to the wing tip. Since the wing was at an angle of attack, the mass injection was not entirely directed along the vortex center, but was slightly skewed.

It appears that the effect of mass injection is primarily that of introducing large amounts of turbulence into the core area during formation of the vortex, resulting in large eddies that help diffuse the vorticity. If this is the case, then it is possible that any method which would cause large amounts of turbulence to be generated in the area of the wing tip would have an equivalent effect. An estimate of the mass injection necessary to eliminate a single vortex is made in Figure 46 for various landing weights assuming a constant approach velocity for all weights. This estimate is made based on the

assumption that for the root circulation on the wind tunnel model the moderate blowing case has produced a sufficient amount of reduction in tangential velocity. In addition, Mironer[31] has recently shown that in order to increase diffusion of the core through heating effects, the heating must be placed in the outer portion of the vortex. Thus very large but perhaps not impossible amounts of injection seem to be required for vortex dispersion through mass injection.

Examination of the axial velocities, V_z (Figures 34, 35), shows that for the no mass injection case there is no large excess or deficit, and it is difficult to detect a trend. In the V_α = 100 fps case it may be possible to conclude that some axial velocity excess exists in the core region and the variations from the freestream are more pronounced. In the mass injection case the effect of the jet is not as pronounced as might be expected. Indeed in the full injection case at far downstream stations the axial velocity on the axis is less than in the moderate blowing case. The chief effect of full mass injection is to "fill out" the velocity profile. It is possible to understand this phenomenon by noting the coupling effect with which the tangential velocity governs the pressure distribution in the vortex, which in turn governs the axial velocity distributions. Thus, as the increase in injection decreases the maximum tangential velocity, the static pressure deficit in the vortex is reduced and the axial velocity appears to lose the large velocity excess that would appear if there were no swirl.

The static pressure distributions obtained are shown in Figure 36

and 37. It should be recalled that the theoretical curve was used to reduce the data in the case of zero mass injection. It can readily be seen that the use of the theory is justified by the excellent correlation of the data, where the theory has been keyed to the experimental data at the conterline. In the V_∞ = 100 fps it is seen that there are few data points. This is the result of the off-scale response of the manometers after the probe was moved slightly from the center of the vortex. Because the probe rotation could cause a large disturbance of the vortex, the probe was not rotated. The results obtained at the V_∞ = 100 fps case show adequate agreement with theory for the few recorded points.

Figures 38 and 39 are typical circulation distributions. It is easily seen that in general the data follows the theoretical prediction. Exceptions are the core region circulation deficiency, the circulation "overshoot" immediately outside the core, and the region far from the core which shows a large degree of data scatter. It is also observed that even at distances of 10 core radii the circulation is still far from the value at the wing root. In the light of the present theory this is to be expected. Previous investigations have obtained similiar results, but were unable to explain the results. For the present work at V_∞ = 70 fps, Γ_{A_C}/Γ_o = .46 and for V_∞ = 100 fps, Γ_{A_C}/Γ_o = .40. This is much lower than the predicted value of .72 for standard viscous theory.

The circulation near the center of the vortex is that expected for a solid body type rotation. At distances of A_C and slightly greater from the core the circulation "overshoots" the predicted inviscid circulation values. This would be expected from examination of the tangential velocity profiles. Donaldson[33] has noted this behavior previously in a more

restrictive class of theoretical examinations which did not account for the inviscid circulation given by the method of Betz. His results showed that this only occurred in turbulent flows. This would seem to indicate that the primary turbulence effect is to "pull" more at the fluid along with the core than would be expected. Indeed this leads to the image of a circular cylinder placed in an external circulation field and suddenly set in rotation (Rayleigh Problem). The result would be an increase of tangential velocity which would be added to the inviscid external tangential velocity. This would cause the circulation to "overshoot" the value in the area of the core. In the region far from the core there is a large degree of data scatter. This would be a result of magnification of experimental error in the farfield. It seems that the error inherent in the long times for settled values and the small changes in reading for each point far from the core could easily result in the high amounts of data scatter. Note that good symmetry is shown in the area of the core. The effects of mass injection are clear in Figure 38. It is seen that the value of the circulation is approaching the expected inviscid prediction and that the circulation is not destroyed on the mass injection.

By the use of standard viscous theory (Eqns (47), and (48)) the effective eddy viscosity ν_T can be calculated. The results are shown in Figure 41. It can be seen that ν_T based on A_C is quite different than ν_T calculated from $V_{\theta max}$. For this reason the standard viscous theory was not compared to the data. Since it is impossible to simultaneously match $V_{\theta max}$ and A_C from the relation

$$V_\theta = \frac{\Gamma_o}{2\pi r}\left(1-e^{-\frac{V_\infty r^2}{4\nu_T z}}\right)$$

it would appear that the concept of using an eddy viscosity at the form

$$\nu_T = k_\nu \ ,$$

where k is a constant, is inadequate in describing turbulent vortex flows, and some other method should be used. One sophisticated method for isolated vortices has been proposed by Donaldson, and this method may be investigated to see if it is possible to generalize Donaldson's "Method of Invariant Modeling" to include aircraft generated vortices. For the low turbulence environment of the present work, Figure 41 shows that $\nu_T \to \nu$ as $z/c \to \infty$ for ν_T based on $V_{\theta max}$. The eddy viscosity based on A_c is less than unity, which is also a violation of the standard viscous theory. In the past, theoreticians have considered ν_T a constant at each downstream station. From the axial velocity profiles it is seen that $(V_z - V_\infty) << V_\infty$, which would imply that standard viscous theory would apply if the motion were laminar, and turbulence must be responsible for the above effects.

CONCLUSIONS AND RECOMMENDATIONS

A vortex was generated in the Virginia Tech 6-Foot Subsonic Wind Tunnel and it has been found possible to use a probe to investigate the detailed structure of the mean flowfield of the vortex over the entire test section length. This contradicts previous investigators who previously concluded that it would be impossible to probe the vortex at large distances downstream.

Summarizing the detailed findings, it is concluded that the axial velocity is nearly constant across the vortex, tangential velocities were found to be higher than the near wing velocities found by Chigier and to show a much smaller rate of decay than the value predicted by standard viscous theory. Also, the core diameter has been found to be approximately 12% of the wing chord and essentially constant as the vortex travels downstream, in agreement with the near wing work of Gasparek and Chigier. Finally, in the very low ambient trubulence level environment of the present work, the turbulent eddy viscosity has been shown to decay rapidly, approaching the molecular viscosity far downstream.

Mass injection at the wing tip has been shown to be an effective means of destroying the high peak tangential velocities in the vortex through the introduction of large scale turbulence into the core area.

It has also been concluded that the generalization of the method of Betz has been shown to fit the outer portion of the experimental vortex excellently.

Use of the existing methods of description for viscous vortex flows

have been shown to be unable to describe both the core radius and maximum tangential velocity simultaneously. Since it was felt that it was the combination of these vortex properties that constitute the most important parameter, it was concluded that present theories are inadequate and must be re-evaluated on the basis of the present findings on the distribution of the outer circulation.

It is recommended that the effect of ambient turbulence on vortex decay be studied experimentally.

Flight test measurements using the apparatus being developed in conjunction with NASA Wallops Station to measure ground wind structure should be used to obtain data on large scale vortices and at long times after initial development.

Alternate methods of introducing large scale turbulence into the core should be investigated.

The present inviscid theory should be modified to include the effects of viscosity, with the final result showing the detailed structure of the vortex for each type of wing.

Advanced instrumentation such as the Laser Doppler Anemometer should be used to measure the vortex flow in order that the probe disturbance error be eliminated.

REFERENCES

1. Garodz, L. J., "Federal Aviation Administration Full-Scale Aircraft Vortex Wake Turbulence Flight Test Investigations: Past, Present, Future," AIAA Paper No. 71-97, January 1971.

2. Aircraft Wake Turbulence Symposium, jointly sponsored by the Boeing Company and AFOSR, September 1970, Seattle, Washington.

3. FAA Sympsoium on Turbulence, March 1971, Washington, D. C.

4. Spreiter, J. D. and Sacks, A. H., "The Rolling Up of the Trailing Vortex Sheet and Its Effect on Downwash Behind Wings," JAS, January 1951, p. 21.

5. Hacket, J. E. and Evans, M. R., "Vortex Wakes Behind High Lift Wings," Journal of Aircraft, May 1971, p. 334.

6. Fage, A. and Simmons, L. F. G., "An Investigation of the Air-Flow Pattern in the Wake of an Aerofoil of Finite Span," Phil. Trans. Roy. Soc. A225, p. 303, 1925.

7. Mowforth, E., "Details of Measurements in a Turbulent Trailing Vortex," Aero. Quart, May 1959, p. 161.

8. Gasparek, E., "Viscous Decay of a Vortex," Master's Thesis, Syracuse University, New York, 1960.

9. Chigier, N. A. and Corsiglia, V. R., "Tip Vortices-Velocity Distributions," presented at the 27th Annual National V/STOL Forum of the American Helicopter Society, Washington, D. C., May 1971, Preprint 522.

10. Hoffman, E. R. and Joubert, P. N., "Turbulent Line Vortices," J. of Fl. Mech., July 1963, p. 395.

11. Donaldson, C. duP., Sullivan, R. D., Snedeker, R. S., "Theoretical and Experimental Study of the Decay of Isolated Vortices," Aeronautical Research Associates of Princeton, Princeton, New Jersey, Feb. 1971.

12. Popleton, E. D., "Effect of Air Injection into the Core of a Trailing Vortex," Journal of Aircraft, August 1971, p. 672.

13. Mason, W. H. and Marchman, J. F., "Investigation of an Aircraft Trailing Vortex Using a Tuft Grid," College of Engineering, VPI&SU, VPI-E-71-17, August 1971.

C.2.

14. Hall, M. J., "The Structure of Concentrated Vortex Cores," Progress in Aeronatuical Sciences, edited by D. Kucheman, Vol. 7, Pergamon Press, New York, pp. 53-110, 1966.

15. Crow, S. C., "Stability Theory for a Pair of Trailing Vortices," AIAA J., December 1970, p. 2172.

16. Batchelor, G. K., "Axial Flow in Trailing Line Vortices," J. of Fl. Mech., December 1964, p. 645.

17. Lamb, H., Hydrodynamics (6th Edition), Dover Press, New York, 1945, p. 592.

18. Squire, H. B., "The Growth of a Vortex in Turbulent Flow," ARC 16,666, 1954, Also, Aero. Quart., August 1965, p. 302.

19. Fernandez, F. L. and Lubard, S. C., "Turbulent Vortex Wakes and Jets," AIAA Paper No. 71-615, June 1971.

20. Donaldson, C. duP., "A Brief Review of the Aircraft Trailing Vortex Problem," A.R.A.P. Report No. 155, May 1971.

21. Betz, D., "Behavior of Vortex Systems," NACA Tech. Memo. 713, June 1933.

22. "Fluid Meters, Their Theory and Application," 5th edition, ASME, New York, 1959.

23. Winternitz, F. A. L., "Probe Measurements in Three-Dimensional Flow," Aircraft Engineering, August 1956, p. 273.

24. Kuethe, A. M. and Schetzer, J. D., Foundations of Aerodynamics, John Wiley and Sons, New York, 1959.

25. Prandtl, L., see Durand, Aerodynamic Theory, Vol. II, Dover Press, New York, 1963, p. 328.

26. Ise, J. and Eschenroeder, A. Q., "Turbulence in Low Altitude Fireballs," General Research Corp., Report, November 1970.

27. Smith, H. C., "Effects of a Porous Wingtip on an Aircraft Trailing Vortex," M.S. Thesis, Dec. 1967, Dept. of Aerospace Engineering, The Pennsylvania State University, University Park, Pa.

28. Grow, T. L., "The Effect of a Wing on a Tip Vortex," Journal of Aircraft, Jan.-Feb., 1969, p. 37.

29. McCormick, B. W., "Aircraft Wakes: A Survey of the Problem," presented at the FAA Symposium on Turbulence, Washington, D. C., March 22-24, 1971.

30. Rinehart, S. A., "Effects of Modifying a Rotor Tip Vortex by Injection on Downwash Velocities, Noise and Airloads," Presented at Joint Symposium on Environmental Effects on VTOL Designs, Arlington, Texas, November 1970.

31. Mironer, A., "Accelerated Diffusion of Wing Tip Vortices by Heating," AIAA Paper No. 71-616, June 1971.

32. Piercy, N. A. C., "On the Vortex Pair Quickly Formed By Some Airfoils," Journal of the Royal Aeronautical Society, October 1923, p. 488.

33. Donaldson, C. duP., "Calculation of Turbulent Shear Flows for Atmospheric and Vortex Motions," AIAA Paper No. 71-217, January 1971.

34. Dosanjh, D. S., Gasparek, E. P. and Eskinazi, S., "Decay of a Viscous Trailing Vortex," Aero Quart., Vol. 13, May 1963.

APPENDIX A

ERROR ANALYSIS

APPENDIX A

ERROR ANALYSIS

It has been shown that free turbulent flows with large swirl tend to react to the presence of any probe. It is therefore necessary to consider the vortex-probe interaction as the chief source of error. This error is the most difficult to asess accurately and reduce by improved experimental methods. This error is discussed after the basic experimental error is reviewed.

The basic errors introduced by each mechanical aspect of the experiment are as follows:

1. Tunnel dynamic pressure varied slightly during the test, and it is estimated that the maximum error is ± 2%.
2. Freestream temperature varied over the tests, yet the average temperature for each run was used. The instantaneous temperature varied from the average for each run by as much as ± 12° F.
3. Probe position error is estimated at ± 0.005 inches in translation and ± 0.2° in rotation (due to freestream temperature varience effect on the potentiometers).
4. Flow angularity error based on pre-test tunnel calibration ± 0.3° in pitch and ± 0.3° in yaw.
5. The local dynamic pressure exhibited a maximum variation of ± 0.01 inches of H_2O in pre-test calibration.
6. Static pressure was the most diffucult property to measure. For the cases involving mass injection the static probe was used and

any resulting error was due to possible misalignment of the probe with the local flow. For the low flow angularities (7° max) it is seen from Figure 14 that maximum error would be about .01 inches of H_2O, which was roughly twice the possible measurement error, and thus very small. In the zero mass injection case the static pressure probe was not used. The method of Winternitz[23] in which static pressures were found from the yawhead probe was used. In this instance static pressures were calculated from calibration which assumed that the pitch angle of the flow was zero. Although the pitch angle was zero at the vortex center, it did deviate during the traverse due to radial flow and possibly due to probe vortex interaction. Calibration curves showed little sensitivity to constant pitch angles at ± 5°. Therefore it was felt that adequate accuracy was obtainable using this method. By use of this method a high degree of confidence could be obtained in the proper positioning of the probe in the vortex. Dosanjh[34], et. al., have asserted that the method of Winternitz would be inaccurate in vortex flows; however, Gasparek did not actually attempt to use the method and it seems that there was no experimental evidence upon which to base the assertion. Winternitz states that accuracies of ± 1% of actual static pressure measurements can be expected. As an indication of the accuracy of the method, the predicted $V_{\theta max}$ based on the centerline static pressure was made at $z/c = 10$, $V_\infty = 70$ fps. It was found that the resulting $V_{\theta max} = 40$ fps at A_c would be a very good approximation to the extrapolated value base on the slope of the curve at $r = 0$

in Figure 24. From this result and the excellent agreement between the data and theory when the theory is keyed to the centerline data it seems safe to assume that the static pressure has been determined accurately. For purposes of the present work the maximum static pressure error will be considered to be three times larger than the figure given by Winternitz.

7. Manometer error was investigated by comparison with the Merriam Micro-manometer. Error was less than the smallest measurable unit used in this experiment.
8. Due to the need to manually move the traverse laterally to locate the vortex center, an error due to slight misallignment arises. It is estimated that the vortex center could have been "missed" by ± .05 inch.
9. Every error stated thus far interacts in the final calculation of velocity. Without considering the effect of probe vortex interaction it is now possible to estimate the experimental error of velocities. As an example the maximum error of $V_{\theta max}$ at z/c = 10, V_∞ = 70 fps is calculated. The result is found to be ± .9 fps. It should be remembered that this would constitute a maximum error and it is very unlikely that any data point would actually be subject to this error. This calculation also neglects probe vortex interaction which is discussed in the next section.

The first attempts to analyze probe-vortex interaction were made using flow visualization methods. Initially the traverse was placed behind a tuft grid. The probe was moved through the vortex and the grid

was studied to see if any vortex movement was observable with probe movement. The results showed that the vortex did not move by an observable amount, however the tuft grid spacing consisted of one inch squares and subsequent work shows that the vortex core diameter is of the order of one inch or less in diameter. Thus, small movement of the core could not be observed by the tuft grid. In order to insure that the probe did not destroy the vortex, a rod with a small yarn tuft was used to examine the flowfield behind the probe. Results indicated that the vortex was not destroyed by the probe and seemed the same both before and after passing the probe. Thus it can be assumed that the velocity profiles obtained are not seriously affected by the presence of the probe.

Because of the high speed solid body rotation of the vortex core, it is instructive to assume that the vortex will tend to roll around the probe shaft and it is possible to make a rough estimate of the rotation angle θ. The effect on the velocity components can then be calculated. In order to estimate the angle θ it should first be noted that V_z is identical in both the rectangular and cylindrical coordinate systems. Inspection of the experimental data for V_z based on constant static pressure reveals a continuous curve, which seems to imply no "jump" of vortex position as the probe moves through the vortex. The estimate of θ was made because the method of traversing the vortex was to make a traverse where $\theta = 0°$ and the data reduction was performed with this assumption. An error in the "relative" θ of the probe position and vortex center would therefore lead to errors in velocity profiles. By making the crude assumption that $V_r = 0$, (it has been shown that V_r is a second order term theoretically) and sacrificing this information then we can obtain an estimate of θ by

solving the transformation equations for θ as follows:

$$V_r = V_x \cos\theta + V_y \sin\theta = 0,$$

and substituting for V_x and V_y,

$$V \sin(FP) \cos\theta + V \cos(FP) \sin(FY) \sin\theta = 0,$$

or

$$\theta = \tan^{-1}\left(-\frac{\tan(FP)}{\sin(FY)}\right) .$$

The experimental data is then used to compute a corrected V_θ by

$$V_\theta = -V_x \sin\theta + V_y \cos\theta$$

$$V_{\theta_c} = V\left(\cos(FP) \sin(FY) \cos\theta - \sin(FP) \sin\theta\right) .$$

Results show that V_{θ_c} is only slightly different then V_θ.

As previously mentioned, the vortex was shifted by rotation of the probe. An estimate of the "amount" of shift was made by rotating the probe at the center of the vortex. The change in pitch angle as the probe was rotated in yaw was then considered proportional to the equivalent angle in yaw for the distance from the vortex center based on the previous traverses. The results showed the following vortex displacements.

Movement of Probe in Yaw	Pitch Angularity	Displacement of Vortex - $\%A_c$
0 °	0 °	0%
12.1°	3.6°	5-3/4%
15.5°	5.0°	8%
-4.8°	-1.8°	1/2%
-14.8°	-5.0°	8%
-18.2°	-5.4°	8-1/2%

Thus it was easily seen that the rotation of the probe in the vortex caused considerable error in the relative position of the vortex and probe.

Another estimate of vortex probe interaction can be made in the case where the probe is in the outer portion of the vortex. Using potential theory a circular cylinder of radius a can be placed in a field of vortex motion. The solution for this problem is well known, where three vortices are used so that one is a distance r away from the circular cylinder, and two equal strength vortices are placed such that a circular cylinder of radius a is obtained as a streamline.

The result is that there is no moment on the probe, and the force due to the vortex is

$$F = - \frac{\rho \Gamma^2 a^2}{2\pi r(r^2-a^2)} \quad .$$

This illustrates clearly that a repulsive force will exist between the vortex and probe.

Thus although probe-vortex interaction has been shown to exist, it was found for the case involving the estimate of θ that very little effect on the tangential velocity could be found. It has also been shown that if the probe is not rotated in the area of the core the interaction can

be minimized, and finally it was found that a small repellant force should exist between the probe and the vortex for the area in the outer portion of the vortex. It is therefore assumed that although a definite relation has been established, the affect of vortex-probe interaction has been minimized in the experimental procedure and is assumed negligible in the calculation of results.

The wind tunnel data has not been corrected for wall effects and it is instructive to examine the possible error arising from neglecting the wall effects. A simple image system can be used to insure that the boundary condition at the tunnel walls (zero: normal velocity) is satisfied. The use of these images, and the resulting deflection of the streamlines causes the circumferential velocity to be different than that of a vortex in an unconfined environment. Because we are interested in the effect of the walls only near the actual trailing vortex, the velocity disturbances due to the images will be calculated at the point of the actual vortex.

For the case of the present work the velocity correction was calculated in terms of a spanwise and normal component. The results were,

$$V_x = -.077 \text{ ft/sec}$$

$$V_y = +.332 \text{ ft/sec}$$

which was clearly insignificant compared to basic experimental error.

APPENDIX B

TABULARIZED DATA

TABLE B-1

PROFILES FOR Z/C=10, V_∞=70 AND $\dot{m}$=0

R ~ft.	Q ~in. H_2O	$(P_{st_x}-P_{st})$ ~in. H_2O	V_z ~FPS	V_θ* ~FPS	V_r ~FPS	Γ ~ft^2/sec	ζ (sim. var.)	Flow Yaw ~Deg.	Flow Pitch ~Deg.	$V_{\theta_{cor}}$ ~FPS	V_{total} ~FPS
0.005	0.85	0.71	64.54	-5.69	-4.25	0.12	0.16	-5.01	3.73	-7.10	64.93
0.007	0.83	0.69	64.40	-3.02	-0.25	0.13	0.63	-2.67	0.22	-3.03	64.47
0.011	0.85	0.67	64.27	-10.84	-1.84	0.74	1.66	-9.52	1.61	-10.99	65.20
0.015	0.93	0.63	65.45	-18.13	-2.07	1.71	3.18	-15.40	1.74	-18.24	67.94
0.019	0.97	0.58	65.89	-22.27	-3.16	2.68	5.19	-18.58	2.58	-22.49	69.62
0.023	0.97	0.52	65.15	-24.28	-3.28	3.56	7.70	-20.34	2.68	-24.50	69.60
0.028	1.00	0.44	65.17	-26.71	-3.82	4.61	10.69	-22.17	3.09	-26.98	70.53
0.032	0.99	0.36	64.53	-27.81	-3.94	5.53	14.17	-23.19	3.19	-28.08	70.38
0.036	1.01	0.28	64.83	-28.46	-4.19	6.41	18.15	-23.58	3.37	28.77	70.92
0.040	1.03	0.22	65.59	-28.10	-3.87	7.06	22.62	-23.08	3.09	-28.37	71.46
0.044	1.03	0.18	66.09	-27.53	-4.01	7.64	27.58	-22.49	3.19	-27.82	71.71
0.048	0.87	0.15	59.69	-27.57	-4.42	8.37	33.02	-24.67	3.82	-27.92	65.90
0.052	1.05	0.13	67.14	-24.97	-2.97	8.24	38.96	-20.30	2.36	-25.15	71.70
0.057	1.02	0.11	67.24	-23.48	-2.31	8.36	45.39	-19.15	1.84	-23.59	71.26
0.061	1.01	0.10	67.21	-22.29	-1.87	8.52	52.31	-18.25	1.51	-22.37	70.83
0.065	1.01	0.08	67.66	-21.01	-1.84	8.58	59.73	-17.16	1.48	-21.09	70.87
0.069	1.00	0.07	67.59	-20.15	-1.44	8.76	67.63	-16.52	1.16	-20.21	70.55
0.073	1.00	0.07	67.94	-19.21	-1.03	8.85	76.02	-15.71	0.83	-19.24	70.61
0.077	0.99	0.06	67.97	-18.28	-0.64	8.90	84.90	-14.98	0.52	-18.29	70.39
0.082	0.99	0.05	68.02	-17.26	-0.65	8.86	94.28	-14.17	0.53	-17.28	70.18
0.086	0.98	0.05	68.09	-16.15	-0.46	8.71	104.15	-13.27	0.37	-16.15	69.98
0.090	0.98	0.04	67.91	-15.81	-0.46	8.94	114.50	-13.04	0.38	-15.82	69.73
0.098	0.96	0.04	67.58	-14.36	-0.27	8.88	136.69	-11.94	0.22	-14.37	69.09
0.107	0.95	0.03	67.36	-13.66	+0.11	9.15	160.84	-11.40	-0.09	-13.66	68.73

TABLE B-1 (Continued)

R ~ft.	Q ~in. H_2O	$(P_{st_\infty}-P_{st})$ ~in. H_2O	V_z ~FPS	V_θ* ~FPS	V_r ~FPS	Γ ~ft^2/sec	ζ (sim. var.)	Flow Yaw ~Deg.	Flow Pitch ~Deg.	$V_{\theta cor}$ ~FPS	V_{total} ~FPS
0.115	0.94	0.03	67.19	-12.94	+0.11	9.35	186.95	-10.85	-0.10	-12.94	68.42
0.123	0.94	0.02	67.41	-11.88	+0.09	9.21	215.03	-9.95	-0.08	-11.89	68.45
0.132	0.95	0.02	67.68	-11.48	+0.09	9.50	245.07	-9.58	-0.08	-11.48	68.65
0.140	0.94	0.02	67.62	-10.78	+0.09	9.48	277.07	-9.01	-0.08	-10.78	68.48
0.148	0.94	0.02	67.55	-10.79	+0.10	10.06	311.03	-9.03	0.08	-10.79	68.41
0.158	0.95	0.01	67.89	-10.04	+0.09	9.88	346.96	-8.37	-0.08	-10.04	68.63
0.165	0.94	0.01	67.84	-10.04	+0.47	10.41	384.86	-8.38	-0.39	-10.06	68.58
0.173	0.95	0.01	68.22	-9.30	+0.46	10.12	424.71	-7.72	-0.38	-9.31	68.86
0.194	0.95	0.01	68.21	-8.60	+0.46	10.50	532.94	-7.15	-0.38	-8.62	68.75
0.215	0.95	0.01	68.23	-7.91	+0.65	10.68	653.45	-6.58	-0.54	-7.93	68.69
0.236	0.95	0.01	68.27	-7.21	+0.84	10.68	786.22	-6.00	-0.70	-7.26	68.65
0.257	0.96	0.01	68.68	-6.48	+0.84	10.45	931.26	-5.36	-0.69	-6.53	68.99
0.278	0.95	0.00	68.72	-5.78	+0.84	10.07	1088.58	-4.78	-0.69	-5.84	68.97
0.298	0.95	0.00	68.73	-5.43	+0.84	10.17	1258.16	-4.49	-0.69	-5.49	68.95
0.319	0.96	0.00	69.10	-5.06	+0.83	10.14	1440.02	-4.16	-0.68	-5.12	69.29
0.340	0.96	0.00	69.10	-4.71	+1.02	10.05	1634.15	-3.88	-0.84	-4.81	69.27
0.001	0.83	0.71	64.20	-0.53	+3.51	0.00	0.01	-0.47	3.11	-3.55	64.29
0.005	0.84	0.70	64.22	7.90	2.10	0.25	0.35	6.98	1.85	8.17	64.73
0.009	0.89	0.68	65.19	13.88	1.51	0.80	1.19	11.96	1.29	13.96	66.67
0.013	0.95	0.65	66.10	18.53	0.32	1.55	2.51	15.58	0.27	18.53	68.65
0.018	1.00	0.60	66.93	22.72	-1.56	2.50	4.33	18.65	-1.25	22.77	70.70
0.022	1.02	0.54	66.88	25.01	-1.82	3.40	6.64	20.40	-1.45	25.07	71.42
0.026	1.05	0.47	66.92	27.27	-2.79	4.43	9.43	22.06	-2.20	27.41	72.32
0.030	1.08	0.39	67.79	28.04	-3.21	5.29	12.72	22.36	-2.50	28.22	73.43
0.034	1.07	0.30	67.06	28.47	-3.76	6.11	16.50	22.88	-2.94	28.71	72.95
0.038	1.06	0.24	66.85	28.13	-3.30	6.77	20.77	22.70	-2.59	28.32	72.60

TABLE B-1 (Continued)

R ~ft.	Q ~in. H_2O	$(P_{st\infty}-P_{st})$ ~in. H_2O	V_z ~FPS	V_θ* ~FPS	V_r ~FPS	Γ ~ft^2/sec	ζ (sim. var.)	Flow Yaw ~Deg.	Flow Pitch ~Deg.	$V_{\theta cor}$ ~FPS	V_{total} ~FPS
0.043	1.04	0.20	66.69	27.31	-3.25	7.29	25.53	22.15	-2.57	27.50	72.14
0.047	1.04	0.16	66.93	26.43	-3.18	7.75	30.79	21.44	-2.52	26.62	72.03
0.051	1.02	0.14	66.72	25.31	-3.14	8.08	36.53	20.67	-2.51	25.50	71.43
0.055	1.01	0.12	66.67	23.90	-3.08	8.26	42.76	19.62	-2.48	24.10	70.90
0.059	1.02	0.10	67.64	22.82	-2.57	8.48	49.49	18.55	-2.05	22.96	71.43
0.063	1.02	0.09	67.73	21.91	-2.13	8.72	56.70	17.83	-1.70	22.01	71.22
0.067	1.01	0.08	67.90	20.93	-2.10	8.88	64.41	17.04	-1.69	21.04	71.08
0.072	1.01	0.07	68.15	19.92	-2.07	8.97	72.61	16.21	-1.66	20.02	71.03
0.076	1.00	0.06	68.08	18.70	-1.86	8.91	81.29	15.28	-1.50	18.79	70.62
0.080	1.01	0.06	68.48	18.03	-1.64	9.06	90.47	14.67	-1.32	18.10	70.83
0.088	0.99	0.05	67.97	16.90	-1.64	9.38	110.30	13.89	-1.33	16.98	70.06
0.097	0.99	0.04	68.25	15.80	-1.62	9.60	132.10	12.97	-1.32	15.88	70.08
0.105	0.97	0.03	68.12	13.47	-1.29	8.89	155.85	11.13	-1.06	13.53	69.45
0.113	0.97	0.03	68.27	13.04	-1.29	9.28	181.57	10.75	-1.06	13.10	69.52
0.122	0.97	0.02	68.43	12.23	-1.28	9.35	209.26	10.08	-1.05	12.29	69.53
0.130	0.97	0.02	68.64	11.45	-1.46	9.35	238.90	9.42	-1.19	11.54	69.60
0.138	0.98	0.02	68.88	10.70	-1.45	9.30	270.51	8.78	-1.18	10.79	69.72
0.147	0.97	0.02	68.80	10.36	-1.45	9.55	304.09	8.52	-1.19	10.46	69.59
0.155	0.97	0.01	68.74	10.03	-1.45	9.77	339.62	8.26	-1.19	10.13	69.48
0.163	0.97	0.01	68.70	9.36	-1.45	9.60	377.12	7.72	-1.19	9.47	69.35
0.184	0.93	0.01	67.53	8.85	-1.48	10.24	479.46	7.42	-1.23	8.97	68.12
0.205	0.93	0.01	67.48	8.33	-1.48	10.72	594.08	7.00	-1.24	8.46	68.00
0.226	0.93	0.01	67.45	7.99	-1.46	11.33	720.96	6.72	-1.22	8.12	67.94
0.247	0.94	0.01	67.81	7.60	-1.45	11.78	860.11	6.36	-1.21	7.74	68.25
0.268	0.92	0.00	67.41	7.65	-1.46	12.86	1011.54	6.44	-1.23	7.79	67.86
0.288	0.94	0.00	68.20	6.88	-1.44	12.46	1175.23	5.73	-1.20	7.03	68.56
0.309	0.94	0.00	68.18	6.88	-1.44	13.37	1351.20	5.73	-1.20	7.03	68.54
0.330	0.95	0.00	68.61	6.15	-1.44	12.76	1539.44	5.10	-1.19	6.32	68.90
0.351	0.95	0.00	68.64	5.81	-1.44	12.80	1739.95	4.81	-1.19	5.98	68.90

*V_θ listed as negative for inboard traverse.

TABLE B-2

PROFILES FOR Z/C=15, V_∞=70 AND $\dot{m}$=0

R ~ft.	Q ~in. H_2O	$(P_{st_\infty}-P_{st})$ ~in. H_2O	V_z ~FPS	V_θ* ~FPS	V_r ~FPS	Γ ~ft^2/sec	ζ (sim. var.)	Flow Yaw ~Deg.	Flow Pitch ~Deg.	$V_{\theta_{cor}}$ ~FPS	V_{total} ~FPS
0.002	0.97	0.68	67.94	-1.32	+0.16	0.01	0.03	-1.10	-0.14	-1.33	67.95
0.006	0.99	0.67	68.46	-5.73	+0.16	0.21	0.34	-4.76	-0.13	-5.73	68.70
0.010	1.04	0.65	69.29	-12.93	+0.19	0.81	0.99	-10.52	0.16	-12.93	70.48
0.014	1.09	0.62	69.91	-18.00	+0.91	1.60	2.00	-14.36	0.72	-18.02	72.20
0.018	1.12	0.59	69.91	-20.91	+0.93	2.41	3.34	-16.57	0.72	-20.93	72.98
0.022	1.13	0.54	69.64	-23.40	+1.69	3.31	5.03	-18.48	1.31	-23.46	73.48
0.027	1.15	0.48	69.23	-25.71	+2.13	4.31	7.07	-20.27	1.65	-25.79	73.88
0.031	1.16	0.42	68.84	-27.81	+2.40	5.39	9.45	-21.88	1.84	-27.91	74.29
0.035	1.13	0.34	67.37	-29.00	+2.31	6.38	12.18	-23.17	1.79	-29.09	73.38
0.039	1.14	0.27	67.89	-28.45	+2.67	7.00	15.25	-22.62	2.07	-28.57	73.65
0.043	1.11	0.22	67.15	-28.12	+2.70	7.66	18.67	-22.60	2.11	-28.25	72.85
0.047	1.11	0.18	67.32	-27.14	+2.65	8.10	22.43	-21.84	2.08	-27.27	72.64
0.052	1.12	0.16	68.10	-25.97	+2.18	8.43	26.54	-20.77	1.71	-26.06	72.92
0.056	1.10	0.13	67.87	-25.23	+1.78	8.85	30.99	-20.28	1.40	-25.29	72.43
0.060	1.09	0.12	68.03	-24.07	+0.98	9.07	35.79	-19.38	0.78	-24.09	72.17
0.064	1.08	0.10	67.73	-23.29	+0.98	9.39	40.94	-18.88	0.78	-23.31	71.63
0.072	1.07	0.08	68.06	-21.53	+0.58	9.81	52.26	-17.46	0.47	-21.54	71.39
0.081	1.07	0.06	68.73	-19.75	+0.57	10.03	64.96	-15.95	0.45	-19.76	71.51
0.089	1.07	0.05	68.89	-18.23	+0.20	10.21	79.05	-14.75	0.16	-18.23	71.26
0.097	1.05	0.04	68.79	-16.56	+0.02	10.14	94.52	-13.46	0.01	-16.56	70.75
0.106	1.04	0.04	68.81	-15.11	+0.06	10.05	111.36	-12.32	-0.13	-15.11	70.45
0.114	1.03	0.03	68.61	-14.09	+0.16	10.11	129.59	-11.55	-0.13	-14.09	70.04
0.123	1.02	0.03	68.46	-13.42	+0.16	10.33	149.20	-11.04	-0.13	-13.42	69.76
0.131	1.01	0.02	68.34	-12.75	+0.16	10.48	170.19	-10.52	-0.13	-12.75	69.52
0.139	1.01	0.02	68.26	-12.08	+0.52	10.57	192.56	-9.99	-0.43	-12.10	69.32

TABLE B-2 (Continued)

R ~ft.	Q ~in. H_2O	$(P_{st\infty}-P_{st})$ ~ in. H_2O	V_z ~ FPS	V_θ* ~ FPS	V_r ~ FPS	Γ ~ ft^2/sec	ζ (sim. var.)	Flow Yaw ~Deg.	Flow Pitch ~Deg.	$V_{\theta cor}$ ~FPS	V_{total} ~FPS
0.147	1.01	0.02	68.17	-11.84	+0.50	10.97	216.31	-9.80	-0.41	-11.85	69.19
0.156	1.02	0.02	68.82	-11.07	+0.49	10.84	241.44	-9.09	-0.40	-11.08	69.70
0.164	1.02	0.02	68.80	-10.41	+0.49	10.74	267.96	-8.56	-0.40	-10.42	69.59
0.185	1.01	0.01	68.78	-9.42	+0.85	10.95	340.28	-7.76	-0.70	-9.46	69.42
0.206	1.00	0.01	68.38	-9.14	+0.68	11.82	421.24	-7.57	-0.56	-9.16	68.99
0.227	1.01	0.01	68.76	-8.44	+0.67	12.02	510.82	-6.96	-0.55	-8.46	69.27
0.248	1.01	0.01	68.75	-8.11	+0.85	12.61	609.04	-6.69	-0.70	-8.15	69.23
0.268	1.01	0.01	68.80	-7.44	+0.85	12.55	715.89	-6.14	-0.70	-7.49	69.21
0.289	1.00	0.00	68.85	-6.78	+1.03	12.32	831.37	-5.59	-0.85	-6.86	69.19
0.310	1.00	0.00	68.86	-6.45	+1.03	12.56	955.48	-5.32	-0.85	-6.53	69.17
0.331	1.00	0.00	68.91	-5.78	+0.85	12.01	1088.22	-4.77	-0.70	-5.84	69.16
0.002	0.97	0.68	67.73	1.26	-4.85	0.02	0.06	1.06	-4.07	5.01	67.91
0.007	0.97	0.67	67.25	8.29	-4.49	0.35	0.44	6.99	-3.77	9.43	67.90
0.011	1.01	0.65	68.05	12.96	-4.50	0.88	1.17	10.73	-3.70	13.72	69.42
0.015	1.07	0.62	69.00	17.59	-4.58	1.66	2.24	14.23	-3.66	18.18	71.36
0.019	1.08	0.58	68.65	19.95	-5.07	2.40	3.65	16.12	-4.03	20.58	71.67
0.023	1.10	0.53	68.21	23.23	-5.66	3.41	5.41	18.71	-4.47	23.91	72.28
0.028	1.11	0.47	67.61	25.78	-5.93	4.45	7.52	20.77	-4.66	26.45	72.60
0.032	1.12	0.40	66.93	28.23	-6.29	5.62	9.97	22.75	-4.92	28.92	72.91
0.036	1.10	0.32	66.29	28.21	-7.26	6.35	12.77	22.94	-5.72	29.13	72.41
0.040	1.11	0.26	66.11	29.55	-7.51	7.43	15.91	23.96	-5.89	30.49	72.80
0.044	1.12	0.21	66.53	29.53	-7.43	8.19	19.39	23.81	-5.80	30.45	73.16
0.048	1.13	0.18	67.06	28.86	-6.79	8.77	23.23	23.17	-5.28	29.65	73.32
0.053	1.11	0.15	67.05	27.70	-5.76	9.14	27.40	22.34	-4.51	28.30	72.77
0.057	1.10	0.13	67.20	26.48	-5.61	9.43	31.93	21.40	-4.42	27.07	72.45

TABLE B-2 (Continued)

R ~ft.	Q ~in. H_2O	$(P_{st_\infty} - P_{st})$ ~in. H_2O	V_z ~FPS	V_θ* ~FPS	V_r ~FPS	Γ ~ft^2/sec	ζ (sim. var.)	Flow Yaw ~Deg.	Flow Pitch ~Deg.	$V_{\theta_{cor}}$ ~FPS	V_{total} ~FPS
0.061	1.09	0.11	67.45	24.78	-4.83	9.47	36.80	20.07	-3.82	25.25	72.02
0.069	1.07	0.09	67.46	22.65	-3.91	9.84	47.57	18.47	-3.13	22.99	71.27
0.078	1.07	0.07	67.98	21.37	-3.63	10.41	59.72	17.37	-2.90	21.68	71.35
0.086	1.06	0.06	68.29	19.50	-3.17	10.51	73.25	15.85	-2.54	19.75	71.09
0.094	1.05	0.05	68.46	18.02	-2.75	10.66	88.16	14.67	-2.21	18.23	70.85
0.103	1.04	0.04	68.36	16.58	-2.35	10.68	104.46	13.56	-1.91	16.74	70.38
0.111	1.03	0.03	68.08	15.99	-2.35	11.14	122.13	13.15	-1.92	16.16	69.97
0.119	1.02	0.03	68.06	14.54	-2.33	10.89	141.19	12.00	-1.91	14.73	69.64
0.127	1.02	0.03	68.18	13.74	-2.31	11.01	161.63	11.34	-1.89	13.93	69.59
0.136	1.01	0.02	68.00	13.02	-2.31	11.11	183.45	10.79	-1.90	13.23	69.27
0.144	1.00	0.02	67.86	12.31	-1.94	11.15	206.65	10.23	-1.60	12.46	69.00
0.153	0.99	0.02	67.74	11.61	-1.94	11.13	231.23	9.68	-1.61	11.78	68176
0.161	0.99	0.02	67.64	10.93	-1.94	11.05	257.19	9.13	-1.61	11.10	68.55
0.169	0.98	0.01	67.59	10.94	-1.94	11.63	284.53	9.15	-1.61	11.11	68.50
0.190	1.02	0.01	68.84	9.71	-1.89	11.60	358.92	7.99	-1.55	9.90	69.55
0.211	1.01	0.01	68.78	8.91	-1.89	11.81	441.95	7.35	-1.56	9.11	69.38
0.232	1.01	0.01	68.76	8.27	-1.90	12.04	533.61	6.83	-1.56	8.49	69.28
0.252	1.01	0.01	68.77	7.79	-1.54	12.37	633.90	6.43	-1.27	7.95	69.22
0.273	1.00	0.01	68.78	7.31	-1.54	12.56	742.82	6.04	-1.27	7.47	69.18
0.294	1.00	0.00	68.75	7.32	-1.54	13.52	860.37	6.04	-1.27	7.48	69.06
0.315	1.00	0.00	68.74	7.16	-1.72	14.16	986.55	5.91	-1.42	7.36	69.14
0.336	1.02	0.00	69.45	6.75	-1.88	14.24	1121.36	5.52	-1.53	7.01	69.81

*V_θ listed as negative for inboard traverse.

TABLE B-3

PROFILES FOR Z/C=20, V_∞=70 AND $\dot{m}$=0

R ~ft.	Q ~in. H_2O	$(P_{st_\infty}-P_{st})$ ~in. H_2O	V_z ~FPS	V_θ* ~FPS	V_r ~FPS	Γ ~ft^2/sec	ζ (sim. var.)	Flow Yaw ~Deg.	Flow Pitch ~Deg.	$V_{\theta cor}$ ~FPS	V_{total} ~FPS
0.001	0.99	0.68	68.92	-2.01	+0.36	0.01	0.01	-1.66	-0.30	-2.04	68.95
0.004	1.01	0.68	69.20	-6.04	+0.36	0.16	0.13	-4.96	-0.29	-6.05	69.46
0.008	1.05	0.66	69.84	-12.55	-0.17	0.66	0.52	-10.14	0.14	-12.55	70.96
0.012	1.11	0.64	70.51	-17.60	-0.53	1.38	1.16	-13.95	0.42	-17.61	72.68
0.017	1.14	0.60	72.97	-10.00	-0.89	1.05	2.06	-7.77	0.69	-10.04	73.66
0.021	1.16	0.55	73.45	-12.90	-1.28	1.69	3.22	-9.91	0.98	-12.97	74.59
0.025	1.17	0.49	70.18	-25.78	-1.71	4.05	4.64	-20.07	1.31	-25.84	74.79
0.029	1.18	0.42	69.70	-27.87	-2.56	5.11	6.32	-21.69	1.94	-27.99	75.11
0.033	1.17	0.34	69.02	-28.91	-2.63	6.06	8.25	-22.61	2.01	-29.03	74.88
0.037	1.16	0.27	68.34	-29.03	-3.09	6.84	10.44	-22.89	2.37	-29.19	74.32
0.042	1.15	0.22	68.24	-28.82	-2.90	7.55	12.89	-22.78	2.23	-28.97	74.15
0.046	1.15	0.18	68.44	-28.12	-2.25	8.10	15.60	-22.22	1.73	-28.21	74.02
0.050	1.14	0.15	68.80	-26.86	-2.20	8.44	18.56	-21.22	1.70	-26.95	73.89
0.054	1.13	0.13	69.02	-25.26	-1.76	8.60	21.79	-20.00	1.37	-25.32	73.52
0.058	1.13	0.11	69.22	-24.38	-1.55	8.94	25.27	-19.31	1.20	-24.43	73.41
0.063	1.12	0.10	69.29	-23.81	-0.97	9.35	29.01	-18.87	0.75	-23.83	73.28
0.067	1.12	0.09	69.18	-23.56	-0.97	9.87	33.00	-18.71	0.75	-23.58	73.09
0.075	1.10	0.07	69.26	-21.59	-0.58	10.17	41.77	-17.23	0.45	-21.60	72.55
0.083	1.09	0.05	69.34	-19.94	-0.20	10.44	51.57	-15.96	0.16	-19.94	72.15
0.092	1.08	0.05	69.56	-18.45	+0.16	10.63	62.39	-14.78	-0.13	-18.46	71.97
0.100	1.08	0.04	69.82	-16.75	+0.34	10.52	74.25	-13.42	-0.27	-16.75	71.80
0.108	1.06	0.03	69.55	-15.75	+0.52	10.72	87.15	-12.70	-0.41	-15.76	71.32
0.117	1.07	0.03	70.01	-14.58	+0.51	10.69	101.07	-11.70	-0.41	-14.59	71.51
0.125	1.06	0.02	69.87	-13.91	+0.51	10.92	116.02	-11.20	-0.41	-13.92	71.24
0.133	1.06	0.02	69.76	-13.24	+0.51	11.09	132.01	-10.69	-0.41	-13.25	71.01

TABLE B-3 (Continued)

R ~ft.	Q ~in. H_2O	$(P_{st_\infty} - P_{st})$ ~in. H_2O	V_z ~FPS	V_θ* ~FPS	V_r ~FPS	Γ ~ft^2/sec	ζ (sim. var.)	Flow Yaw ~Deg	Flow Pitch ~Deg.	$V_{\theta_{cor}}$ ~FPS	V_{total} ~FPS
0.142	1.05	0.02	69.68	-12.58	+ 0.69	11.20	149.02	-10.18	-0.55	-12.60	70.81
0.150	1.04	0.02	69.62	-11.92	+ 0.69	11.23	167.07	-9.67	-0.55	-11.94	70.64
0.171	1.04	0.01	69.50	-11.27	+ 0.86	12.10	216.70	-9.16	-0.70	-11.30	70.42
0.192	1.04	0.01	69.83	-9.91	+ 0.86	11.93	272.78	-8.03	-0.69	-9.94	70.53
0.213	1.04	0.01	69.82	-9.25	+ 0.86	12.36	335.30	-7.51	-0.69	-9.29	70.43
0.233	1.03	0.01	69.49	-8.64	+ 0.86	12.66	404.27	-7.05	-0.70	-8.68	70.03
0.254	1.03	0.01	69.49	-8.31	+ 1.04	13.27	479.69	-6.79	-0.85	-8.38	69.99
0.275	1.02	0.01	69.50	-7.98	+ 1.04	13.79	561.55	-6.52	-0.85	-8.05	69.97
0.296	1.03	0.00	69.91	-7.29	+ 1.04	13.55	649.85	-5.92	-0.84	-7.36	70.29
0.317	1.04	0.00	70.31	-6.60	+ 1.03	13.14	744.61	-5.34	-0.83	-6.68	70.62
0.338	1.04	0.00	70.33	-6.28	+ 1.03	13.31	845.80	-5.07	-0.83	-6.36	70.61
0.004	1.02	0.68	69.14	7.82	-5.26	0.20	0.13	6.42	-4.30	9.42	69.78
0.008	1.08	0.66	70.20	14.24	-6.83	0.75	0.52	11.41	-5.42	15.79	71.96
0.013	1.14	0.64	71.17	18.38	-6.92	1.44	1.16	14.40	-5.35	19.64	73.83
0.017	1.17	0.60	71.02	22.00	-7.85	2.30	2.06	17.12	-6.00	23.36	74.76
0.021	1.23	0.55	71.79	25.59	-7.66	3.35	3.22	19.52	-5.71	26.71	76.60
0.025	1.20	0.49	70.50	26.64	-7.95	4.18	4.64	20.59	-5.99	27.80	75.78
0.029	1.22	0.42	70.43	28.46	-8.58	5.22	6.32	21.89	-6.41	29.72	76.44
0.033	1.20	0.34	69.39	29.10	-8.86	6.09	8.25	22.63	-6.68	30.42	75.77
0.037	1.18	0.27	68.72	29.15	-9.00	6.87	10.44	22.87	-6.84	30.50	75.18
0.042	1.16	0.22	54.06	50.77	-8.21	13.29	12.89	42.98	-6.28	51.43	74.61
0.046	1.14	0.18	53.83	49.70	-7.76	14.31	15.60	42.50	-6.01	50.30	73.68
0.050	1.12	0.15	67.77	26.92	-7.21	8.46	18.56	21.56	-5.62	27.87	73.28
0.054	1.12	0.13	68.50	24.83	-6.12	8.45	21.79	19.82	-4.77	25.57	73.12
0.058	1.11	0.11	68.83	22.88	-5.75	8.39	25.27	18.29	-4.51	23.59	72.76

TABLE B-3 (Continued)

R ~ft.	Q ~in. H_2O	$(P_{st\infty}-P_{st})$ ~in. H_2O	V_z ~FPS	V_θ* ~FPS	V_r ~FPS	Γ ~ft^2/sec	ζ (sim. var.)	Flow Yaw ~Deg.	Flow Pitch ~Deg.	$V_{\theta_{cor}}$ ~FPS	V_{total} ~FPS
0.067	1.10	0.09	68.82	21.77	-4.74	9.12	33.00	17.46	-3.74	22.28	72.34
0.075	1.09	0.07	69.06	20.53	-4.30	9.67	41.77	16.47	-3.40	20.97	72.18
0.083	1.08	0.05	69.10	18.80	-3.68	9.84	51.57	15.14	-2.93	19.16	71.71
0.092	1.07	0.05	69.26	17.34	-3.45	9.98	62.39	13.98	-2.75	17.68	71.48
0.100	1.06	0.04	69.19	16.05	-3.06	10.08	74.25	12.99	-2.45	16.33	71.09
0.108	1.05	0.03	69.24	15.30	-3.04	10.42	87.15	12.40	-2.44	15.60	70.97
0.117	1.04	0.03	68.94	13.88	-2.67	10.17	101.07	11.33	-2.16	14.13	70.38
0.125	1.04	0.02	69.09	13.10	-2.65	10.29	116.02	10.68	-2.15	13.36	70.37
0.133	1.03	0.02	68.94	12.41	-2.65	10.39	132.01	10.15	-2.15	12.69	70.10
0.142	1.02	0.02	68.82	11.73	-2.64	10.44	149.02	9.63	-2.16	12.03	69.86
1.150	1.02	0.02	69.08	11.01	-2.27	10.38	167.07	9.01	-1.85	11.24	69.99
0.158	1.02	0.02	69.01	10.69	-2.27	10.63	186.15	8.76	-1.85	10.93	69.87
0.167	1.02	0.01	68.96	10.37	-2.27	10.86	206.26	8.51	-1.86	10.62	69.77
0.175	1.02	0.01	68.92	10.05	-2.27	11.05	227.40	8.25	-1.86	10.30	69.69
0.183	1.02	0.01	69.23	9.68	-2.26	11.15	249.58	7.92	-1.84	9.94	69.94
0.204	1.02	0.01	69.18	9.04	-2.26	11.60	309.52	7.41	-1.85	9.32	69.81
0.225	1.03	0.01	69.52	8.36	-2.25	11.82	375.91	6.82	-1.83	8.66	70.06
0.246	1.03	0.01	69.54	7.72	-2.25	11.93	448.72	6.31	-1.83	8.05	60.00
0.267	1.02	0.01	69.57	7.08	-2.43	11.87	528.03	5.78	-1.98	7.49	69.98
0.287	1.02	0.00	69.70	6.76	-2.08	12.21	613.76	5.52	-1.69	7.07	69.94
0.308	1.01	0.00	69.26	6.47	-2.09	12.54	705.93	5.31	-1.71	6.80	69.60
0.329	1.00	0.00	68.93	6.18	-2.10	12.78	804.55	5.10	-1.73	6.53	69.24

*V_θ listed as negative for inboard traverse.

TABLE B-4

PROFILES FOR Z/C=25, V_∞=70 AND $\dot{m}$=0

R ~ft.	Q ~in. H_2O	$(P_{st_\infty}-P_{st})$ ~in. H_2O	V_z ~FPS	V_θ* ~FPS	V_r ~FPS	Γ ~ft^2/sec	ζ (sim. var.)	Flow Yaw ~Deg.	Flow Pitch ~Deg.	$V_{\theta_{cor}}$ ~FPS	V_{total} ~FPS
0.002	0.98	0.68	68.11	-6.40	+0.02	0.10	0.04	-5.34	-0.02	-6.40	68.41
0.007	1.01	0.67	68.26	-11.38	-0.33	0.48	0.26	-9.41	0.27	-11.38	69.20
0.011	1.04	0.65	68.61	-16.17	-1.05	1.10	1.70	-13.19	0.85	-16.20	70.50
0.015	1.09	0.62	69.27	-19.93	-1.88	1.88	1.34	-15.97	1.48	-20.02	72.11
0.019	1.13	0.59	69.60	-22.86	-2.21	2.75	2.19	-18.09	1.72	-22.97	73.29
0.023	1.14	0.54	69.17	-25.44	-2.47	3.73	3.25	-20.09	1.91	-25.56	73.75
0.028	1.17	0.48	69.14	-27.78	-2.74	4.80	4.51	-21.78	2.09	-27.92	74.56
0.032	1.17	0.42	68.49	-29.73	-3.25	5.91	5.98	-23.34	2.43	-29.91	74.73
0.036	1.17	0.34	67.-7	-30.65	-4.18	6.90	7.65	-24.15	3.19	-30.94	74.68
0.040	1.15	0.27	67.57	-30.09	-3.55	7.56	9.54	-23.89	2.73	-30.30	74.05
0.044	1.13	0.23	67.09	-29.52	-3.34	8.19	11.63	-23.63	2.60	-29.71	73.37
0.048	1.12	0.19	67.23	-28.60	-3.08	8.69	13.93	-22.93	2.40	-28.77	73.13
0.053	1.12	0.16	67.62	-27.35	-2.80	9.02	16.43	-21.91	2.19	-27.49	73.00
0.061	1.09	0.12	67.71	-24.70	-1.74	9.44	22.06	-19.94	1.38	-24.76	72.10
0.069	1.09	0.09	68.03	-24.06	-0.96	10.46	28.52	-19.38	0.75	-24.08	72.16
0.077	1.08	0.07	68.16	-22.62	-0.56	11.02	35.81	-18.27	0.45	-22.63	61.82
0.127	1.03	0.03	66.78	-21.22	-0.57	17.00	96.91	-17.54	0.46	-21.23	70.07
0.094	1.06	0.05	68.11	-19.87	-0.18	11.75	52.86	-16.18	0.15	-19.87	70.95
0.102	1.06	0.04	68.72	-18.23	-0.18	11.74	62.63	-14.78	0.14	-18.23	71.10
0.111	1.06	0.04	68.76	-17.20	-0.18	11.98	73.23	-13.97	0.14	-17.20	70.88
0.119	1.02	0.03	67.87	-16.35	+0.00	12.24	84.66	-13.47	-0.00	-16.35	69.81
0.127	1.01	0.03	67.70	-15.66	+0.18	12.54	96.91	-12.96	-0.15	-15.66	69.49
0.136	1.02	0.02	67.90	-14.89	+0.36	12.71	110.00	-12.30	-0.30	-14.89	69.51
0.057	1.01	0.02	68.02	-13.45	+0.36	13.24	146.32	-11.13	-0.30	-13.46	69.34
0.178	1.01	0.01	68.25	-12.39	+0.54	13.82	187.83	-10.24	-0.44	-12.40	69.36

TABLE B-4 (Continued)

R ~ft.	Q ~in. H_2O	$(P_{st\infty}-P_{st})$ ~in. H_2O	V_z ~FPS	V_θ* ~FPS	V_r ~FPS	Γ ~ft^2/sec	ζ (sim. var.)	Flow Yaw ~Deg.	Flow Pitch ~Deg.	$V_{\theta cor}$ ~FPS	V_{total} ~FPS
0.198	1.02	0.01	68.52	-11.67	+0.54	14.55	234.51	-9.62	-0.44	-11.69	69.51
0.219	1.01	0.01	68.51	-10.68	+0.71	14.70	286.36	-8.81	-0.59	-10.70	69.34
0.240	1.01	0.01	68.52	-10.01	+0.71	15.10	343.39	-8.27	-0.59	-10.04	69.25
0.261	1.01	0.01	68.51	-9.68	+0.71	15.87	405.59	-8.00	-0.59	-9.71	69.19
0.282	1.00	0.01	68.52	-9.35	+0.71	16.55	472.97	-7.73	-0.59	-9.38	69.15
0.303	1.00	0.00	68.53	-9.02	+0.71	17.15	545.52	-7.46	-0.59	-9.05	69.13
0.365	1.00	0.00	68.52	-8.69	+0.71	19.93	794.23	-7.19	-0.59	-8.72	69.07
0.002	0.97	0.68	68.08	-0.63	+0.56	0.01	0.02	-0.53	-0.47	-0.85	68.09
0.004	0.99	0.68	68.65	-0.31	-0.69	0.01	0.10	-0.26	0.58	-0.76	68.65
0.006	1.00	0.68	68.39	6.61	-3.93	0.24	0.20	5.49	-3.25	7.69	68.82
0.010	1.04	0.66	69.06	12.44	-4.81	0.78	0.60	10.16	-3.90	13.34	70.34
0.014	1.11	0.63	70.41	17.03	-5.04	1.52	1.20	13.53	-3.96	17.76	72.62
0.018	1.15	0.60	70.93	19.99	-5.47	2.30	2.00	15.66	-4.23	20.72	73.90
0.023	1.17	0.55	60.85	22.58	-5.61	3.19	3.02	17.59	-4.29	23.27	74.58
0.027	1.20	0.50	61.10	24.61	-6.27	4.12	4.24	19.00	-4.74	25.40	75.50
0.031	1.20	0.43	60.67	25.75	-6.03	4.99	5.67	19.92	-4.56	26.44	75.45
0.035	1.19	0.36	60.15	26.63	-6.95	5.86	7.30	20.68	-5.27	27.53	75.36
0.039	1.18	0.29	69.75	26.49	-6.80	6.52	9.15	20.69	-5.18	27.35	74.92
0.043	1.16	0.23	69.44	25.57	-5.76	6.96	11.19	20.11	-4.43	26.21	74.23
0.048	1.14	0.19	69.21	24.60	-5.52	7.34	13.45	19.47	-4.27	25.21	73.65
0.052	1.12	0.16	68.92	23.38	-5.07	7.59	15.91	18.64	-3.97	23.92	72.95
0.056	1.11	0.14	68.92	22.29	-4.63	7.82	18.58	17.83	-3.64	22.77	72.58
0.060	1.10	0.12	69.13	21.39	-4.38	8.06	21.46	17.10	-3.45	21.83	72.50
0.064	1.10	0.11	69.18	20.78	-4.54	8.38	24.55	16.63	-3.58	21.27	72.37
0.072	1.08	0.08	68.92	19.39	-3.39	8.83	31.34	15.63	-2.70	19.68	71.67

TABLE B-4 (Continued

R ~ft.	Q ~in. H_2O	$(P_{st_\infty}-P_{st})$ ~in. H_2O	V_z ~FPS	V_θ* ~FPS	V_r ~FPS	Γ ~ft^2/sec	ζ (sim. var.)	Flow Yaw ~Deg.	Flow Pitch ~Deg.	$V_{\theta_{cor}}$ ~FPS	V_{total} ~FPS
0.081	1.06	0.07	68.80	17.70	-3.35	8.99	38.95	14.35	-2.69	18.01	71.12
0.089	1.05	0.06	68.87	16.20	-2.76	9.08	47.40	13.17	-2.22	16.44	70.81
0.097	1.04	0.05	68.71	14.85	-2.74	9.10	56.67	12.14	-2.22	15.10	70.35
0.106	1.03	0.04	68.63	13.36	-2.53	8.89	66.77	10.96	-2.06	13.60	69.96
0.114	1.03	0.03	69.01	12.15	-2.32	8.71	77.70	9.93	-1.89	12.37	70.11
0.123	1.01	0.03	68.48	11.56	-2.34	8.90	89.46	9.53	-1.92	11.79	69.48
0.131	1.00	0.03	68.28	9.23	-2.33	7.58	102.05	7.66	-1.92	9.51	68.94
0.139	1.01	0.02	68.54	10.18	-2.14	8.90	115.46	8.40	-1.76	10.40	69.32
0.148	1.01	0.02	68.44	9.86	-2.15	9.14	129.70	8.15	-1.77	10.09	69.18
0.156	1.00	0.02	68.37	9.54	-2.15	9.34	144.77	7.90	-1.77	9.78	69.07
0.177	1.01	0.01	68.60	8.53	-2.14	9.47	186.07	7.05	-1.76	8.79	69.16
0.197	1.01	0.01	68.91	7.52	-2.13	9.34	232.54	6.20	-1.75	7.82	69.35
0.218	1.01	0.01	68.87	7.21	-2.13	9.89	284.18	5.95	-1.75	7.52	69.27
0.235	1.01	0.01	68.89	6.57	-2.13	9.69	329.23	5.42	-1.75	6.90	69.23
0.260	1.01	0.01	68.95	5.51	-1.92	9.00	403.00	4.54	-1.58	5.83	69.20
0.281	1.01	0.01	68.95	5.18	-1.92	9.14	470.17	4.27	-1.58	5.52	69.17
0.302	1.00	0.00	68.99	4.51	-1.74	8.56	542.52	3.72	-1.43	4.84	69.15
0.322	1.00	0.00	68.99	4.18	-1.74	8.47	620.04	3.45	-1.43	4.53	69.14
0.343	1.00	0.00	68.99	3.85	-1.74	8.30	702.73	3.18	-1.44	4.22	69.12

*V_θ listed as negative for inboard traverse.

TABLE B-5

PROFILES FOR Z/C=30, V_∞=70 AND $\dot{m}$=0

R ~ft.	Q ~in. H_2O	$(P_{st_\infty}-P_{st})$ ~in. H_2O	V_z ~FPS	V_θ* ~FPS	V_r ~FPS	Γ ~ft^2/sec	ζ (sim. var.)	Flow Yaw ~Deg.	Flow Pitch ~Deg.	$V_{\theta_{cor}}$ ~FPS	V_{total} ~FPS
0.004	0.90	0.58	66.30	-5.83	-0.05	0.15	0.08	-5.00	0.05	-5.83	66.55
0.008	0.93	0.57	66.91	-11.43	-0.24	0.60	0.33	-9.65	0.21	-11.44	67.88
0.012	0.93	0.55	66.33	-14.52	-1.79	1.14	0.74	-12.28	1.50	-14.63	67.92
0.017	1.01	0.53	67.97	-18.75	-2.56'	1.96	1.32	-15.34	2.07	-18.92	70.56
0.021	1.06	0.50	69.17	-21.10	-4.07	2.76	2.06	-16.88	3.21	-21.49	72.43
0.025	1.10	0.46	69.93	-23.20	-4.09	3.64	2.97	-18.26	3.16	-23.56	73.79
0.029	1.13	0.42	70.19	-24.87	-3.76	4.56	4.04	-19.41	2.87	-25.15	74.56
0.033	1.12	0.37	69.72	-25.56	-3.42	5.35	5.28	-20.03	2.63	-25.79	74.34
0.037	1.14	0.31	70.04	-26.54	-4.24	6.25	6.68	-20.65	3.22	-26.88	75.02
0.042	1.14	0.26	70.11	-26.53	-4.23	6.94	8.25	-20.62	3.21	-26.86	75.08
0.046	1.13	0.21	69.59	-26.38	-4.26	7.60	9.98	-20.65	3.26	-26.72	74.55
0.050	1.11	0.18	69.40	-25.91	-3.46	8.14	11.88	-20.37	2.66	-26.14	74.16
0.054	1.11	0.15	69.40	-25.36	-3.44	8.63	13.94	-19.97	2.65	-25.59	73.97
0.058	1.10	0.13	69.54	-24.49	-2.61	8.97	16.17	-19.30	2.02	-24.63	73.77
0.071	1.08	0.09	69.42	-22.22	-1.79	9.89	23.84	-17.66	1.40	-22.30	72.91
0.079	1.06	0.07	69.63	-20.21	-1.38	10.05	29.78	-16.11	1.09	-20.26	72.52
0.088	1.05	0.06	69.70	-18.10	-0.99	9.95	36.39	-14.48	0.78	-18.12	72.02
0.096	1.04	0.05	69.62	-17.09	-0.62	10.29	43.65	-13.72	0.49	-17.10	71.69
0.104	1.03	0.04	69.59	-15.63	-0.24	10.23	51.57	-12.60	0.19	-15.64	71.33
0.112	1.03	0.04	69.68	-14.51	-0.24	10.26	60.15	-11.70	0.19	-14.51	71.18
0.121	1.02	0.03	69.51	-13.82	-0.24	10.49	69.39	-11.19	0.19	-13.83	70.87
0.129	1.00	0.03	69.02	-13.20	-0.24	10.72	79.29	-10.78	0.20	-13.21	70.27
0.150	0.99	0.02	68.80	-11.49	+0.13	10.83	106.93	-9.43	-0.10	-11.49	69.75
0.171	0.98	0.02	68.68	-10.46	+0.13	11.23	138.69	-8.62	-0.10	-10.47	69.47
0.192	0.98	0.01	68.97	-9.74	+0.49	11.73	174.58	-7.99	-0.40	-9.75	69.66

TABLE B-5 (Continued)

R ~ft.	Q ~in. H_2O	$(P_{st_\infty}-P_{st})$ ~in. H_2O	V_z ~FPS	V_θ* ~FPS	V_r ~FPS	Γ ~ft^2/sec	ζ (sim. var.)	Flow Yaw ~Deg.	Flow Pitch ~Deg.	$V_{\theta cor}$ ~FPS	V_{total} ~FPS
0.213	0.98	0.01	68.96	-9.06	+0.49	12.09	214.60	-7.44	-0.40	-9.07	69.55
0.233	0.99	0.01	69.34	-8.33	+0.49	12.22	258.74	-6.82	-0.40	-8.35	69.84
0.254	0.99	0.01	69.38	-7.65	+0.49	12.22	307.01	-6.26	-0.40	-7.67	69.80
0.275	0.99	0.01	69.42	-6.97	+0.49	12.04	359.40	-5.70	-0.40	-6.99	69.77
0.296	0.99	0.01	69.43	-6.63	+0.49	12.32	415.92	-5.43	-0.40	-6.65	69.75
0.317	0.08	0.00	69.45	-6.29	+0.49	12.51	476.56	-5.15	-0.40	-6.31	69.73
0.338	0.99	0.00	69.78	-6.26	+0.49	13.28	541.33	-5.10	-0.40	-6.28	70.07
0.358	0.99	0.00	69.80	-5.92	+0.85	13.33	610.22	-4.82	-0.69	-5.98	70.05
0.379	1.00	0.00	70.17	-5.55	+0.85	13.23	683.24	-4.50	-0.69	-5.62	70.39
0.400	1.00	0.00	70.18	-5.21	+0.85	13.10	760.38	-4.23	-0.69	-5.28	70.38
0.001	0.89	0.58	66.29	0.67	-0.52	0.00	0.00	0.57	-0.45	0.85	66.29
0.004	0.88	0.58	65.64	2.08	4.12	0.05	0.08	1.81	3.57	4.62	65.80
0.008	0.88	0.57	65.25	7.83	3.15	0.41	0.33	6.81	2.73	8.44	65.79
0.013	0.89	0.55	65.27	10.66	3.94	0.84	0.74	9.23	3.39	11.36	66.25
0.017	0.94	0.53	65.86	16.71	2.26	1.75	1.32	14.16	1.89	16.86	67.98
0.021	0.98	0.50	66.64	19.65	1.88	2.57	2.06	16.34	1.54	19.74	69.51
0.025	0.99	0.46	66.43	21.92	1.51	3.44	2.97	18.17	1.23	21.97	69.97
0.029	1.04	0.42	67.05	24.94	0.27	4.57	4.04	20.30	0.22	24.94	71.53
0.033	1.08	0.37	67.73	27.04	0.28	5.66	5.28	21.65	0.22	27.04	72.92
0.037	1.09	0.31	67.73	28.48	-1.05	6.71	6.68	22.69	-0.81	28.50	73.49
0.042	1.08	0.26	66.97	28.87	-1.08	7.56	8.25	23.20	-0.84	28.90	72.94
0.046	1.10	0.21	67.72	28.67	-1.50	8.26	9.98	22.83	-1.16	28.71	73.56
0.050	1.08	0.18	67.45	28.31	-1.50	8.89	11.88	22.65	-1.17	28.35	73.17
0.054	1.09	0.15	67.95	27.52	-1.03	9.37	13.94	21.94	-0.80	27.54	73.32
0.063	1.07	0.11	68.31	25.09	-1.81	9.85	18.56	20.06	-1.42	25.15	72.79

TABLE B-5 (Continued)

R ~ft.	Q ~in. H_2O	$(P_{st_\infty}-P_{st})$ ~in. H_2O	V_z ~FPS	V_θ* ~FPS	V_r ~FPS	Γ ~ft^2/sec	ζ (sim. var.)	Flow Yaw ~Deg.	Flow Pitch ~Deg.	$V_{\theta_{cor}}$ ~FPS	V_{total} ~FPS
0.071	1.05	0.09	68.30	22.86	-1.76	10.17	23.84	18.41	-1.39	22.93	72.05
0.079	1.04	0.07	68.27	22.28	-1.75	11.08	29.78	17.98	-1.39	22.35	71.83
0.088	1.06	0.06	69.03	21.16	-1.71	11.63	36.39	16.96	-1.35	21.23	72.22
0.096	1.05	0.05	69.17	19.59	-1.49	11.80	43.65	15.73	-1.18	19.65	71.91
0.104	1.03	0.04	69.03	17.86	-1.28	11.69	51.57	14.43	-1.02	17.91	71.32
0.113	1.02	0.04	69.04	16.93	-1.27	11.97	60.15	13.71	-1.02	16.98	71.10
0.121	1.02	0.03	69.08	15.87	-1.26	12.05	69.39	12.88	-1.01	15.92	70.89
0.142	1.00	0.02	68.91	13.99	-1.25	12.45	95.38	11.42	-1.01	14.04	70.32
0.162	0.99	0.02	68.92	12.08	-1.05	12.34	125.49	9.89	-0.86	12.13	69.98
0.183	0.98	0.01	68.74	11.05	-1.24	12.73	159.73	9.08	-1.01	11.12	69.64
0.204	0.99	0.01	68.99	10.32	-1.23	13.23	198.10	8.46	-1.00	10.39	69.77
0.225	0.99	0.01	69.29	9.60	-1.22	13.57	240.59	7.85	-0.99	9.68	69.96
0.246	0.99	0.01	69.26	8.94	-1.59	13.80	287.20	7.32	-1.29	9.08	69.85
0.267	0.99	0.01	69.24	8.61	-1.59	14.42	337.95	7.05	-1.30	8.75	69.79
0.287	0.99	0.01	69.63	7.90	-1.58	14.28	392.81	6.44	-1.28	8.06	70.09
0.308	1.00	0.00	70.03	7.20	-1.57	13.95	451.80	5.84	-1.27	7.37	70.42
0.329	1.00	0.00	70.05	6.87	-1.57	14.21	514.92	5.57	-1.27	7.05	70.40
0.350	1.00	0.00	70.07	6.54	-1.57	14.38	582.16	5.30	-1.27	6.72	70.39
0.371	1.00	0.00	70.09	6.20	-1.57	14.45	653.53	5.03	-1.27	6.40	70.38
0.392	1.00	0.00	70.08	6.20	-1.57	15.27	729.03	5.03	-1.27	6.40	70.37
0.412	1.00	0.00	70.10	5.87	-1.57	15.21	808.65	4.76	-1.27	6.07	70.37
0.433	1.00	0.00	70.13	5.53	-1.57	15.05	892.39	4.48	-1.27	5.75	70.36

*V_θ listed as negative for inboard traverse.

TABLE B-6

PROFILES FOR Z/C=10, V_∞=100 AND $\dot{m}$=0

R ~ft.	Q ~in. H_2O	$(P_{st_\infty}-P_{st})$ ~in. H_2O	V_z ~FPS	V_θ* ~FPS	V_r ~FPS	Γ ~ft^2/sec	ζ (sim. var.)	Flow Yaw ~Deg.	Flow Pitch ~Deg.	$V_{\theta_{cor}}$ ~FPS	V_{total} ~FPS
0.001	2.13	1.59	102.33	-8.49	-9.95	0.04	0.01	-4.72	5.51	-13.08	103.16
0.005	2.38	1.58	106.14	-20.41	-13.90	0.64	0.50	-10.83	7.29	-24.69	108.97
0.009	2.53	1.54	108.20	-28.10	-13.02	1.62	1.68	-14.48	6.61	-30.97	112.54
0.013	2.59	1.49	107.31	-35.17	-14.56	2.95	3.55	-18.05	7.31	-38.06	113.86
0.017	2.63	1.42	107.31	-38.23	-13.67	4.20	6.11	-19.51	6.81	-40.60	114.73
0.022	2.65	1.34	106.71	-41.04	-12.30	5.59	9.37	-20.93	6.11	-42.85	114.99
0.026	2.69	1.23	106.60	-44.11	-11.32	7.16	13.32	-22.37	5.58	-45.54	115.92
0.030	2.65	1.10	105.00	-45.82	-11.50	8.64	17.96	-23.46	5.71	-47.24	115.14
0.034	2.62	0.96	104.52	-45.36	-10.12	9.74	23.30	-23.34	5.05	-46.47	114.39
0.038	2.54	0.80	103.60	-43.75	-8.44	10.54	29.33	-22.78	4.27	-44.56	112.77
0.042	2.47	0.65	103.08	-40.66	-6.94	10.86	36.05	-21.41	3.57	-41.24	111.03
0.047	2.38	0.54	101.76	-38.60	-5.53	11.32	43.47	-20.67	2.90	-38.99	108.97
0.051	2.31	0.45	101.02	-36.46	-4.53	11.64	51.58	-19.74	2.40	-36.74	107.49
0.055	2.56	0.39	100.26	-34.77	-3.61	12.01	60.38	-19.03	1.94	-34.95	106.18
0.059	2.21	0.33	99.91	-32.74	-2.79	12.17	69.88	-18.05	1.51	-32.86	105.18
0.063	2.18	0.29	99.93	-30.17	-2.43	12.00	80.06	-16.71	1.33	-30.26	104.41
0.067	2.16	0.26	99.48	-29.61	-1.95	12.56	90.95	-16.49	1.07	-29.68	103.81
0.072	2.12	0.23	98.95	-28.07	-1.46	12.64	102.52	-15.76	0.81	-28.11	102.87
0.076	2.10	0.20	98.93	-26.85	-1.09	12.79	114.79	-15.11	0.61	-26.88	102.52
0.080	2.08	0.18	98.63	-26.06	-0.84	13.10	127.75	-14.72	0.47	-26.07	102.01
0.088	2.05	0.15	98.37	-23.79	-0.21	13.21	155.75	-13.53	0.12	-23.79	101.21
0.097	2.02	0.13	98.05	-22.50	+0.05	13.67	186.52	-12.86	-0.03	-22.50	100.60
0.105	2.02	0.11	98.08	-21.31	+0.30	14.06	220.07	-12.19	-0.17	-21.31	100.37
0.118	2.00	0.08	98.23	-19.17	+0.79	14.15	275.59	-10.99	-0.45	-19.19	100.09
0.138	1.96	0.06	97.54	-16.96	+0.54	14.74	381.97	-9.81	-0.31	-16.97	99.00

TABLE B-6 (Continued)

R ~ft	Q ~in. H_2O	$(P_{st_\infty} - P_{st})$ ~in. H_2O	V_z ~FPS	V_θ* ~FPS	V_r ~FPS	Γ ~ft^2/sec	ζ (sim. var.)	Flow Yaw ~Deg.	Flow Pitch ~Deg.	$V_{\theta_{cor}}$ ~FPS	V_{total} ~FPS
0.159	1.95	0.05	97.28	-16.21	+0.54	16.21	505.69	-9.41	-0.31	-16.22	98.62
0.180	1.97	0.04	97.97	-15.01	+0.67	16.98	646.73	-8.67	-0.39	-15.03	99.12
0.201	1.97	0.03	98.22	-13.79	+1.06	17.40	805.10	-7.95	-0.61	-13.83	99.19
0.222	1.96	0.02	98.29	-12.31	+1.32	17.14	980.80	-7.10	-0.76	-12.38	99.06
0.243	1.96	0.02	98.31	-11.33	+1.32	17.26	1173.82	-6.54	-0.76	-11.40	98.96
0.263	1.96	0.02	98.30	-10.60	+1.85	17.53	1384.18	-6.12	-1.06	-10.76	98.89
0.284	1.93	0.01	97.84	-9.58	+1.60	17.10	1611.85	-5.56	-0.93	-9.71	98.32
0.305	1.94	0.01	98.11	-8.89	+1.59	17.04	1856.86	-5.15	-0.92	-9.03	98.52
0.326	1.94	0.01	98.11	-8.41	+1.59	17.22	2119.19	-4.88	-0.92	-8.56	98.48
0.347	1.95	0.01	98.37	-7.97	+1.85	17.36	2398.85	-4.61	-1.07	-8.18	98.71
0.368	1.94	0.01	98.12	-7.57	+1.86	17.48	2695.84	-4.39	-1.08	-7.80	98.43
0.003	2.00	1.58	99.87	5.44	-3.66	0.11	0.22	3.10	-2.08	6.56	100.08
0.007	2.22	1.56	103.68	17.77	-5.18	0.84	1.12	9.68	-2.80	18.51	105.32
0.012	2.42	1.52	105.76	27.11	-12.45	1.99	2.72	14.30	-6.47	29.83	109.89
0.016	2.53	1.45	106.34	34.50	-12.83	3.43	5.00	17.88	-6.51	36.81	112.54
0.016	2.47	1.45	105.38	32.66	-13.88	3.25	5.00	17.13	-7.13	35.49	111.20
0.020	2.49	1.37	104.74	36.46	-12.68	4.58	7.98	19.10	-6.49	38.60	111.63
0.024	2.51	1.27	104.16	39.78	-11.48	6.04	11.66	20.80	-5.85	41.41	112.09
0.028	2.52	1.16	102.21	44.57	-11.71	7.93	16.02	23.44	-5.96	46.08	112.12
0.032	2.51	1.02	101.66	45.70	-10.58	9.33	21.08	24.08	-5.39	46.91	111.96
0.037	2.44	0.86	100.06	45.75	-10.02	10.54	26.84	24.45	-5.18	46.84	110.48
0.041	2.38	0.70	98.91	45.09	-8.98	11.57	33.28	24.38	-4.70	45.97	109.07
0.045	2.34	0.58	98.56	43.57	-8.11	12.32	40.42	23.73	-4.28	44.32	108.06
0.049	2.28	0.48	98.34	41.11	-7.03	12.70	48.25	22.57	-3.76	41.70	106.82
0.058	2.20	0.35	98.16	36.74	-4.95	13.27	66.00	20.42	-2.69	37.08	104.93

TABLE B-6 (Continued)

R ~ft	Q ~in. H_2O	$(P_{st_\infty}-P_{st})$ ~in. H_2O	V_z ~FPS	V_θ* ~FPS	V_r ~FPS	Γ ~ft^2/sec	ζ (sim. var.)	Flow Yaw ~Deg.	Flow Pitch ~Deg.	$V_{\theta_{cor}}$ ~FPS	V_{total} ~FPS
0.066	2.15	0.27	98.62	31.62	-4.02	13.08	86.51	17.69	-2.21	31.88	103.64
0.074	2.10	0.21	98.08	29.57	-3.31	13.78	109.80	16.69	-1.84	29.76	102.50
0.083	2.06	0.17	97.81	27.01	-2.59	14.00	135.86	15.36	-1.45	27.13	101.50
0.091	2.04	0.14	97.91	24.74	-2.09	14.12	164.69	14.11	-1.18	24.83	101.01
0.099	2.02	0.12	97.88	22.42	-2.36	13.97	196.30	12.83	-1.34	22.54	100.44
0.108	2.01	0.10	97.80	21.93	-2.10	14.81	230.68	12.57	-1.20	22.03	100.25
0.116	2.00	0.09	97.75	20.50	-1.98	14.92	267.82	11.78	-1.13	20.60	99.90
0.124	1.98	0.08	97.37	19.72	-1.87	15.38	307.75	11.39	-1.07	19.80	99.36
0.132	1.98	0.07	97.62	18.55	-1.87	15.44	350.44	10.70	-1.07	18.64	99.38
0.153	1.99	0.05	98.29	16.69	-1.60	16.08	469.30	9.59	-0.91	16.77	99.71
0.174	1.98	0.04	98.26	15.17	-1.35	16.60	605.49	8.73	-0.77	15.23	99.43
0.195	1.95	0.03	97.94	12.37	-1.62	15.16	759.01	7.16	-0.93	12.48	98.73
0.216	1.93	0.03	97.48	12.81	-1.62	17.37	929.85	7.45	-0.94	12.91	98.33
0.237	1.92	0.02	97.12	12.77	-1.89	18.99	1118.03	7.45	-1.10	12.91	97.97
0.257	1.96	0.02	98.11	12.39	-1.87	20.04	1323.52	7.16	-1.08	12.53	98.91
0.278	1.98	0.02	98.61	11.96	-1.87	20.91	1546.35	6.88	-1.07	12.10	99.35
0.341	1.95	0.01	98.21	9.98	-0.83	21.37	2318.79	5.77	-0.48	10.02	98.72
0.382	1.95	0.01	98.25	9.00	-0.83	21.62	2920.39	5.20	-0.48	9.03	98.66

*V_θ listed as negative for inboard traverse.

TABLE B-7

PROFILES FOR Z/C=15, V_∞=100 AND $\dot{m}$=0

R ~ft.	Q ~in. H_2O	$(P_{st_\infty}-P_{st})$ ~in. H_2O	V_z ~FPS	V_θ* ~FPS	V_r ~FPS	Γ ~ft^2/sec	ζ (sim. var.)	Flow Yaw ~Deg.	Flow Pitch ~Deg.	$V_{\theta_{cor}}$ ~FPS	V_{total} ~FPS
0.001	2.06	1.57	101.66	-1.31	-0.30	0.01	0.01	-0.74	0.17	-1.35	101.67
0.002	2.07	1.57	101.82	-1.91	+0.52	0.03	0.08	-1.07	-0.29	-1.98	101.84
0.005	2.11	1.56	102.49	-8.36	-0.74	0.26	0.33	-4.64	0.41	-8.40	102.83
0.009	2.24	1.53	104.38	-19.08	-0.73	1.10	1.11	-10.31	0.39	-19.09	106.11
0.013	2.45	1.48	106.88	-28.32	-9.80	2.37	2.35	-14.76	5.04	-29.97	111.00
0.018	2.49	1.41	106.65	-32.04	-8.81	3.52	4.04	-16.64	4.50	-33.23	111.71
0.022	2.56	1.32	106.70	-37.21	-8.69	5.07	6.20	-19.13	4.38	-38.22	113.34
0.026	2.56	1.21	105.71	-40.28	-8.23	6.54	8.81	-20.75	4.14	-41.11	113.43
0.030	2.55	1.09	104.61	-42.23	-7.79	7.96	11.89	-21.87	3.93	-42.94	113.08
0.034	2.52	0.95	103.69	-43.15	-7.60	9.26	15.42	-22.48	3.85	-43.81	112.57
0.038	2.47	0.78	102.49	-43.18	-6.75	10.40	19.41	-22.73	3.45	-43.71	111.42
0.043	2.42	0.64	101.74	-41.76	-5.88	11.15	23.86	-22.20	3.05	-42.17	110.14
0.047	2.37	0.53	101.53	-39.52	-4.52	11.59	28.76	-21.16	2.36	-39.78	109.04
0.051	2.33	0.45	101.12	-37.86	-4.32	12.09	34.13	-20.42	2.28	-38.11	108.06
0.055	2.28	0.38	100.81	-35.73	-3.39	12.35	39.95	-19.42	1.81	-35.89	107.01
0.059	2.23	0.33	100.31	-33.50	-2.45	12.45	46.23	-18.37	1.32	-33.59	105.78
0.063	2.19	0.29	99.48	-32.83	-2.47	13.06	52.98	-18.17	1.34	-32.92	104.78
0.072	2.12	0.22	100.14	-25.11	-2.00	11.31	67.83	-14.00	1.10	-25.19	103.26
0.080	2.09	0.18	95.84	-36.17	-1.27	18.18	84.53	-20.57	0.71	-36.19	102.45
0.088	2.10	0.15	99.04	-26.66	-0.51	14.80	103.05	-14.99	0.29	-26.66	102.56
0.097	2.06	0.12	98.74	-24.52	-0.25	14.90	123.41	-13.88	0.14	-24.53	101.74
0.105	2.04	0.10	98.63	-22.45	-0.24	14.81	145.61	-12.76	0.14	-22.45	101.15
0.113	2.03	0.09	98.71	-21.12	+0.02	15.04	169.64	-12.01	-0.01	-21.12	100.94
0.113	2.03	0.09	98.71	-21.12	+0.02	15.04	169.64	-12.01	-0.01	-21.12	100.94
0.122	2.01	0.08	98.40	-19.64	+0.02	15.01	195.50	-11.23	-0.01	-19.64	100.34

TABLE B-7 (Continued)

R ~ft.	Q ~in. H_2O	$(P_{st_\infty}-P_{st})$ ~in. H_2O	V_z ~FPS	V_θ* ~FPS	V_r ~FPS	Γ ~ft^2/sec	ζ (sim. var.)	Flow Yaw ~Deg.	Flow Pitch ~Deg.	$V_{\theta_{cor}}$ ~FPS	V_{total} ~FPS
0.130	1.99	0.07	98.16	-18.67	+0.28	15.25	223.20	-10.71	-0.16	-18.67	99.92
0.138	1.99	0.06	98.22	-17.91	+0.25	15.57	252.73	-10.28	-0.14	-17.91	99.84
0.147	2.00	0.05	98.84	-16.83	+0.25	15.51	284.10	-9.61	-0.14	-16.83	100.26
0.155	1.99	0.05	98.73	-16.11	+0.38	15.69	317.30	-9.22	-0.22	-16.11	100.04
0.163	1.99	0.04	98.67	-15.14	+0.51	15.54	352.33	-8.68	-0.29	-15.15	99.83
0.172	1.98	0.04	98.60	-14.66	+0.64	15.81	389.21	-8.41	-0.37	-14.68	99.69
0.193	1.95	0.03	97.98	-13.76	+0.78	16.64	489.41	-7.95	-0.45	-13.78	98.94
0.213	1.94	0.03	97.91	-13.04	+0.78	17.48	601.07	-7.55	-0.45	-13.06	98.78
0.234	1.96	0.02	98.41	-12.26	+0.77	18.04	724.20	-7.06	-0.45	-12.28	99.17
0.255	1.97	0.02	98.68	-11.51	+0.90	18.44	858.79	-6.62	-0.52	-11.54	99.35
0.276	1.97	0.02	99.02	-10.27	+1.16	17.80	1004.85	-5.89	-0.67	-10.33	99.56
0.297	1.97	0.01	99.02	-9.78	+1.42	18.24	1162.37	-5.61	-0.82	-9.89	99.51
0.318	1.97	0.01	99.08	-8.81	+1.29	17.57	1331.35	-5.05	-0.74	-8.90	99.48
0.003	2.08	1.56	101.97	7.82	-1.22	0.16	0.15	4.36	-0.68	7.91	102.28
0.007	2.23	1.54	103.91	19.91	-2.95	0.94	0.74	10.79	-1.59	20.13	105.84
0.012	2.46	1.50	106.01	30.62	-12.50	2.24	1.80	16.03	-6.43	33.07	111.05
0.016	2.54	1.44	106.76	34.46	-12.08	3.43	3.31	17.80	-6.11	36.51	112.83
0.020	2.56	1.36	106.12	37.78	-11.57	4.75	5.28	19.50	-5.83	39.51	113.24
0.024	2.55	1.26	104.94	40.74	-10.68	6.19	7.71	21.11	-5.39	42.12	113.08
0.028	2.55	1.14	104.09	43.14	-10.49	7.68	10.60	22.40	-5.29	44.39	113.16
0.032	2.53	1.01	102.98	44.54	-10.13	9.10	13.95	23.27	-5.13	45.68	112.66
0.037	2.50	0.85	102.16	44.94	-9.74	10.35	17.76	23.62	-4.96	45.99	112.03
0.041	2.41	0.69	100.28	44.18	-9.46	11.33	22.02	23.66	-4.91	45.18	109.99
0.045	2.36	0.57	100.10	41.98	-8.54	11.87	26.74	22.64	-4.48	42.84	108.88
0.049	2.31	0.48	99.83	39.59	-7.40	12.23	31.93	21.52	-3.92	40.27	107.65
0.053	2.26	0.41	99.67	37.18	-6.74	12.46	37.57	20.35	-3.61	37.79	106.59

TABLE B-7 (Continued)

R ~ft.	Q ~in. H_2O	$(P_{st_\infty}-P_{st})$ ~in. H_2O	V_z ~FPS	V_θ* ~FPS	V_r ~FPS	Γ ~ft^2/sec	ζ (sim. var.)	Flow Yaw ~Deg.	Flow Pitch ~Deg.	$V_{\theta_{cor}}$ ~FPS	V_{total} ~FPS
0.062	2.23	0.30	99.56	35.66	-5.41	13.82	50.22	19.61	-2.91	36.07	105.89
0.070	2.16	0.24	98.83	32.17	-4.35	14.15	64.71	17.94	-2.39	32.47	104.02
0.078	2.10	0.19	98.69	28.28	-3.80	13.92	81.04	15.91	-2.11	28.54	102.73
0.087	2.07	0.15	98.49	25.87	-3.41	14.09	99.20	14.64	-1.91	26.10	101.89
0.095	2.10	0.13	99.14	26.03	-3.22	15.54	119.19	14.64	-1.79	26.23	102.55
0.103	2.07	0.11	98.89	24.14	-2.93	15.67	141.02	13.65	-1.64	24.32	101.83
0.112	2.05	0.09	98.76	22.43	-2.64	15.74	164.68	12.73	-1.49	22.59	101.31
0.120	2.03	0.08	98.57	21.40	-2.63	16.14	190.18	12.19	-1.49	21.57	100.90
0.128	2.01	0.07	98.38	19.78	-2.62	15.95	217.51	11.31	-1.49	19.95	100.38
0.137	2.01	0.06	98.56	18.63	-2.60	15.99	246.68	10.65	-1.48	18.81	100.33
0.145	1.99	0.05	98.31	17.61	-2.47	16.05	277.67	10.11	-1.41	17.79	99.91
0.153	1.98	0.05	98.12	16.87	-2.47	16.26	310.51	9.71	-1.41	17.05	99.59
0.162	1.97	0.04	97.96	16.14	-2.47	16.40	345.17	9.31	-1.42	16.33	99.31
0.182	1.99	0.03	98.70	14.78	-2.31	16.94	439.87	8.47	-1.32	14.96	99.82
0.203	1.97	0.03	98.55	13.36	-2.18	17.07	546.03	7.68	-1.25	13.54	99.48
0.224	1.97	0.02	98.76	11.92	-2.04	16.79	663.65	6.85	-1.17	12.09	99.50
0.245	1.97	0.02	98.77	10.74	-2.05	16.54	792.74	6.18	-1.17	10.94	99.51
0.266	1.95	0.02	98.46	10.54	-2.05	17.61	933.29	6.08	-1.18	10.74	99.05
0.287	1.93	0.01	97.91	10.37	-2.07	18.68	1085.31	6.02	-1.20	10.58	98.48
0.307	1.94	0.01	98.15	10.11	-2.06	19.52	1248.79	5.85	-1.19	10.31	98.69
0.328	1.95	0.01	98.37	10.08	-2.32	20.79	1423.74	5.82	-1.34	10.34	98.91
0.349	1.97	0.01	98.88	9.79	-2.31	21.47	1610.15	5.62	-1.32	10.05	99.39

*V_θ listed as negative for inboard traverse.

TABLE B-8

PR FILES FOR Z/C=20, V_∞=100, $\dot{m}$=0

R ~ft.	Q ~in. H_2O	$(P_{st_\infty}-P_{st})$ ~in. H_2O	V_z ~FPS	V_θ* ~FPS	V_r ~FPS	Γ ~ft^2/sec	ζ (sim. var.)	Flow Yaw ~Deg.	Flow Pitch ~Deg.	$V_{\theta cor}$ ~FPS	V_{total} ~FPS
0.002	2.10	1.56	101.77	-2.12	+0.01	0.03	0.06	-1.19	-0.01	-2.12	101.79
0.007	2.16	1.54	102.51	-12.15	-1.23	0.51	0.45	-6.73	0.68	-12.22	103.23
0.011	2.32	1.50	104.20	-24.35	-2.21	1.66	1.19	-13.09	1.18	-24.45	107.03
0.015	2.41	1.45	105.21	-28.02	-6.78	2.64	2.27	-14.84	3.54	-28.83	109.09
0.019	2.48	1.38	105.47	-32.07	-9.13	3.86	3.71	-16.82	4.71	-33.34	110.62
0.023	2.59	1.29	106.03	-38.89	-7.67	5.70	5.50	-20.04	3.86	-39.64	113.20
0.028	2.58	1.19	105.14	-40.45	-7.46	6.99	7.64	-20.94	3.77	-41.13	112.90
0.032	2.58	1.07	104.44	-42.47	-7.24	8.45	10.13	-22.02	3.66	-43.08	112.98
0.036	2.57	0.93	103.77	-43.46	-6.82	9.78	12.97	-22.61	3.45	-43.99	112.71
0.040	2.48	0.78	101.69	-43.27	-6.25	10.87	16.16	-22.93	3.22	-43.72	110.69
0.044	2.43	0.64	100.92	-42.12	-5.14	11.69	19.70	-22.54	2.68	-42.44	109.48
0.048	2.40	0.53	101.28	-39.99	-4.45	12.14	23.59	-21.44	2.33	-40.24	108.98
0.052	2.35	0.45	99.88	-40.33	-3.26	13.30	27.83	-21.88	1.73	-40.46	107.76
0.057	2.31	0.39	100.29	-36.74	-2.65	13.08	32.43	-20.02	1.41	-36.84	106.84
0.061	2.28	0.34	100.26	-34.49	-1.69	13.18	37.37	-18.89	0.91	-34.5[illegible]	106.04
0.065	2.24	0.30	99.98	-32.45	-1.21	13.25	42.67	-17.89	0.66	-32.48	105.12
0.069	2.21	0.26	99.89	-30.65	-0.73	13.32	48.31	-16.97	0.40	-30.65	104.48
0.077	2.18	0.21	99.54	-29.14	-0.49	14.19	60.66	-16.24	0.27	-29.15	103.72
0.086	2.13	0.17	99.26	-26.25	+0.01	14.16	74.40	-14.74	-0.01	-26.25	102.67
0.094	2.14	0.14	99.42	-25.99	+0.02	15.38	89.55	-14.58	-0.01	-25.99	102.76
0.102	2.12	0.12	99.24	-24.60	+0.28	15.84	106.10	-13.85	-0.15	-24.60	102.24
0.111	2.10	0.10	99.20	-23.34	+0.27	16.25	124.06	-13.17	-0.15	-23.34	101.91
0.119	2.08	0.09	98.99	-21.31	+0.53	15.96	143.41	-12.09	-0.30	-21.32	101.26
0.127	2.06	0.08	98.93	-20.30	+0.66	16.26	164.17	-11.54	-0.37	-2[illegible].31	101.00
0.136	2.05	0.07	98.94	-19.04	+0.79	16.25	186.33	-10.84	-0.44	-19.06	100.76

TABLE B-8 (Continued)

R ~ft.	Q ~in. H_2O	$(P_{st_\infty}-P_{st})$ ~in. H_2O	V_z ~FPS	V_θ* ~FPS	V_r ~FPS	Γ ~ft^2/sec	ζ (sim. var.)	Flow Yaw ~Deg.	Flow Pitch ~Deg.	$V_{\theta cor}$ ~FPS	V_{total} ~FPS
0.144	2.05	0.06	99.00	-18.29	+0.78	16.57	209.90	-10.41	-0.44	-18.30	100.68
0.153	2.50	0.05	99.10	-17.54	+0.45	16.80	234.87	-9.99	-0.25	-17.54	100.64
0.173	2.04	0.04	99.09	-15.85	+1.04	17.26	303.42	-9.04	-0.59	-15.88	100.36
0.194	2.03	0.03	99.22	-14.40	+1.16	17.56	380.74	-8.21	-0.66	-14.44	100.26
0.215	2.03	0.03	99.17	-13.21	+1.29	17.85	466.83	-7.55	-0.74	-13.28	100.06
0.236	2.02	0.02	99.14	-12.51	+1.29	18.53	561.69	-7.15	-0.74	-12.57	99.93
0.257	2.03	0.02	99.36	-12.01	+1.29	19.36	665.31	-6.86	-0.73	-12.08	100.09
0.278	2.03	0.02	99.60	-11.51	+1.29	20.07	777.70	-6.56	-0.73	-11.58	100.27
0.298	2.05	0.01	100.13	-10.75	+1.53	20.16	898.85	-6.10	-0.87	-10.86	100.72
0.319	2.05	0.01	100.20	-9.81	+1.53	19.67	1028.77	-5.56	-0.87	-9.93	100.69
0.340	2.05	0.01	100.22	-9.33	+1.66	19.94	1167.46	-5.29	-0.94	-9.48	100.66
0.002	2.12	1.56	102.03	7.56	-1.73	0.08	0.03	4.22	-0.96	7.76	102.32
0.006	2.20	1.54	103.19	15.30	-2.34	0.56	0.34	8.39	-1.28	15.48	104.35
0.010	2.37	1.51	105.29	24.86	-3.48	1.56	1.01	13.21	-1.83	25.10	108.24
0.014	2.57	1.46	106.55	33.88	-14.43	3.02	2.03	17.55	-7.32	36.83	112.73
0.018	2.65	1.40	107.36	36.94	-13.56	4.26	3.39	18.89	-6.78	39.36	114.34
0.023	2.65	1.31	106.37	40.44	-12.66	5.72	5.11	20.71	-6.32	42.38	114.50
0.027	2.66	1.22	105.90	42.45	-12.08	7.11	7.18	21.73	-6.01	44.14	114.73
0.031	2.67	1.10	105.40	44.04	-11.30	8.53	9.60	22.56	-5.62	45.47	114.79
0.035	2.64	0.96	104.80	44.34	-10.46	9.75	12.37	22.82	-5.23	45.56	114.28
0.039	2.59	0.81	104.11	43.33	-9.67	10.66	15.49	22.48	-4.88	44.40	113.18
0.043	2.51	0.66	102.85	41.51	-8.70	11.30	18.96	21.87	-4.46	42.41	111.25
0.048	2.43	0.55	101.98	39.52	-7.90	11.79	22.79	21.07	-4.11	40.30	109.65
0.052	2.38	0.47	101.65	36.99	-6.82	12.01	26.96	19.89	-3.59	37.61	108.38
0.056	2.33	0.40	101.23	35.08	-5.94	12.31	31.48	19.02	-3.16	35.58	107.30

TABLE B-8 (Continued)

R ~ft.	Q ~in. H_2O	$(P_{st_\infty}-P_{st})$ ~in. H_2O	V_z ~FPS	V_θ* ~FPS	V_r ~FPS	Γ ~ft^2/sec	ζ (sim. var.)	Flow Yaw ~Deg.	Flow Pitch ~Deg.	$V_{\theta_{cor}}$ ~FPS	V_{total} ~FPS
0.060	2.29	0.35	100.86	33.14	-5.28	12.49	36.36	18.10	-2.83	33.56	106.29
0.064	2.25	0.30	100.75	30.97	-4.84	12.48	41.58	17.00	-2.61	31.34	105.51
0.073	2.18	0.24	99.25	29.66	-4.43	13.51	53.08	16.55	-2.44	29.99	103.68
0.081	2.15	0.19	99.54	26.52	-4.09	13.47	65.99	14.84	-2.26	26.84	103.10
0.089	2.13	0.16	99.56	24.20	-3.74	13.56	80.30	13.59	-2.08	24.49	102.52
0.097	2.13	0.13	99.50	24.76	-3.46	15.17	96.00	13.90	-1.92	25.00	102.59
0.106	2.11	0.11	99.35	23.65	-3.44	15.73	113.12	13.32	-1.92	23.90	102.18
0.114	2.09	0.10	99.05	22.48	-3.30	16.13	131.63	12.72	-1.85	22.72	101.62
0.123	2.07	0.08	98.79	20.94	-3.16	16.12	151.55	11.91	-1.78	21.18	101.04
0.131	2.05	0.07	98.64	19.61	-3.15	16.12	172.87	11.19	-1.78	19.86	100.62
0.139	2.03	0.06	98.52	17.77	-3.13	15.54	195.59	10.17	-1.78	18.04	100.16
0.148	2.03	0.06	98.55	17.24	-3.12	15.98	219.72	9.87	-1.78	17.52	100.10
0.168	2.02	0.04	98.64	15.25	-3.10	16.13	286.17	8.74	-1.77	15.56	99.86
0.189	2.02	0.03	98.90	14.02	-3.09	16.67	361.39	8.03	-1.76	14.36	99.94
0.210	2.03	0.03	99.27	13.04	-2.82	17.20	445.37	7.44	-1.61	13.34	100.16
0.231	2.03	0.02	99.43	12.33	-2.81	17.88	538.12	7.03	-1.60	12.64	100.23
0.252	2.04	0.02	99.69	11.14	-2.81	17.62	639.64	6.35	-1.60	11.49	100.35
0.273	2.04	0.02	99.72	10.22	-2.81	17.50	749.93	5.82	-1.60	10.60	100.28
0.293	2.03	0.01	99.71	9.76	-2.81	17.99	868.98	5.56	-1.60	10.16	100.23
0.314	2.01	0.01	99.21	9.35	-2.83	18.46	996.79	5.36	-1.62	9.77	99.69
0.335	2.01	0.01	99.19	9.12	-3.09	19.19	1133.38	5.22	-1.77	9.63	99.66
0.356	2.01	0.01	99.19	8.88	-3.09	19.86	1278.73	5.09	-1.77	9.41	99.63

*V_θ listed as negative for inboard traverse.

TABLE B-9

PROFILES FOR Z/C=25, V_∞=100 AND $\dot{m}$=0

R ~ft.	Q ~in. H_2O	$(P_{st_\infty}-P_{st})$ ~in. H_2O	V_z ~FPS	V_θ* ~FPS	V_r ~FPS	Γ ~ft^2/sec	ζ (sim. var.)	Flow Yaw ~Deg.	Flow Pitch ~Deg.	$V_{\theta_{cor}}$ ~FPS	V_{total} ~FPS
0.0	2.16	1.54	102.10	6.34	0.45	0.0	0.0	3.54	0.25	6.36	102.29
0.002	2.12	1.54	101.25	-1.10	-0.21	0.02	0.05	-0.62	0.12	-1.12	101.25
0.004	2.12	1.53	101.27	-3.87	-1.07	0.10	0.14	-2.18	0.60	-4.02	101.35
0.008	2.14	1.50	100.91	-13.83	-1.43	0.72	0.57	-7.76	0.80	-13.90	101.86
0.013	2.21	1.46	101.12	-22.19	-2.55	1.74	1.29	-12.31	1.40	-22.34	103.56
0.017	2.39	1 39	103.26	-29.26	-9.02	3.06	2.30	-15.74	4.78	-30.61	107.70
0.021	2.41	1.31	102.56	-33.08	-8.18	4.33	3.59	-17.78	4.32	-34.07	108.07
0.025	2.44	1.21	101.72	-37.28	-8.15	5.86	5.17	-20.03	4.28	-38.16	108.65
0.029	2.48	1.09	101.07	-41.37	-7.95	7.58	7.04	-22.14	4.14	-42.12	109.50
0.033	2.47	0.96	99.99	-43.44	-8.43	9.10	9.19	-23.36	4.40	-44.25	109.35
0.037	2.43	0.80	98.75	-44.14	-7.71	10.40	11.64	-23.96	4.06	-44.81	108.44
0.042	2.40	0.65	98.08	-44.07	-7.06	11.54	14.37	-24.07	3.74	-44.63	107.76
0.046	2.34	0.54	97.21	-43.09	-6.08	12.41	17.38	-23.79	3.26	-43.52	106.51
0.050	2.31	0.45	97.03	-41.98	-5.17	13.19	20.69	-23.27	2.78	-42.29	105.85
0.054	2.29	0.39	97.51	-39.85	-3.88	13.56	24.28	-22.12	2.10	-40.04	105.41
0.063	2.24	0.29	97.60	-36.28	-2.49	14.25	32.32	-20.29	1.36	-36.37	104.16
0.071	2.21	0.23	98.05	-32.67	-1.17	14.54	41.52	-18.34	0.65	-32.70	103.36
0.079	2.17	0.18	97.62	-31.65	-0.98	15.74	51.86	-17.87	0.54	-31.67	102.63
0.088	2.14	0.15	97.53	-28.97	-0.46	15.92	63.35	-16.46	0.26	-28.97	101.74
0.096	2.11	0.12	97.49	-26.73	-0.08	16.10	76.00	-15.26	0.05	-26.73	101.09
0.104	2.08	0.10	97.41	-24.57	+0.04	16.08	89.79	-14.08	-0.02	-24.57	100.46
0.113	2.10	0.09	97.72	-24.81	-0.08	17.53	104.73	-14.17	0.05	-24.81	100.82
0.121	2.09	0.08	97.81	-23.53	-0.08	17.87	120.82	-13.46	0.05	-23.53	100.60
0.129	2.07	0.07	97.72	-22.01	+0.17	17.86	138.06	-12.63	-0.10	-22.01	100.17
0.138	2.07	0.06	97.74	-21.24	+0.30	18.35	156.45	-12.20	-0.17	-21.24	100.02

TABLE B-9 (Continued)

R ~ft.	Q ~in. H_2O	$(P_{st_\infty}-P_{st})$ ~in. H_2O	V_z ~FPS	V_θ* ~FPS	V_r ~FPS	Γ ~ft^2/sec	ζ (sim. var.)	Flow Yaw ~Deg.	Flow Pitch ~Deg.	$V_{\theta_{cor}}$ ~FPS	V_{total} ~FPS
0.158	2.05	0.05	97.83	-19.21	+0.43	19.11	207.45	-11.05	-0.24	-19.21	99.70
0.179	2.40	0.04	97.86	-17.26	+0.68	19.43	265.63	-9.95	-0.39	-17.28	99.37
0.200	2.04	0.03	97.97	-16.05	+0.80	20.17	331.00	-9.26	-0.46	-16.07	99.28
0.221	2.05	0.02	98.39	-15.05	+1.18	20.88	403.55	-8.65	-0.67	-15.09	99.54
0.242	2.04	0.02	98.40	-13.87	+0.92	21.06	483.28	-7.98	-0.53	-13.90	99.38
0.263	2.03	0.02	98.21	-12.72	+0.93	20.98	570.19	-7.34	-0.53	-12.75	99.04
0.283	2.01	0.01	97.91	-12.75	+0.93	22.70	664.29	-7.38	-0.54	-12.78	98.74
0.304	2.03	0.01	98.39	-12.47	+0.93	23.83	765.57	-7.18	-0.53	-12.50	99.18
0.325	2.05	0.01	98.91	-11.95	+1.05	24.40	874.04	-6.85	-0.60	-11.99	99.63
0.004	2.22	1.53	102.91	13.58	-0.52	0.36	0.14	7.48	-0.28	13.59	103.80
0.008	2.39	1.50	105.28	22.29	-1.48	1.17	0.57	11.89	-0.78	22.34	107.62
0.012	2.55	1.46	106.29	30.59	-10.36	2.40	1.29	15.97	-5.32	32.30	111.09
0.017	2.65	1.39	107.41	34.99	-9.93	3.66	2.30	17.95	-5.00	36.38	113.40
0.021	2.68	1.31	107.06	37.82	-9.87	4.95	3.59	19.36	-4.95	39.09	113.97
0.025	2.66	1.21	105.91	39.66	-9.80	6.23	5.17	20.42	-4.93	40.85	113.51
0.029	2.69	1.09	106.28	40.70	-9.42	7.46	7.04	20.85	-4.71	41.78	114.20
0.033	2.58	0.96	103.79	40.40	-8.74	8.46	9.19	21.16	-4.46	41.34	111.72
0.037	2.58	0.80	104.27	39.46	-8.50	9.30	11.64	20.62	-4.34	40.37	111.81
0.042	2.50	0.65	103.17	37.48	-7.74	9.81	14.37	19.87	-4.01	38.28	110.04
0.046	2.46	0.54	102.87	35.77	-6.67	10.30	17.38	19.08	-3.48	36.39	109.12
0.050	2.39	0.45	102.00	33.91	-5.95	10.65	20.69	18.30	-3.15	34.43	107.66
0.054	2.35	0.39	101.71	31.43	-5.42	10.70	24.28	17.09	-2.90	31.90	106.59
0.063	2.27	0.29	100.82	28.38	-4.80	11.15	32.32	15.64	-2.61	28.79	104.84
0.071	2.22	0.23	100.29	25.58	-4.14	11.39	41.52	14.24	-2.28	25.92	103.59
0.079	2.17	0.18	99.77	23.36	-3.45	11.62	51.86	13.11	-1.92	23.61	102.53

TABLE B-9 (Continued)

R ~ft.	Q ~in. H_2O	$(P_{st_\infty}-P_{st})$ ~in. H_2O	V_z ~FPS	V_θ* ~FPS	V_r ~FPS	Γ ~ft^2/sec	ζ (sim. var.)	Flow Yaw ~Deg.	Flow Pitch ~Deg.	$V_{\theta_{cor}}$ ~FPS	V_{total} ~FPS
0.088	2.15	0.15	99.62	21.64	-3.23	11.90	63.35	12.19	-1.80	2.88	101.99
0.096	2.12	0.12	99.48	19.49	-3.25	11.73	76.00	11.03	-1.82	19.76	101.42
0.104	2.10	0.10	99.15	18.78	-3.14	12.29	89.79	10.67	-1.77	19.04	100.96
0.112	2.09	0.09	98.96	17.84	-3.02	12.61	104.73	10.17	-1.71	18.09	100.60
0.121	2.08	0.08	98.84	16.91	-2.78	12.84	120.82	9.66	-1.58	17.14	100.31
0.129	2.07	0.07	98.78	15.76	-2.92	12.79	138.06	9.02	-1.66	16.03	100.07
0.137	2.06	0.06	98.70	15.07	-2.80	13.02	156.45	8.64	-1.60	15.33	99.88
0.146	2.05	0.05	98.67	14.16	-2.80	12.97	175.98	8.12	-1.60	14.43	99.72
0.154	2.05	0.05	98.61	13.69	-2.55	13.26	196.67	7.86	-1.46	13.93	99.59
0.175	2.04	0.04	98.68	10.83	-2.56	11.90	253.42	6.23	-1.47	11.13	99.31
0.196	2.03	0.03	98.53	10.61	-2.57	13.05	317.34	6.11	-1.48	10.92	99.13
0.217	2.02	0.02	98.45	10.15	-2.57	13.82	388.46	5.86	-1.48	10.47	99.01
0.237	2.02	0.02	98.43	9.45	-2.57	14.10	466.75	5.46	-1.48	9.79	98.92
0.258	2.03	0.02	98.67	8.73	-2.57	14.16	552.23	5.03	-1.48	9.10	99.09
0.279	2.03	0.01	98.94	7.77	-2.56	13.62	644.89	4.46	-1.47	8.18	99.28
0.300	2.03	0.01	98.96	6.82	-2.44	12.86	744.73	3.92	-1.40	7.25	99.23
0.321	2.03	0.01	98.97	6.12	-2.44	12.34	851.76	3.52	-1.40	6.59	99.18
0.342	2.03	0.01	98.96	5.65	-2.44	12.14	965.97	3.25	-1.40	6.16	99.15

*V_θ listed as negative for inboard traverse.

TABLE B-10

PROFILES FOR Z/C=30, V_∞=100 AND $\dot{m}$=0

R ~ft.	Q ~in. H_2O	$(P_{st_\infty}-P_{st})$ ~in. H_2O	V_z ~FPS	V_θ* ~FPS	V_r ~FPS	Γ ~ft^2/sec	ζ (sim. var.)	Flow Yaw ~Deg.	Flow Pitch ~Deg.	$V_{\theta_{cor}}$ ~FPS	V_{total} ~FPS
0.001	1.96	1.44	97.12	-2.11	-0.31	0.01	0.00	-1.24	0.18	-2.13	97.15
0.002	2.04	1.44	98.88	-5.44	-1.69	0.09	0.04	-3.13	0.97	-5.70	99.05
0.007	2.14	1.42	100.74	-11.82	-2.63	0.50	0.31	-6.66	1.48	-12.11	101.47
0.011	2.21	1.38	100.87	-21.54	-3.13	1.47	0.82	-11.99	1.73	-21.77	103.19
0.015	2.39	1.33	102.90	-29.09	-9.89	2.74	1.56	-15.70	5.26	-30.72	107.38
0.019	2.47	1.27	103.56	-32.61	-9.74	3.93	2.55	-17.39	5.10	-34.03	109.01
0.023	2.52	1.18	103.78	-35.98	-9.63	5.28	3.78	-19.03	4.99	-37.25	110.26
0.028	2.60	1.09	104.52	-38.53	-9.50	6.66	5.26	-20.13	4.85	-39.68	111.80
0.032	2.58	0.97	103.62	-40.04	-9.09	7.97	6.97	-21.02	4.65	-41.05	111.46
0.036	2.56	0.84	103.00	-40.56	-7.78	9.13	8.93	-21.38	4.00	-41.30	110.97
0.040	2.47	0.69	101.29	-39.80	-7.23	10.00	11.12	-21.34	3.78	-40.45	109.07
0.044	2.43	0.57	100.70	-38.83	-6.15	10.77	13.56	-20.98	3.25	-39.31	108.10
0.048	2.38	0.47	100.32	-37.22	-5.28	11.30	16.24	-20.25	2.81	-37.59	107.13
0.057	2.26	0.34	99.03	-32.95	-3.03	11.73	22.32	-18.31	1.66	-33.09	104.42
0.065	2.21	0.26	98.84	-29.62	-1.86	12.09	29.37	-16.59	1.03	-29.67	103.20
0.073	2.17	0.21	98.31	-27.60	-1.15	12.71	37.38	-15.60	0.64	-27.62	102.12
0.082	2.11	0.17	97.88	-24.51	-0.92	12.58	46.36	-13.99	0.52	-24.53	100.91
0.090	2.10	0.14	97.81	-22.91	-0.43	12.96	56.31	-13.12	0.24	-22.91	100.45
0.098	2.08	0.11	97.84	-21.53	-0.18	13.30	67.22	-12.35	0.10	-21.53	100.18
0.107	2.07	0.10	97.63	-20.60	-0.05	13.80	79.09	-11.85	0.03	-20.60	99.78
0.115	2.06	0.08	97.83	-19.21	+0.07	13.88	91.93	-11.05	-0.04	-19.21	99.70
0.123	2.00	0.07	96.47	-18.41	+0.33	14.27	105.74	-10.75	-0.19	-18.41	98.21
0.132	2.04	0.06	97.69	-17.31	+0.57	14.32	120.51	-10.00	-0.33	-17.32	99.21
0.153	2.03	0.05	97.57	-15.62	+0.83	14.96	161.66	-9.05	-0.48	-15.64	98.81
0.173	2.03	0.04	97.83	-13.73	+0.83	14.95	208.85	-7.95	-0.48	-13.75	98.80

TABLE B-10 (Continued)

R ~ft.	Q ~in. H_2O	$(P_{st_\infty}-P_{st})$ ~in. H_2O	V_z ~FPS	V_θ* ~FPS	V_r ~FPS	Γ ~ft^2/sec	ζ (sim. var.)	Flow Yaw ~Deg.	Flow Pitch ~Deg.	$V_{\theta_{cor}}$ ~FPS	V_{total} ~FPS
0.194	2.02	0.03	97.92	-11.70	+0.83	14.28	262.07	-6.78	-0.48	-11.73	98.62
0.215	2.01	0.02	97.78	-11.71	+0.83	15.82	321.33	-6.79	-0.48	-11.74	98.48
0.236	2.02	0.02	98.02	-10.99	+0.83	16.29	386.62	-6.37	-0.48	-11.02	98.64
0.257	2.02	0.02	98.02	-10.28	+0.83	16.58	457.94	-5.96	-0.48	-10.32	98.56
0.278	2.01	0.01	98.05	-9.34	+0.83	16.28	535.30	-5.41	-0.48	-9.37	98.50
0.298	2.01	0.01	98.05	-8.86	+0.83	16.61	618.70	-5.14	-0.48	-8.90	98.45
0.319	2.00	0.01	97.78	-8.63	+0.83	17.30	708.12	-5.02	-0.48	-8.67	98.17
0.340	2.00	0.01	97.77	-8.39	+0.83	17.91	803.58	-4.88	-0.48	-8.43	98.13
0.002	2.01	1.44	98.34	0.47	1.44	0.00	0.02	0.27	0.84	1.52	98.35
0.006	2.03	1.42	98.60	8.59	0.18	0.31	0.24	4.95	0.10	8.59	98.97
0.010	2.09	1.39	98.77	17.76	0.18	1.12	0.70	10.14	0.10	17.76	100.36
0.014	2.24	1.35	100.29	27.08	-1.87	2.41	1.40	15.03	-1.03	27.14	103.90
0.018	2.36	1.28	100.53	34.10	-10.30	3.93	2.34	18.64	-5.51	35.62	106.66
0.023	2.41	1.20	100.77	36.79	-10.42	5.20	3.52	19.95	-5.52	38.24	107.78
0.027	2.47	1.11	101.12	39.51	-9.63	6.62	4.94	21.23	-5.04	40.67	108.99
0.031	2.49	0.99	100.93	41.64	-9.57	8.07	6.61	22.31	-4.99	42.73	109.60
0.035	2.50	0.87	100.66	42.45	-9.01	9.34	8.52	22.75	-4.69	43.40	109.62
0.039	2.43	0.72	99.30	42.15	-8.09	10.37	10.66	22.88	-4.27	42.92	108.18
0.043	2.37	0.59	98.31	41.05	-7.50	11.18	13.05	22.55	-4.01	41.73	106.80
0.048	2.31	0.49	97.63	39.33	-6.90	11.74	15.68	21.83	-3.73	39.93	105.47
0.052	2.27	0.41	97.44	37.69	-6.00	12.24	18.56	21.04	-3.27	38.17	104.65
0.060	2.12	0.31	96.97	34.61	-5.13	13.05	25.03	19.54	-2.84	34.99	103.09
0.068	2.16	0.24	96.96	31.14	-3.73	13.37	32.46	17.72	-2.08	31.37	101.91
0.077	2.13	0.19	97.27	27.83	-3.26	13.41	40.86	15.88	-1.84	28.02	101.23
0.085	2.07	0.15	96.77	24.57	-2.81	13.12	50.22	14.17	-1.60	24.73	99.88

TABLE B-10 (Continued)

R ~ft.	Q ~in. H_2O	$(P_{st_\infty}-P_{st})$ ~in. H_2O	V_z ~FPS	V_θ* ~FPS	V_r ~FPS	Γ ~ft^2/sec	ζ (sim. var.)	Flow Yaw ~Deg.	Flow Pitch ~Deg.	$V_{\theta_{cor}}$ ~FPS	V_{total} ~FPS
0.093	2.07	0.13	96.73	24.12	-2.56	14.15	60.56	13.93	-1.46	24.26	99.73
0.102	2.05	0.11	96.63	22.55	-2.33	14.40	71.85	13.07	-1.34	22.67	99.26
0.110	2.04	0.09	96.78	21.41	-2.08	14.80	84.11	12.41	-1.20	21.51	99.14
0.118	2.03	0.08	96.69	20.48	-2.09	15.22	97.34	11.90	-1.20	20.58	98.85
0.139	2.02	0.06	96.78	18.60	-1.84	16.26	134.63	10.82	-1.06	18.69	98.57
0.160	2.01	0.04	97.01	16.74	-1.84	16.83	177.96	9.74	-1.07	16.84	98.46
0.181	1.99	0.03	96.76	15.33	-1.85	17.41	227.32	8.95	-1.08	15.44	97.99
0.202	2.00	0.03	97.02	14.20	-1.85	17.99	282.71	8.28	-1.07	14.32	98.07
0.222	1.99	0.02	97.07	13.04	-1.72	18.23	344.14	7.61	-1.00	13.15	97.95
0.243	1.99	0.02	97.04	12.57	-1.83	19.21	411.60	7.34	-1.06	12.70	97.86
0.264	1.98	0.02	96.86	11.45	-1.81	19.00	485.10	6.71	-1.06	11.59	97.55
0.285	1.98	0.01	97.11	10.96	-1.86	19.63	564.63	6.41	-1.08	11.12	97.75
0.306	1.99	0.01	97.37	10.47	-1.85	20.13	650.19	6.11	-1.08	10.64	97.95
0.327	1.99	0.01	97.39	10.00	-1.85	20.52	741.79	5.83	-1.08	10.17	97.92
0.347	1.99	0.01	97.40	9.52	-1.85	20.79	839.43	5.55	-1.08	9.70	97.88

*V_θ listed as negative for inboard traverse.

TABLE B-11

PROFILES FOR Z/C=10, V_∞=70 AND $\dot{m}$=0.000215 slugs/sec

R ~ft.	Q ~in. H_2O	$(P_{st_\infty}-P_{st})$ ~in. H_2O	V_z ~FPS	V_θ* ~FPS	V_r ~FPS	Γ ~ft^2/sec	ζ (sim. var.)	Flow Yaw ~Deg.	Flow Pitch ~Deg.	$V_{\theta cor}$ ~FPS	V_{total} ~FPS
0.003	1.14	-0.02	75.66	-0.62	+0.21	0.01	0.16	-0.47	-0.16	-0.66	75.66
0.007	1.14	-0.02	75.49	-0.94	-0.13	0.04	0.79	-0.71	0.10	-0.95	75.50
0.012	1.40	0.24	83.75	-0.88	-0.73	0.06	1.92	-0.60	0.50	-1.14	83.75
0.016	1.38	0.24	82.96	-1.46	-0.74	0.14	3.53	-1.00	0.51	-1.63	82.97
0.020	1.37	0.23	82.73	-2.05	-0.58	0.26	5.64	-1.41	0.40	-2.13	82.76
0.024	1.37	0.21	82.87	-2.63	-0.58	0.40	8.23	-1.81	0.40	-2.70	82.91
0.028	1.35	0.19	82.24	-3.24	-0.59	0.58	11.31	-2.25	0.41	-3.29	82.31
0.037	1.34	0.19	81.76	-3.85	-0.59	0.89	18.94	-2.69	0.41	-3.90	81.85
0.041	1.34	0.19	81.59	-4.16	-0.59	1.07	23.49	-2.90	0.41	-4.20	81.70
0.045	1.33	0.19	81.25	-4.78	-0.59	1.35	28.53	-3.35	0.41	-4.81	81.39
0.049	1.30	0.17	80.46	-5.11	-0.59	1.58	34.06	-3.62	0.42	-5.15	80.63
0.053	1.27	0.14	79.34	-5.48	-0.60	1.84	40.08	-3.93	0.43	-5.51	79.53
0.058	1.25	0.13	78.75	-5.82	-0.60	2.10	46.58	-4.20	0.43	-5.85	78.97
0.062	1.24	0.12	78.26	-7.08	-0.44	2.74	53.58	-5.14	0.32	-7.09	78.58
0.066	1.21	0.12	77.58	-7.44	-0.44	3.08	61.06	-5.45	0.32	-7.45	77.94
0.070	1.20	0.10	77.26	-7.46	-0.61	3.28	69.04	-5.49	0.45	-7.49	77.62
0.074	1.18	0.09	76.43	-7.84	-0.44	3.65	77.50	-5.83	0.33	-7.85	76.83
0.078	1.16	0.08	75.79	-8.21	-0.45	4.04	86.45	-6.15	0.33	-8.22	76.24
0.083	1.14	0.06	75.15	-8.59	-0.45	4.45	95.90	-6.48	0.34	-8.60	75.64
0.087	1.14	0.06	74.98	-8.60	-0.45	4.68	105.82	-6.51	0.34	-8.61	75.47
0.091	1.13	0.06	74.54	-8.65	-0.28	4.93	116.25	-6.58	0.21	-8.65	75.04
0.095	1.11	0.05	74.06	-8.69	-0.28	5.19	127.16	-6.66	0.21	-8.70	74.57
0.103	1.09	0.05	73.21	-8.78	-0.10	5.70	150.44	-6.80	0.08	-8.78	73.73
0.112	1.08	0.04	73.03	-8.80	-0.10	6.17	175.68	-6.83	0.08	-8.80	73.56
0.120	1.07	0.04	72.51	-8.85	+0.07	6.67	202.89	-6.92	-0.06	-8.85	73.05

TABLE B-11 (Continued)

R ~ft.	Q ~in. H_2O	$(P_{st}-P_{st_\infty})$ ~in. H_2O	V_z ~FPS	V_θ* ~FPS	V_r ~FPS	Γ ~ft^2/sec	ζ (sim. var.)	Flow Yaw ~Deg.	Flow Pitch ~Deg.	$V_{\theta_{cor}}$ ~FPS	V_{total} ~FPS
0.128	1.06	0.03	72.34	-8.87	+0.25	7.15	232.04	-6.95	-0.20	-8.87	72.88
0.137	1.06	0.03	72.20	-8.55	+0.43	7.34	263.16	-6.72	-0.34	-8.56	72.71
0.145	1.04	0.02	71.71	-8.36	+0.43	7.61	296.23	-6.61	-0.34	-8.37	72.19
0.166	1.04	0.02	71.57	-8.04	+0.42	8.37	387.47	-6.37	-0.33	-8.05	72.02
0.187	1.05	0.01	72.21	-7.65	+0.77	8.97	490.94	-6.01	-0.60	-7.69	72.62
0.208	1.03	0.01	71.51	-7.04	+0.96	9.18	606.63	-5.59	-0.76	-7.11	71.86
0.228	1.01	0.01	70.66	-7.11	+0.97	10.20	734.56	-5.72	-0.78	-7.17	7-.02
0.249	1.00	0.00	70.55	-6.78	+0.07	10.61	874.72	-5.46	-0.78	-6.85	70.89
0.270	0.98	0.0	69.69	-6.50	+0.99	11.03	1027.11	-5.30	-0.80	-6.58	70.00
0.291	0.97	0.0	69.39	-5.83	+0.99	10.66	1191.73	-4.78	-0.81	-5.92	69.65
0.312	0.96	-0.00	68.95	-5.51	+1.00	10.79	1368.58	-4.55	-0.83	-5.60	69.18
0.333	0.95	-0.01	68.83	-5.17	+1.01	10.80	1557.66	-4.27	-0.83	-5.27	69.03
0.353	0.94	-0.01	68.36	-5.20	+1.01	11.54	1758.97	-4.32	-0.84	-5.29	68.56
0.374	0.95	-0.01	68.67	-4.82	+1.20	11.34	1972.51	-4.00	-0.99	-4.97	68.85
0.395	0.95	-0.01	68.62	-4.47	+1.20	11.10	2198.28	-3.71	-0.99	-4.63	68.78
0.001	1.42	0.25	84.41	-0.41	+0.32	0.00	0.01	-0.28	-0.21	-0.52	84.41
0.005	1.42	0.25	84.40	0.43	-0.47	0.01	0.35	0.29	-0.32	0.63	84.41
0.009	1.42	0.23	84.25	0.99	-0.62	0.06	1.18	0.67	-0.42	1.17	84.26
0.013	1.41	0.22	83.95	1.27	-0.63	0.11	2.50	0.86	-0.43	1.42	83.96
0.018	1.36	0.20	82.42	2.56	-0.80	0.27	4.32	1.70	-0.55	2.58	82.46
0.022	1.33	0.18	81.65	2.78	-0.97	0.38	6.61	1.94	-0.68	2.95	81.70
0.026	1.34	0.17	81.79	3.06	-1.28	0.50	9.40	2.14	-0.89	3.32	81.85
0.030	1.33	0.16	81.47	3.37	-1.44	0.64	12.68	2.36	-1.01	3.67	81.55
0.034	1.28	0.14	79.90	3.77	-1.48	0.81	16.45	2.69	-1.05	4.05	80.00
0.038	1.26	0.12	79.04	5.05	-1.82	1.22	20.70	3.63	-1.31	5.36	79.22
0.042	1.26	0.10	79.04	5.04	-1.98	1.35	25.45	3.63	-1.43	5.42	79.22

TABLE B-11 (Continued)

R ~ft.	Q ~in. H_2O	$(P_{st}-P_{st_\infty})$ ~in. H_2O	V_z ~FPS	V_θ* ~FPS	V_r ~FPS	Γ ~ft^2/sec	ζ (sim. var.)	Flow Yaw ~Deg.	Flow Pitch ~Deg.	$V_{\theta_{cor}}$ ~FPS	V_{total} ~FPS
0.047	1.25	0.09	78.86	5.37	-1.99	1.57	30.68	3.87	-1.43	5.72	79.06
0.051	1.24	0.07	78.40	5.10	-2.00	1.63	36.41	3.70	-14.5	5.48	78.59
0.055	1.23	0.07	78.14	5.12	-2.01	1.77	42.62	3.73	-1.46	5.50	78.33
0.063	1.19	0.06	76.99	6.46	-2.04	2.57	56.51	4.77	-1.50	6.78	77.29
0.072	1.15	0.06	75.53	7.85	-2.06	3.54	72.36	5.90	-1.54	8.12	75.96
0.080	1.16	0.04	75.86	7.81	-2.05	3.93	90.17	5.85	-1.53	8.08	76.29
0.088	1.16	0.04	75.69	7.83	-2.07	4.35	109.93	5.88	-1.55	8.10	76.13
0.097	1.15	0.03	75.53	7.85	-2.06	4.77	131.66	5.90	-1.54	8.12	75.96
.105	1.14	0.02	5.19	7.89	-2.07	5.21	155.33	5.96	-1.56	8.16	75.63
0.113	1.11	0.02	74.02	8.65	-1.93	6.16	180.97	6.64	-1.48	8.87	74.54
0.122	1.09	0.01	73.41	9.05	-1.95	6.92	208.56	6.99	-1.50	9.25	73.99
0.130	1.08	0.01	72.95	8.79	-1.96	7.18	238.11	6.84	-1.52	9.01	73.51
.138	1.08	0.01	72.82	8.81	-1.97	7.66	269.	6.86	-1.53	9.03	73.37
0.147	1.06	0.00	72.40	8.86	-2.15	8.17	303.07	6.94	-1.68	9.12	72.97
0.167	1.03	0.0	71.18	9.03	-2.02	9.50	395.29	7.19	-1.60	9.25	71.78
0.188	0.99	-0.00	69.69	8.57	-2.25	10.15	499.74	6.98	-1.83	8.86	70.25
0.209	0.97	-0.00	68.89	8.68	-2.28	11.41	616.41	7.15	-1-87	8.98	69.47
0.230	0.95	-0.00	68.55	8.39	-2.29	12.13	745.32	6.94	-1.89	8.70	69.10
0.251	0.93	-0.00	67.87	7.80	-2.32	12.30	886.46	6.52	-1.93	8.14	68.35
0.272	0.91	-0.02	67.15	7.55	-2.35	12.88	1039.82	6.38	-1.98	7.90	67.61
0.292	0.91	-0.02	67.19	7.20	-2.15	13.23	1205.42	6.09	-1.82	7.52	67.61
0.313	0.91	-0.02	67.23	7.85	-2.15	13.49	1383.25	5.79	-1.82	7.18	67.61
0.334	0.91	-0.02	67.31	6.15	-1.96	12.91	1573.31	5.19	-1.66	6.45	67.62
0.355	0.92	-0.02	67.73	5.76	-1.76	12.84	1775.60	4.83	-1.48	6.02	68.00
0.397	0.92	-0.02	67.77	5.40	-1.57	13.46	2216.86	4.53	-1.32	5.63	68.01

*V_θ listed as negative for inboard traverse.

TABLE B-12

PROFILES FOR Z/C=10, V_∞=70 fps, $\dot{m}$=0.00038 slugs/sec

R ~ft.	Q ~in. H_2O	$(P_{st_\infty}-P_{st})$ ~in. H_2O	V_z ~FPS	V_θ* ~FPS	V_r ~FPS	Γ ~ft^2/sec	ζ (sim. var.)	Flow Yaw ~Deg.	Flow Pitch ~Deg.	$V_{\theta_{cor}}$ ~FPS	V_{total} ~FPS
0.004	1.39	0.06	82.94	-0.49	+0.37	0.01	0.25	-0.34	-0.25	-0.61	82.94
0.012	1.39	0.06	83.15	-0.39	+0.13	0.03	2.23	-0.27	-0.09	-0.41	83.15
0.021	1.40	0.06	83.44	-0.68	+0.26	0.09	6.20	-0.46	-0.18	-0.73	83.45
0.029	1.40	0.06	83.44	-0.96	+0.44	0.18	12.15	-0.66	-0.30	-1.06	83.45
0.037	1.39	0.05	83.08	-1.25	+0.11	0.30	20.08	-0.86	-0.08	-1.26	83.09
0.046	1.39	0.05	83.07	-1.54	+0.26	0.44	30.00	-1.06	-0.18	-1.56	83.09
0.054	1.39	0.05	83.07	-1.83	+0.42	0.62	41.90	-1.26	-0.29	-1.88	83.09
0.063	1.39	0.05	82.88	-2.23	+0.42	0.87	55.78	-1.53	-0.29	-2.26	82.91
0.071	1.38	0.04	82.81	-2.52	+0.26	1.12	71.65	-1.73	-0.18	-2.53	82.85
0.079	1.37	0.04	82.50	-2.82	+0.27	1.40	89.50	-1.95	-0.18	-2.83	82.55
0.088	1.36	0.04	82.07	-3.13	+0.42	1.72	109.34	-2.17	-0.29	-3.15	82.13
0.096	1.35	0.04	81.63	-3.44	+0.43	2.07	131.15	-2.40	-0.30	-3.46	81.70
0.104	1.34	0.03	81.53	-3.64	+0.40	2.38	154.95	-2.54	-0.28	-3.66	81.61
0.112	1.33	0.03	81.12	-4.05	+0.41	2.86	180.74	-2.84	-0.28	-4.07	81.22
0.121	1.31	0.03	80.43	-4.38	+0.41	3.33	208.51	-3.10	-0.29	-4.40	80.55
0.129	1.31	0.03	80.38	-4.68	+0.41	3.80	238.26	-3.32	-0.29	-4.70	80.52
0.150	1.27	0.03	79.08	-5.05	+0.42	4.76	321.31	-3.64	-0.30	-5.07	79.25
0.171	1.23	0.02	77.71	-5.74	+0.43	6.16	416.77	-4.20	-0.31	-5.76	77.92
0.192	1.18	0.02	76.26	-5.83	+0.27	7.02	524.62	-4.35	-0.20	-5.84	76.48
0.213	1.14	0.01	74.75	-6.25	+0.11	8.34	644.86	-4.75	-0.08	-6.25	75.01
0.233	1.12	0.01	74.08	-6.30	+0.11	9.23	777.50	-4.83	-0.08	-6.30	74.34
0.254	1.19	0.11	76.68	-5.81	+0.27	9.27	922.54	-4.31	-0.20	-5.81	76.90
0.275	1.04	0.01	71.56	-5.82	+0.30	10.05	1079.97	-4.62	-0.24	-5.82	71.89
0.296	1.03	0.01	71.14	-5.51	+0.30	10.24	1249.81	-4.41	-0.24	-5.52	71.53
0.317	1.02	0.00	70.41	-4.88	+0.49	9.70	1432.03	-3.94	-0.39	-4.90	71.04

TABLE B-12 (Continued)

R ~ft.	Q ~in. H_2O	$(P_{st_\infty}-P_{st})$ ~in. H_2O	V_z ~FPS	V_θ* ~FPS	V_r ~FPS	Γ ~ft^2/sec	ζ (sim. var.)	Flow Yaw ~Deg.	Flow Pitch ~Deg.	$V_{\theta_{cor}}$ ~FPS	V_{total} ~FPS
0.358	1.01	0.00	70.45	-4.19	+0.65	9.43	1833.68	-3.39	-0.52	-4.24	70.58
0.400	0.90	0.0	66.66	-4.02	+0.88	10.10	2284.91	-3.43	-0.75	-4.11	66.79
0.442	0.98	-0.00	69.42	-3.54	+1.03	9.83	2785.72	-2.91	-0.84	-3.69	69.51
0.483	0.97	-0.01	69.25	-3.20	+1.03	9.71	3336.12	-2.63	-0.85	-3.36	69.33
0.525	0.97	-0.01	69.25	-3.20	+1.03	10.54	3936.10	-2.63	-0.85	-3.36	69.33
0.567	0.93	-0.01	68.00	-2.88	+1.05	10.27	4585.67	-2.42	-0.88	-3.07	68.07
0.004	1.38	0.06	82.64	0.08	-0.06	0.00	0.25	0.06	-0.01	0.10	82.64
0.013	1.37	0.06	82.40	0.37	-0.06	0.03	2.23	0.26	-0.04	0.38	82.40
0.021	1.38	0.06	82.61	0.65	-0.06	0.09	6.20	0.45	-0.04	0.65	82.61
0.029	1.36	0.06	82.24	0.94	-0.06	0.17	12.15	0.65	-0.04	0.94	82.25
0.037	1.35	0.06	81.94	1.23	-0.06	0.29	20.08	0.86	-0.05	1.23	81.95
0.046	1.35	0.05	81.87	1.51	0.09	0.44	30.00	1.05	0.06	1.52	81.89
0.054	1.35	0.05	81.76	2.37	0.25	0.81	41.90	1.65	0.17	2.38	81.79
0.063	1.32	0.05	80.81	2.70	0.25	1.06	55.78	1.90	0.18	2.71	80.85
0.071	1.31	0.05	80.43	3.01	0.25	1.34	71.65	2.13	0.18	3.02	80.48
0.079	1.31	0.04	80.35	3.30	0.25	1.64	89.50	2.34	0.18	3.31	80.42
0.088	1.29	0.04	79.71	3.93	0.25	2.16	109.34	2.81	0.18	3.94	79.81
0.096	1.29	0.04	79.70	4.23	0.25	2.55	131.16	3.02	0.18	4.24	79.81
0.104	1.27	0.04	79.05	4.58	0.25	2.99	154.95	3.30	0.18	4.58	79.19
0.113	1.23	0.04	77.90	5.27	0.44	3.73	180.74	3.85	0.32	5.29	78.08
0.121	1.22	0.04	77.54	5.92	0.44	4.50	208.51	4.34	0.32	5.94	77.76
0.142	1.17	0.03	76.01	6.68	0.27	5.95	286.60	5.00	0.21	6.69	76.30
0.162	1.14	0.03	74.81	7.12	0.28	7.27	377.10	5.41	0.21	7.12	75.15
0.183	1.10	0.02	73.60	7.47	0.10	8.61	479.99	5.77	0.08	7.47	73.98
0.204	1.06	0.02	72.05	7.65	-0.07	9.81	595.27	6.03	-0.06	7.65	72.45

TABLE B-12 (Continued)

R ~ft.	Q ~in. H_2O	$(P_{st_\infty}-P_{st})$ ~in. H_2O	V_z ~FPS	V_θ* ~FPS	V_r ~FPS	Γ ~ft^2/sec	ζ (sim. var.)	Flow Yaw ~Deg.	Flow Pitch ~Deg.	$V_{\theta_{cor}}$ ~FPS	V_{total} ~FPS
0.225	1.02	0.01	70.82	7.79	-0.26	11.02	722.96	6.25	-0.21	7.80	71.25
0.246	1.01	0.01	70.28	7.86	-0.44	12.13	863.03	6.34	-0.36	7.87	70.72
0.267	1.00	0.00	70.18	7.21	-0.44	12.09	1015.51	5.84	-0.36	7.23	70.55
0.287	0.99	0.0	69.68	6.94	-0.63	12.53	1180.38	5.66	-0.51	6.97	70.02
0.308	0.98	-0.00	69.53	6.62	-0.82	12.83	1357.65	5.41	-0.67	6.67	69.85
0.350	0.98	-0.00	69.64	5.60	-1.00	12.31	1749.38	4.57	-0.82	5.69	69.87
0.392	0.98	-0.01	69.49	5.27	-1.19	12.97	2190.69	4.31	-0.97	5.40	69.70
0.433	0.98	-0.01	69.54	4.58	-1.19	12.46	2681.58	3.75	-0.97	4.73	69.70
0.475	0.98	-0.01	69.40	3.90	-1.19	11.64	3222.07	3.20	-0.98	4.08	69.52
0.517	0.98	-0.01	69.42	3.55	-1.19	11.54	3812.13	2.92	-0.98	3.75	69.52
0.558	0.98	-0.01	69.43	3.21	-1.19	11.26	4451.78	2.63	-0.98	3.42	69.52
0.600	0.98	-0.01	69.45	2.87	-1.19	10.81	5141.02	2.35	-0.98	3.11	69.52

*V_θ listed as negative for inboard traverse.

TABLE B-13

PROFILES FOR Z/C=20, V_∞=70 fps, $\dot{m}$=0.000215 slugs/sec

R ~ft.	Q ~in. H_2O	$(P_{st_\infty}-P_{st})$ ~in. H_2O	V_z ~FPS	V_θ* ~FPS	V_r ~FPS	Γ ~ft^2/sec	ζ (sim. var.)	Flow Yaw ~Deg.	Flow Pitch ~Deg.	$V_{\theta_{cor}}$ ~FPS	V_{total} ~FPS
0.003	1.42	0.20	83.10	-0.52	+0.03	0.01	0.08	-0.36	-0.02	-0.52	83.10
0.007	1.42	0.20	82.95	-0.80	-0.12	0.04	0.41	-0.55	0.08	-0.81	82.96
0.010	1.38	0.19	81.92	-1.35	-0.04	0.08	0.73	-0.94	-0.03	-1.35	81.93
0.012	1.38	0.19	81.92	-1.35	-0.27	0.10	0.99	-0.94	0.19	-1.37	81.93
0.016	1.38	0.19	81.91	-1.92	-0.27	0.19	1.83	-1.33	0.19	-1.94	81.93
0.020	1.38	0.19	81.74	-2.49	-0.11	0.31	2.91	-1.74	0.08	-2.50	81.78
0.024	1.37	0.19	81.58	-2.78	-0.11	0.42	4.25	-1.94	0.08	-2.79	81.63
0.028	1.38	0.17	81.81	-3.07	-0.57	0.55	5.84	-2.14	0.40	-3.12	81.87
0.032	1.37	0.16	81.47	-3.95	-0.42	0.81	7.69	-2.76	0.29	-3.97	81.57
0.037	1.36	0.14	81.22	-4.25	-0.42	0.98	9.79	-2.98	0.30	-4.27	81.33
0.041	1.35	0.13	80.91	-4.55	-0.42	1.17	12.14	-3.20	0.30	-4.57	81.04
0.045	1.35	0.13	80.83	-4.85	-0.42	1.37	14.74	-3.42	0.30	-4.87	80.98
0.049	1.31	0.13	79.34	-5.50	-0.27	1.70	17.60	-3.94	0.19	-5.50	79.53
0.053	1.30	0.12	79.19	-5.50	-0.27	1.84	20.71	-3.96	0.19	-5.51	79.38
0.058	1.29	0.10	78.73	-5.52	-0.27	2.00	24.07	-3.99	0.19	-5.53	78.92
0.062	1.27	0.09	78.26	-5.54	-0.27	2.15	27.69	-4.03	0.20	-5.55	78.46
0.070	1.27	0.09	78.22	-6.15	-0.27	2.70	35.67	-4.47	0.20	-6.15	78.46
0.078	1.27	0.09	78.11	-7.35	-0.27	3.62	44.67	-5.35	0.20	-7.35	78.46
0.087	1.25	0.08	77.33	-7.40	-0.11	4.03	54.68	-5.44	0.08	-7.40	77.68
0.095	1.24	0.08	77.26	-7.41	+0.05	4.42	65.70	-5.45	-0.04	-7.41	77.62
0.103	1.23	0.08	76.85	-7.43	+0.05	4.83	77.74	-5.50	-0.04	-7.43	77.21
0.112	1.21	0.07	76.34	-7.77	+0.06	5.45	90.78	-5.78	-0.04	-7.77	76.73
0.120	1.19	0.07	75.59	-8.13	+0.06	6.13	104.84	-6.11	-0.04	-8.13	76.03
0.128	1.19	0.07	75.40	-8.15	+0.22	6.57	119.90	-6.14	-0.17	-8.15	75.84
0.149	1.17	0.06	74.84	-8.19	+0.39	7.68	161.99	-6.22	-0.30	-8.20	75.29

TABLE B-13 (Continued)

R ~ft.	Q ~ in. H_2O	$(P_{st_\infty}-P_{st})$ ~ in. H_2O	V_z ~ FPS	V_θ* ~ FPS	V_r ~ FPS	Γ ~ft^2/sec	ζ (sim. var.)	Flow Yaw ~Deg.	Flow Pitch ~Deg.	$V_{\theta_{cor}}$ ~FPS	V_{total} ~FPS
0.170	1.14	0.06	74.06	-7.94	+0.40	8.49	210.40	-6.09	-0.31	-7.95	74.49
0.191	1.13	0.05	73.56	-7.98	+0.74	9.57	265.13	-6.16	-0.57	-8.02	73.99
0.212	1.10	0.04	72.76	-7.73	+0.75	10.28	326.18	-6.03	-0.59	-7.77	73.17
0.233	1.11	0.04	72.83	-7.09	+0.75	10.35	393.55	-5.53	-0.59	-7.13	73.18
0.253	1.10	0.04	72.80	-6.77	+0.92	10.78	467.24	-5.29	-0.72	-6.83	73.12
0.274	1.10	0.04	72.73	-6.46	+1.10	11.12	547.25	-5.05	-0.86	-6.55	73.02
0.295	1.10	0.03	72.59	-6.14	+1.10	11.38	633.57	-4.81	-0.86	-6.24	72.85
0.316	1.09	0.03	72.47	-5.50	+1.10	10.92	726.22	-4.32	-0.87	-5.61	72.69
0.337	1.09	0.03	72.39	-5.18	+1.28	10.96	825.19	-4.07	-1.00	-5.34	72.59
0.001	1.42	0.20	83.10	0.03	0.12	0.00	0.01	0.02	0.08	0.12	83.10
0.005	1.42	0.20	83.10	0.48	-0.08	0.01	0.18	0.33	-0.06	0.48	83.10
0.009	1.42	0.20	83.10	0.75	-0.08	0.04	0.61	0.51	-0.06	0.75	83.10
0.013	1.42	0.20	82.95	1.03	-0.08	0.09	1.29	0.71	-0.06	1.03	82.96
0.017	1.41	0.19	82.79	1.86	-0.08	0.20	2.23	1.28	-0.06	1.86	82.81
0.022	1.40	0.19	82.50	1.87	-0.08	0.25	3.42	1.29	-0.06	1.87	82.52
0.026	1.39	0.18	81.89	2.46	-0.09	0.40	4.86	1.71	-0.06	2.46	81.93
0.030	1.37	0.15	81.29	2.78	-0.09	0.52	6.55	1.95	-0.06	2.78	81.34
0.034	1.35	0.13	80.69	2.82	-0.09	0.61	8.50	1.99	-0.06	2.82	80.74
0.038	1.33	0.12	80.05	3.73	-0.09	0.90	10.70	2.66	-0.06	3.73	80.14
0.047	1.31	0.10	79.40	4.67	-0.09	1.37	15.85	3.35	-0.07	4.67	79.54
0.055	1.29	0.08	78.76	5.02	-0.09	1.74	22.02	3.63	-0.07	5.03	78.92
0.063	1.26	0.07	77.98	5.10	-0.10	2.03	29.20	3.72	-0.07	5.10	78.15
0.072	1.23	0.06	77.06	6.69	-0.10	3.01	37.39	4.93	-0.07	6.69	77.35
0.080	1.22	0.04	76.77	6.42	-0.10	3.23	46.59	4.76	-0.07	6.42	77.04
0.088	1.20	0.04	75.80	7.13	-0.43	3.96	56.81	5.35	-0.32	7.14	76.14

TABLE B-13 (Continued)

R ~ft.	Q ~in. H_2O	$(P_{st_\infty}-P_{st})$ ~in. H_2O	V_z ~FPS	V_θ* ~FPS	V_r ~FPS	Γ ~ft^2/sec	ζ (sim. var.)	Flow Yaw ~Deg.	Flow Pitch ~Deg.	$V_{\theta cor}$ ~FPS	V_{total} ~FPS
0.088	1.19	0.03	75.74	7.14	-0.43	3.96	56.81	5.36	-0.32	7.15	76.07
0.105	1.17	0.03	74.86	7.84	-0.60	5.17	80.26	5.95	-0.46	7.87	75.27
0.113	1.15	0.02	74.37	7.91	-0.77	5.63	93.51	6.04	-0.59	7.94	74.79
0.122	1.15	0.02	74.34	7.90	-2.28	6.04	107.77	6.04	-1.74	8.22	74.79
0.142	1.14	0.02	73.93	7.66	-0.78	6.86	147.83	5.88	-0.60	7.70	74.33
0.158	1.12	0.02	73.23	7.75	-1.13	7.71	182.51	6.01	-0.87	7.83	73.65
0.184	1.10	0.01	72.75	7.50	-1.31	8.68	246.93	5.85	-1.02	7.61	73.15
0.205	1.09	0.01	72.48	6.91	-1.14	8.90	305.95	5.42	-0.89	7.01	72.82
0.209	1.08	0.01	72.00	6.66	-1.32	8.75	318.52	5.25	-1.04	6.79	72.32
0.247	1.06	0.00	71.52	6.39	-1.51	9.91	442.96	5.08	-1.20	6.57	71.82
0.267	1.05	0.01	71.04	6.13	-1.52	10.30	520.95	4.91	-1.21	6.32	71.32
0.288	1.04	0.01	70.69	5.85	-1.70	10.59	605.25	4.70	-1.37	6.09	70.95
0.309	1.03	0.01	70.27	5.89	-1.71	11.45	695.88	4.77	-1.39	6.14	70.54
0.330	1.02	0.00	70.20	5.90	-1.72	12.23	792.82	4.78	-1.39	6.14	70.47
0.351	1.04	0.02	70.92	5.50	-1.87	12.11	896.09	4.41	-1.50	5.81	71.16
0.372	1.03	0.02	70.47	5.22	-1.89	12.18	1005.67	4.21	-1.52	5.55	70.69
0.392	1.04	0.02	70.78	5.18	-1.88	12.78	1121.58	4.17	-1.51	5.51	70.99
0.413	1.04	0.02	70.68	5.19	-1.88	13.49	1243.80	4.18	-1.51	5.52	70.89

*V_θ listed as negative for inboard traverse.

TABLE B-14

PROFILES FOR Z/C=20, V_∞=70 fps, $\dot{m}$=0.00038 slugs/sec

R ~ft.	Q ~in. H_2O	$(P_{st_\infty}-P_{st})$ ~in. H_2O	V_z ~FPS	V_θ* ~FPS	V_r ~FPS	Γ ~ft^2/sec	ζ (sim. var.)	Flow Yaw ~Deg.	Flow Pitch ~Deg.	$V_{\theta cor}$ ~FPS	V_{total} ~FPS
0.002	1.27	0.05	78.53	-0.33	-0.27	0.01	0.05	-0.24	0.20	-0.42	78.53
0.011	1.26	0.06	78.28	-0.32	-0.11	0.02	0.86	-0.23	0.08	-0.34	78.28
0.019	1.25	0.06	77.97	-0.60	-0.11	0.07	2.68	-0.44	0.08	-0.61	77.97
0.028	1.27	0.06	78.58	-0.91	-0.11	0.16	5.52	-0.66	0.08	-0.92	78.59
0.036	1.27	0.06	78.58	-1.11	-0.06	0.25	9.37	-0.81	0.05	-1.11	78.59
0.044	1.27	0.06	78.58	-1.41	-0.22	0.39	14.23	-1.02	0.16	-1.43	78.59
0.053	1.27	0.06	78.58	-1.41	-0.22	0.46	20.10	-1.02	0.16	-1.43	78.59
0.061	1.26	0.04	78.26	-1.70	-0.22	0.65	26.99	-1.24	0.16	-1.72	78.28
0.069	1.26	0.04	78.25	-2.00	-0.22	0.87	34.89	-1.46	0.16	-2.01	78.28
0.078	1.26	0.04	78.25	-2.30	-0.06	1.12	43.81	-1.68	0.05	-2.30	78.28
0.086	1.24	0.04	77.46	-2.61	-0.23	1.41	53.73	-1.92	0.17	-2.62	77.50
0.094	1.24	0.04	77.45	-2.92	-0.23	1.72	64.67	-2.14	0.17	-2.92	77.50
0.103	1.24	0.04	77.37	-3.22	-0.06	2.08	76.63	-2.37	0.05	-3.22	77.44
0.111	1.21	0.03	76.63	-3.54	-0.23	2.47	89.59	-2.63	0.17	-3.55	76.72
0.119	1.22	0.03	76.94	-3.85	-0.23	2.88	103.57	-2.85	0.17	-3.85	77.03
0.123	1.22	0.03	76.94	-3.85	-0.23	2.98	110.94	-2.85	0.17	-3.85	77.03
0.144	1.21	0.03	76.44	-4.17	-0.55	3.78	151.59	-3.11	0.41	-4.21	76.56
0.165	1.20	0.03	76.11	-4.49	-0.23	4.65	198.57	-3.36	0.17	-4.50	76.24
0.186	1.20	0.02	75.91	-5.12	-0.23	5.98	251.88	-3.84	0.17	-5.12	76.09
0.207	1.19	0.02	75.59	-5.13	-0.23	6.66	311.52	-3.86	0.17	-5.14	75.77
0.228	1.17	0.02	75.09	-5.47	+0.44	7.81	377.49	-4.14	-0.33	-5.48	75.29
0.248	1.17	0.01	74.95	-5.16	+0.77	8.05	449.79	-3.92	-0.58	-5.21	75.13
0.269	1.18	0.01	75.27	-5.14	+0.77	8.70	528.42	-3.89	-0.58	-5.20	75.45
0.290	1.16	0.01	74.88	-5.16	+0.77	9.40	613.38	-3.92	-0.59	-5.22	75.06
0.311	1.16	0.01	74.78	-5.16	+0.77	10.08	704.68	-3.93	-0.59	-5.22	74.96

TABLE B-14 (Continued)

R ~ft.	Q ~in. H_2O	$(P_{st}-P_{st})_\infty$ ~in. H_2O	V_z ~FPS	V_θ* ~FPS	V_r ~FPS	Γ ~ft^2/sec	ζ (sim. var.)	Flow Yaw ~Deg.	Flow Pitch ~Deg.	$V_{\theta_{cor}}$ ~FPS	V_{total} ~FPS
0.336	1.16	0.01	74.78	-5.16	+1.11	10.90	822.59	-3.93	-0.84	-5.28	74.96
0.361	1.08	0.01	72.10	-5.28	+1.15	11.96	949.62	-4.16	-0.91	-5.40	72.30
0.373	1.06	0.01	71.40	-4.98	+1.51	11.68	1016.55	-3.97	-1.20	-5.20	71.59
0.394	1.05	0.01	70.99	-5.08	+1.48	12.58	1133.17	-4.07	-1.19	-5.29	71.19
0.415	1.04	0.00	70.94	-4.75	+1.48	12.38	1256.13	-3.81	-1.19	-4.97	71.12
0.436	1.03	0.0	70.46	-4.77	+1.49	13.05	1385.41	-3.85	-1.21	-4.99	70.64
0.457	1.02	0.0	70.14	-4.44	+1.15	12.74	1521.02	-3.60	-0.93	-4.59	70.29
0.478	1.02	0.0	70.14	-4.44	+1.15	13.32	1662.97	-3.60	-0.93	-4.59	70.29
0.498	1.02	0.0	70.16	-4.10	+1.15	12.85	1811.24	-3.33	-0.93	-4.26	70.29
0.519	1.02	0.0	70.16	-4.10	+1.15	13.38	1965.85	-3.33	-0.93	-4.26	70.29
0.540	1.02	0.0	70.16	-4.10	+1.15	13.92	2126.79	-3.33	-0.93	-4.26	70.29
0.006	1.26	0.05	78.22	0.26	0.11	0.01	0.25	0.19	0.08	0.29	78.22
0.014	1.27	0.05	78.46	0.54	0.11	0.05	1.46	0.40	0.08	0.56	78.46
0.022	1.28	0.05	78.74	0.82	0.11	0.12	3.69	0.59	0.08	0.83	78.74
0.031	1.28	0.05	78.74	0.82	0.11	0.16	6.93	0.59	0.08	0.83	78.74
0.039	1.27	0.05	78.42	1.41	0.11	0.35	11.19	1.03	0.08	1.42	78.43
0.047	1.27	0.05	78.42	1.70	-0.05	0.51	16.46	1.24	-0.04	1.70	78.43
0.064	1.27	0.05	78.41	1.99	-0.05	0.80	30.03	1.45	-0.04	2.00	78.43
0.085	1.27	0.05	78.40	2.29	-0.21	1.22	52.69	1.66	-0.15	2.30	78.44
0.106	1.26	0.04	77.92	2.91	-0.21	1.93	81.69	2.13	-0.15	2.92	77.97
0.127	1.25	0.04	77.57	3.84	-0.37	3.05	117.02	2.82	-0.27	3.86	77.67
0.147	1.22	0.04	76.88	3.89	-0.54	3.61	158.68	2.89	-0.40	3.93	76.98
0.127	1.20	0.04	76.22	4.26	-0.71	3.39	117.02	3.18	-0.53	4.32	76.35
0.189	1.17	0.03	74.96	5.00	-0.89	5.94	260.99	3.79	-0.68	5.08	75.13
0.210	1.15	0.03	74.50	5.04	-1.07	6.65	321.64	3.85	-0.81	5.15	74.67

TABLE B-14 (Continued)

R ~ft.	Q ~in. H_2O	$(P_{st_\infty}-P_{st})$ ~in. H_2O	V_z ~FPS	V_θ* ~FPS	V_r ~FPS	Γ ~ft^2/sec	ζ (sim. var.)	Flow Yaw ~Deg.	Flow Pitch ~Deg.	$V_{\theta_{cor}}$ ~FPS	V_{total} ~FPS
0.231	1.12	0.03	73.41	5.47	-1.09	7.93	388.62	4.24	-0.84	5.57	73.62
0.252	1.09	0.03	72.33	5.58	-1.28	8.83	461.94	4.39	-1.00	5.73	72.56
0.272	1.08	0.02	72.26	5.59	-1.45	9.57	541.58	4.40	-1.14	5.77	72.49
0.293	1.05	0.02	71.17	5.71	-1.48	10.52	627.56	4.56	-1.18	5.90	71.41
0.31	1.04	0.02	70.71	5.76	-1.70	11.36	719.87	4.63	-1.36	6.00	70.9
0.335	1.04	0.02	70.61	5.77	-1.66	12.14	818.51	4.65	-1.34	6.00	70.86
0.356	1.02	0.01	70.22	5.48	-1.85	12.26	923.48	4.44	-1.50	5.79	70.46
0.377	1.01	0.01	69.90	5.19	-1.86	12.28	1034.78	4.22	-1.51	5.51	70.12
0.397	1.01	0.01	69.83	5.20	-1.87	12.98	1152.41	4.23	-1.52	5.52	70.05
0.418	1.01	0.01	69.79	4.87	-1.87	12.80	1276.37	3.97	-1.52	5.21	69.98
0.439	1.01	0.01	69.78	4.54	-1.87	12.52	1406.67	3.70	-1.52	4.91	69.95
0.460	1.01	0.01	69.71	4.54	-1.87	13.13	1543.29	3.71	-1.53	4.91	69.88
0.502	1.01	0.01	69.68	3.87	-1.91	12.21	1835.54	3.17	-1.56	4.32	69.82
0.543	1.01	0.00	69.67	3.54	-1.87	12.08	2153.11	2.89	-1.53	4.00	69.78
0.585	1.01	0.00	69.68	3.20	-1.87	11.77	2496.00	2.62	-1.53	3.71	69.78

*V_θ listed as negative for inboard traverse.

TABLE B-15

PROFILES FOR Z/C=30, V_∞=70 fps AND $\dot{m}$=0.000215 slugs/sec

R ~ft.	Q ~in. H_2O	$(P_{st_\infty}-P_{st})$ ~in. H_2O	V_z ~FPS	V_θ* ~FPS	V_r ~FPS	Γ ~ft^2/sec	ζ (sim. var.)	Flow Yaw ~Deg.	Flow Pitch ~Deg.	$V_{\theta_{cor}}$ ~FPS	V_{total} ~FPS
0.005	1.28	0.16	80.19	-0.27	0.11	0.01	0.12	.19	0.08	-0.29	80.20
0.013	1.27	0.15	79.87	-1.47	-0.05	0.12	0.83	-1.05	-0.04	-1.47	79.88
0.022	1.26	0.14	79.51	-3.01	-0.05	0.41	2.19	-2.16	-0.04	-3.01	79.57
0.030	1.26	0.14	79.20	-4.26	0.27	0.80	4.21	-3.06	0.20	-4.27	79.32
0.038	1.26	0.13	79.11	-4.88	0.11	1.18	6.87	-3.51	0.08	-4.88	79.26
0.047	1.25	0.14	78.84	-6.43	-0.05	1.89	10.18	-4.64	-0.04	-6.43	79.10
0.055	1.23	0.13	78.05	-6.39	-0.06	2.21	14.14	-4.66	-0.04	-6.39	78.31
0.063	1.21	0.11	77.49	-7.14	-0.22	2.84	18.74	-5.24	-0.16	-7.14	77.82
0.072	1.20	0.10	77.17	-7.17	-0.06	3.23	24.00	-5.28	-0.04	-7.17	77.50
0.080	1.17	0.09	76.04	-7.88	-0.23	3.96	29.91	-5.89	-0.17	-7.89	76.45
0.088	1.16	0.08	75.90	-8.21	-0.06	4.56	36.46	-6.14	-0.05	-8.21	76.34
0.097	1.15	0.07	75.57	-8.24	-0.06	5.00	43.67	-6.19	-0.05	-8.24	76.01
0.105	1.14	0.07	75.02	-8.61	-0.24	5.68	51.52	-6.51	-0.18	-8.61	75.51
0.113	1.12	0.06	74.55	-8.33	-0.24	5.93	60.03	-6.35	-0.18	-8.34	75.02
0.122	1.11	0.06	74.21	-8.37	-0.24	6.39	69.18	-6.41	-0.18	-8.37	74.68
0.130	1.09	0.05	73.39	-8.12	-0.25	6.63	78.98	-6.28	-0.19	-8.12	73.84
0.138	1.08	0.04	73.18	-8.46	-0.25	7.36	89.43	-6.56	-0.19	-8.47	73.67
0.159	1.07	0.04	72.70	-8.18	-0.25	8.18	118.39	-6.39	-0.20	-8.19	73.16
0.180	1.05	0.03	72.22	-7.90	-0.25	8.94	151.41	-6.21	-0.20	-7.90	72.65
0.201	1.04	0.03	71.84	-7.60	-0.26	9.59	188.49	-6.01	-0.20	-7.61	72.24
0.222	1.03	0.03	71.42	-7.31	-0.26	10.18	229.63	-5.81	-0.21	-7.31	71.79
0.243	1.03	0.03	71.35	-6.98	-0.26	10.63	274.82	-5.56	-0.21	-6.98	71.69
0.263	1.02	0.02	71.10	-7.00	-0.26	11.58	324.07	-5.59	-0.21	-7.00	71.45
0.284	1.02	0.01	70.91	-6.67	-2.62	11.90	377.37	-5.34	-2.09	-7.16	71.27
0.305	1.01	0.01	70.85	-6.42	-0.33	12.31	434.73	-5.16	-0.26	-6.43	71.14

TABLE B-15 (Continued)

R ~ft.	Q ~in. H_2O	$(P_{st}-P_{st})$ ~in.~H_2O	V_z ~FPS	V_θ* ~FPS	V_r ~FPS	Γ ~ft^2/sec	ζ (sim. var.)	Flow Yaw ~Deg.	Flow Pitch ~Deg.	$V_{\theta cor}$ ~FPS	V_{total} ~FPS
0.326	1.01	0.01	70.70	-6.43	-0.51	13.17	496.15	-5.17	-0.41	-6.45	71.00
0.347	1.01	0.00	70.69	-5.75	-0.51	12.53	561.62	-4.63	-0.41	-5.78	70.93
0.368	1.00	0.00	70.62	-5.76	-0.51	13.30	631.16	-4.64	-0.41	-5.78	70.86
0.388	0.98	0.00	69.86	-5.46	-0.52	13.33	704.74	-4.45	-0.42	-5.49	70.08
0.409	0.97	0.0	69.49	-5.14	-0.89	13.20	782.39	-4.21	-0.73	-5.21	69.68
0.430	0.97	0.0	69.51	-4.79	-0.89	12.93	864.09	-3.92	-0.73	-4.87	69.68
0.451	0.97	-0.00	69.46	-4.44	-0.89	12.57	949.85	-3.64	-0.73	-4.53	69.61
0.472	0.97	-0.00	69.46	-4.44	-0.89	13.15	1039.66	-3.64	-0.73	-4.53	69.61
0.003	1.09	-0.00	74.03	0.35	-0.48	0.01	0.05	0.27	-0.37	0.60	74.03
0.012	1.26	0.14	79.55	1.42	-0.44	0.10	0.64	1.02	-0.32	1.49	79.57
0.020	1.25	0.13	79.21	2.62	-0.77	0.33	1.87	1.88	-0.56	2.73	79.25
0.028	1.26	0.13	79.19	3.22	-0.77	0.57	3.75	2.31	-0.56	3.31	79.26
0.037	1.24	0.13	78.53	3.87	-0.78	0.89	6.28	2.80	-0.57	3.94	78.63
0.045	1.22	0.12	77.79	5.47	-0.79	1.55	9.46	4.00	-0.58	5.53	77.99
0.053	1.21	0.11	77.57	5.80	-0.79	1.94	13.29	4.25	-0.58	5.85	77.79
0.062	1.19	0.10	77.05	6.47	-1.13	2.51	17.77	4.77	-0.83	6.57	77.33
0.070	1.17	0.09	76.16	7.18	-1.14	3.16	22.90	5.36	-0.85	7.27	76.50
0.078	1.14	0.06	75.32	7.27	-1.15	3.58	28.68	5.48	-0.87	7.36	75.68
0.087	1.10	0.04	73.89	8.06	-1.18	4.39	35.10	6.19	-0.90	8.14	74.34
0.095	1.10	0.04	73.72	8.08	-1.18	4.82	42.18	6.22	-0.91	8.16	74.17
0.112	1.07	0.03	72.65	8.53	-1.20	5.98	58.27	6.66	-0.93	8.61	73.16
0.132	1.05	0.02	72.08	8.28	-1.56	6.89	82.04	6.52	-1.23	8.42	72.57
0.153	1.03	0.01	71.41	8.36	-1.58	8.06	109.87	6.64	-1.25	8.51	71.92
0.174	1.02	0.01	71.05	8.08	-1.59	8.84	141.76	6.46	-1.26	8.24	71.53
0.195	1.01	0.01	70.66	7.81	-1.41	9.56	177.70	6.27	-1.13	7.93	71.11

TABLE B-15 (Continued)

R ~ft.	Q ~ in. H_2O	$(P_{st_\infty}-P_{st})$ ~in. H_2O	V_z ~FPS	V_θ* ~FPS	V_r ~FPS	Γ ~ft^2/sec	ζ (sim. var.)	Flow Yaw ~Deg.	Flow Pitch ~Deg.	$V_{\theta_{cor}}$ ~FPS	V_{total} ~FPS
0.216	1.01	0.01	70.63	7.15	-1.42	9.70	217.70	5.75	-1.14	7.29	71.00
0.237	1.00	0.00	70.56	6.83	-1.42	10.15	261.75	5.50	-1.14	6.98	70.90
0.262	1.00	0.00	70.56	6.50	-1.24	10.68	319.98	5.23	-1.00	6.61	70.87
0.278	0.99	0.00	70.17	6.20	-1.25	10.85	362.04	5.03	-1.01	6.33	70.45
0.299	0.98	0.00	69.80	5.90	-1.25	11.09	418.26	4.81	-1.02	6.03	70.06
0.320	0.98	0.0	69.80	5.56	-1.44	11.18	478.54	4.53	-1.17	5.74	60.03
0.341	0.97	-0.00	69.28	5.26	-1.45	11.27	542.88	4.32	-1.19	5.46	69.50
0.362	0.97	-0.00	69.28	5.26	-1.45	11.96	611.28	4.32	-1.19	5.46	69.50
0.382	0.96	-0.00	68.94	4.95	-1.64	11.89	683.73	4.08	-1.36	5.21	69.14
0.424	0.95	-0.00	68.58	4.98	-1.65	13.27	840.80	4.13	-1.37	5.25	68.78

*V_θ listed as negative for inboard traverse.

TABLE B-16

PROFILES FOR Z/C=30, V_∞=70 fps, $\dot{m}$=0.00038 slugs/sec

R ~ft.	Q ~in. H_2O	$(P_{st_\infty}-P_{st})$ ~in. H_2O	V_z ~FPS	V_θ* ~FPS	V_r ~FPS	Γ ~ft^2/sec	ζ (sim. var.)	Flow Yaw ~Deg.	Flow Pitch ~Deg.	$V_{\theta_{cor}}$ ~FPS	V_{total} ~FPS
0.007	1.26	0.06	78.06	-0.18	-0.13	0.01	0.22	-0.13	0.10	-0.23	78.06
0.019	1.26	0.06	78.06	-0.48	-0.13	0.06	1.80	-0.35	0.10	-0.50	78.06
0.032	1.26	0.06	78.06	-1.07	-0.29	0.21	4.92	-0.78	0.21	-1.11	78.06
0.044	1.26	0.06	78.05	-1.47	-0.29	0.41	9.56	-1.07	0.21	-1.50	78.06
0.057	1.26	0.06	78.04	-1.77	-0.29	0.63	15.74	-1.29	0.21	-1.79	78.06
0.069	1.26	0.06	77.87	-2.38	-0.29	1.03	23.45	-1.74	0.21	-2.39	77.91
0.082	1.24	0.06	77.40	-2.69	-0.30	1.38	32.69	-1.98	0.22	-2.71	77.44
0.094	1.23	0.06	77.07	-3.01	-0.30	1.78	43.47	-2.23	0.22	-3.02	77.13
0.115	1.22	0.05	76.59	-3.33	-0.14	2.41	64.83	-2.48	0.10	-3.34	76.66
0.136	1.21	0.04	76.10	-3.66	-0.30	3.13	90.44	-2.74	0.23	-3.68	76.19
0.157	1.19	0.04	75.69	-4.30	-0.30	4.24	120.31	-3.24	0.23	-4.31	75.81
0.178	1.18	0.04	75.26	-4.64	-0.14	5.17	154.44	-3.51	0.11	-4.64	75.40
0.198	1.16	0.03	74.43	-5.00	-0.14	6.23	192.82	-3.82	0.11	-5.00	74.60
0.219	1.15	0.03	74.11	-5.02	-0.14	6.91	235.46	-3.85	0.11	-5.02	74.28
0.240	1.15	0.03	74.11	-5.02	-0.14	7.56	282.35	-3.85	0.11	-5.02	74.28
0.261	1.12	0.03	73.35	-5.06	+0.02	8.30	333.49	-3.93	-0.02	-5.06	73.53
0.303	1.11	0.03	72.88	-4.77	+0.02	9.07	448.55	-3.73	-0.02	-4.77	73.03
0.344	1.11	0.02	72.83	-4.45	+0.36	9.63	580.63	-3.48	-0.29	-4.47	72.96
0.386	1.09	0.02	72.35	-4.15	+0.54	10.07	729.73	-3.27	-0.42	-4.19	72.47
0.428	1.09	0.01	72.20	-3.83	+0.54	10.30	895.84	-3.03	-0.43	-3.87	72.30
0.469	1.08	0.01	71.87	-3.52	+0.89	10.38	1078.98	-2.79	-0.70	-3.63	71.96
0.511	1.07	0.01	71.82	-3.19	+0.89	10.25	1279.14	-2.53	-0.70	-3.32	71.90
0.553	1.06	0.01	71.35	-3.21	+0.89	11.15	1496.32	-2.57	-0.71	-3.33	71.43
0.594	1.06	0.01	71.36	-2.88	+0.89	10.75	1730.52	-2.30	-0.71	-3.02	71.42
0.006	1.23	0.06	77.13	0.43	0.18	0.02	0.17	0.32	0.13	0.47	77.13

TABLE B-16 (Continued)

R ~ft.	Q ~in. H_2O	$(P_{st_\infty}-P_{st})$ ~in. H_2O	V_z ~FPS	V_θ* ~FPS	V_r ~FPS	Γ ~ ft^2/sec	ζ (sim. var.)	Flow Yaw ~Deg.	Flow Pitch ~Deg.	$V_{\theta_{cor}}$ ~FPS	V_{total} ~FPS
0.018	1.23	0.06	77.13	0.73	0.18	0.08	1.65	0.54	0.13	0.75	77.13
0.031	1.23	0.06	77.13	1.02	0.02	0.20	4.66	0.75	0.01	1.02	77.13
0.043	1.23	0.06	77.11	1.61	0.02	0.44	9.20	1.19	0.01	1.61	77.13
0.056	1.23	0.06	77.05	1.90	0.02	0.67	15.28	1.41	0.01	1.90	77.07
0.068	1.23	0.06	76.88	2.20	0.02	0.94	22.89	1.63	0.01	2.20	76.91
0.081	1.21	0.06	76.46	2.51	0.02	1.28	32.03	1.87	0.01	2.51	76.51
0.097	1.21	0.06	76.45	2.81	0.02	1.72	46.60	2.09	0.01	2.81	76.51
0.114	1.22	0.06	76.43	3.41	0.02	2.45	63.89	2.54	0.01	3.41	76.51
0.135	1.21	0.06	76.10	3.73	0.02	3.17	89.34	2.79	0.01	3.73	76.19
0.156	1.19	0.06	75.45	4.08	-0.31	4.00	119.04	3.08	-0.23	4.09	75.56
0.197	1.17	0.05	74.95	4.43	-0.48	5.49	191.20	3.36	-0.36	4.45	75.08
0.239	1.18	0.04	75.11	4.41	-0.48	6.63	280.39	3.35	-0.36	4.44	75.24
0 281	1.16	0.04	74.53	4.46	-0.48	7.86	386.59	3.40	-0.37	4.48	74.67
0.322	1.13	0.03	73.73	4.83	-0.49	9.79	509.82	3.73	-0.38	4.86	73.89
0.364	1.11	0.03	72.93	4.90	-0.83	11.20	650.07	3.82	-0.65	4.97	73.10
0.406	1.07	0.03	71.48	5.02	-1.20	12.79	807.33	3 99	-0.95	5.16	71.67
0.447	1.06	0.02	71.11	5.05	-1.20	14.19	981.62	4.04	-0.96	5.19	71.30
0.489	1.04	0.02	70.70	5.08	-1.21	15.62	1172.93	4.09	-0.97	5.22	70.89
0.531	1.03	0.02	70.27	4.79	-1.22	15.97	1381.26	3.88	-0.99	4.94	70.45
0.572	1.02	0.02	69.92	4.82	-1.58	17.32	1606.61	3.92	-1.28	5.07	70.11
0.614	1.02	0.01	69.77	4.50	-1.58	17.35	1848.97	3.67	-1.29	4.77	69.93
0.656	1.01	0.01	69.72	4.17	-1.59	17.17	2108.36	3.40	-1.29	4.46	69.86
0.697	1.01	0.01	69.60	3.84	-1.59	16.83	2384.77	3.14	-1.30	4.06	69.73
0.739	1.01	0.00	69.46	3.85	-1.59	17.88	2678.20	3.16	-1.30	4.17	69.59
0.781	1.01	0.00	69.48	3.52	-1.59	17.25	2988.65	2.88	-1.30	3.86	69.59

*V_θ iisted as negative for inboard traverse.

C 3

TABLE I

SUMMARY OF DETAILED AIRCRAFT VORTEX EXPERIMENTS OF INTEREST

Investigator	Date	Ref.	Instrumentation	Model	V_∞	Distance Downstream	Mass Injection	Comments
Fage & Simmons	1926	6	Hot Wire	Rect. Wing b/2=3', c=.5'	50FPS	z/c = .573, 2, 13	---	8% over velocity in core
Mowforth	1959	7	Pitot Tube Static Probe Yawmeter	Rect. Wing b/c=4.2", c=1.5" α=6°	100FPS	z/c = 7.7, 10.25	---	No velocity profiles present
Gasparek	1961	8	Yawmeter	Rect. Wing b/2=10.5", c=3" α=8°	9FPS	z/c = 1,2,4, 6,8.7	---	Neglects static pressure
Hoffman & Joubert	1963	10	Yawmeter	Split Wing 6" chord	65FPS	z/c = 8.3, 9.8	---	Circulation results
Chigier & Corsiglia	1971	9	Hot Wire	Rect. Wing b/2 =4', c = 1.5' α = 12°	100FPS	z/c = -.75, -.5 -.25, 0., 2.0, 4.0	---	Over velocity in core

TABLE I (Continued)

Investigator	Date	Ref.	Instrumentation	Model	V_∞	Distance Downstream	Mass Injection	Comments
Poppleton	1971	12	Hot Wire	Split Wing	70FPS	90", 157", 213"	X	Effects of mass injection
Mason	1971	--	Yawmeter	Rect. Wing, b/2=4', c=.666' $\alpha=7\frac{1}{2}°$	70FPS	z/c=10,15, 20,25, 30	X	Complete data

TABLE 2

WING CHARACTERISTICS INCLUDING JET OPERATING CONDITIONS

Wing Characteristics
Chord = 2/3 ft.
Semi-span = 4 ft.
Angle of Attack = 7-1/2°
Airfoil = NACA 0012
$Re_C = 2.5 \times 10^5, 3.5 \times 10^5$
$C_L = .674$
$\dot{m} = 2.15 \times 10^{-4}, 3.3 \times 10^{-4}$ slugs/sec

TABLE 3

PARAMETER STUDY

Test	Z/C	Q (Dyn. Press)	Wing	Mass Injection[(a)]
1	10	1" H_2O	Clean	----
2		2" H_2O	Clean	----
3		1" H_2O	Mod.	0
4		1" H_2O	Mod.	Moderate
5		1" H_2O	Mod.	Full
6	15	1" H_2O	Clean	----
7		2" H_2O	Clean	----
8	20	1" H_2O	Clean	----
9		2" H_2O	Clean	----
10		1" H_2O	Mod.	0
11		1" H_2O	Mod.	Moderate
12		1" H_2O	Mod.	Full
13	25	1" H_2O	Clean	----
14		2" H_2O	Clean	----
15	30	1" H_2O	Clean	----
16		2" H_2O	Clean	----
17		1" H_2O	Mod.	0
18		1" H_2O	Mod.	Moderate
19		1" H_2O	Mod.	Full

(a) moderate - $\dot{m}$ = 0.000215 slugs/sec
full $\dot{m}$ = 8.00035 slugs/sec

TABLE 4

SUMMARY OF DATA FIGURES

Figure No.	Variables	Parameter	Comments
20	Γ/Γ_o vs R/S	Aspect Ratio	Rectangular Wings
21	Γ/Γ_o vs R/S	Twist Angle	Rectangular Wings
22	Γ/Γ_o vs R/S	Taper Ratio	Tapered Wings
23	V_θ vs R	Angle of Attack	Wind Tunnel Model
24	V_θ vs R	Mass Flow	V_∞ = 70 FPS, Z/C = 10
25	V_θ vs R	----	V_∞ = 70 FPS, Z/C = 15
26	V_θ vs R	Mass Flow	V_∞ = 70 FPS, Z/C = 20
27	V_θ vs R	----	V_∞ = 70 FPS, Z/C = 25
28	V_θ vs R	Mass Flow	V_∞ = 70 FPS, Z/C = 30
29	V_θ vs R	----	V_∞ = 100 FPS, Z/C = 10
30	V_θ vs R	----	V_∞ = 100 FPS, Z/C = 15
31	V_θ vs R	----	V_∞ = 100 FPS, Z/C = 20
32	V_θ vs R	----	V_∞ = 100 FPS, Z/C = 25
33	V_θ vs R	----	V_∞ = 100 FPS, Z/C = 30
34	V_z vs R	Mass Flow	V_∞ = 70 FPS
35	V_z vs R	----	V_∞ = 100 FPS
36	P_{st} vs R	Mass Flow	V_∞ = 70 FPS
37	P_{st} vs R	----	V_∞ = 100 FPS
38	Γ vs R	Mass Flow	V_∞ = 70 FPS
39	Γ vs R	----	V_∞ = 100 FPS
40	Γ vs lnR	----	V_∞ = 70 FPS
41	ν_T/ν vs Z/C	$V_{\theta max}$, A_c	Based on Std. Viscous Theory
42	$V_{\theta max}$ vs Z/C	V_∞, $\dot{m}$	----
43	A_c vs Z/C	V_∞, $\dot{m}$	----
44	$P_{st_{r=0}}$ vs Z/C	V_∞, $\dot{m}$	----
45	$V_{\theta max}$, A_c vs $\dot{m}$	----	Z/C = 30

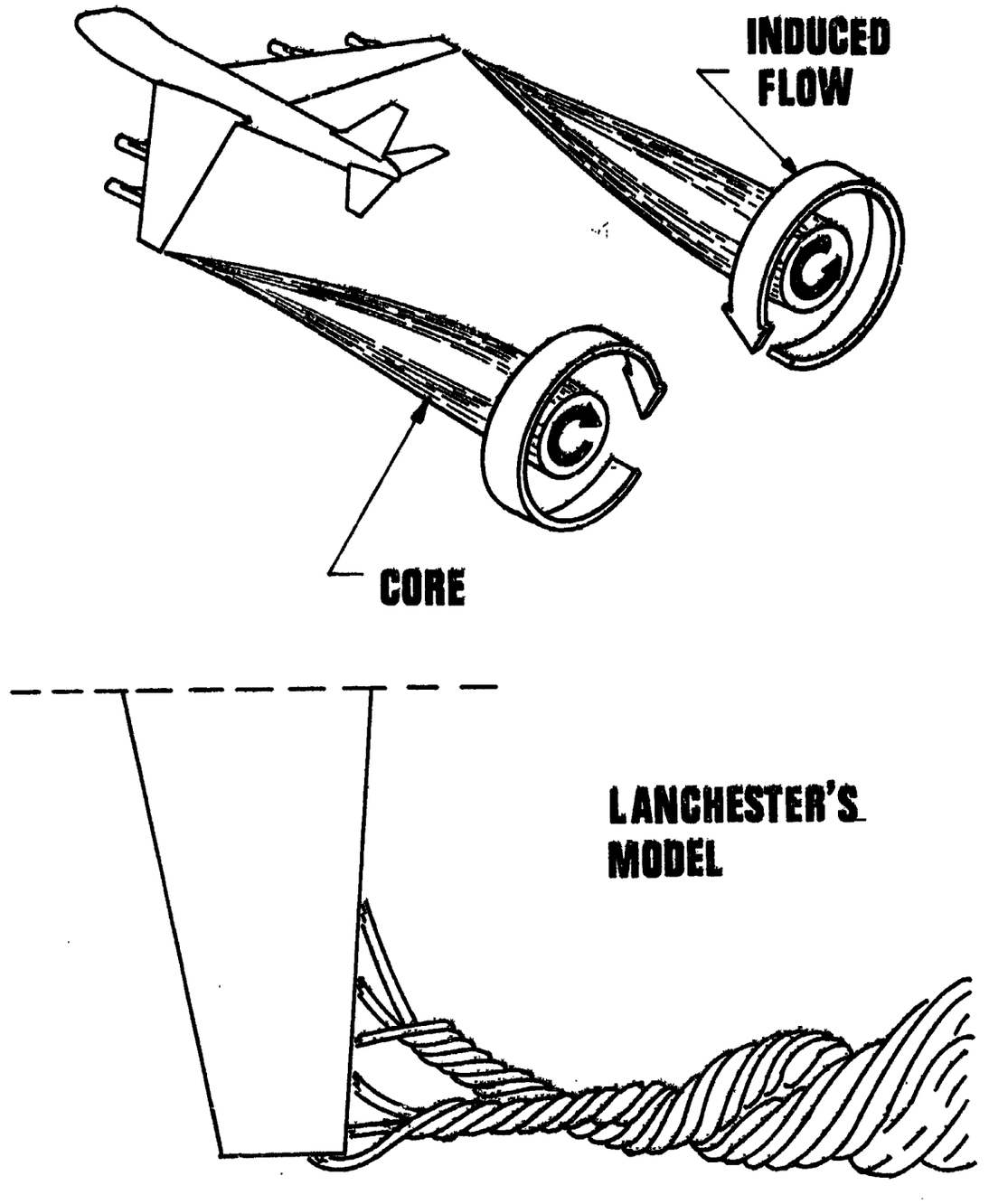

FIG 1 ILLUSTRATION OF TRAILING VORTEX

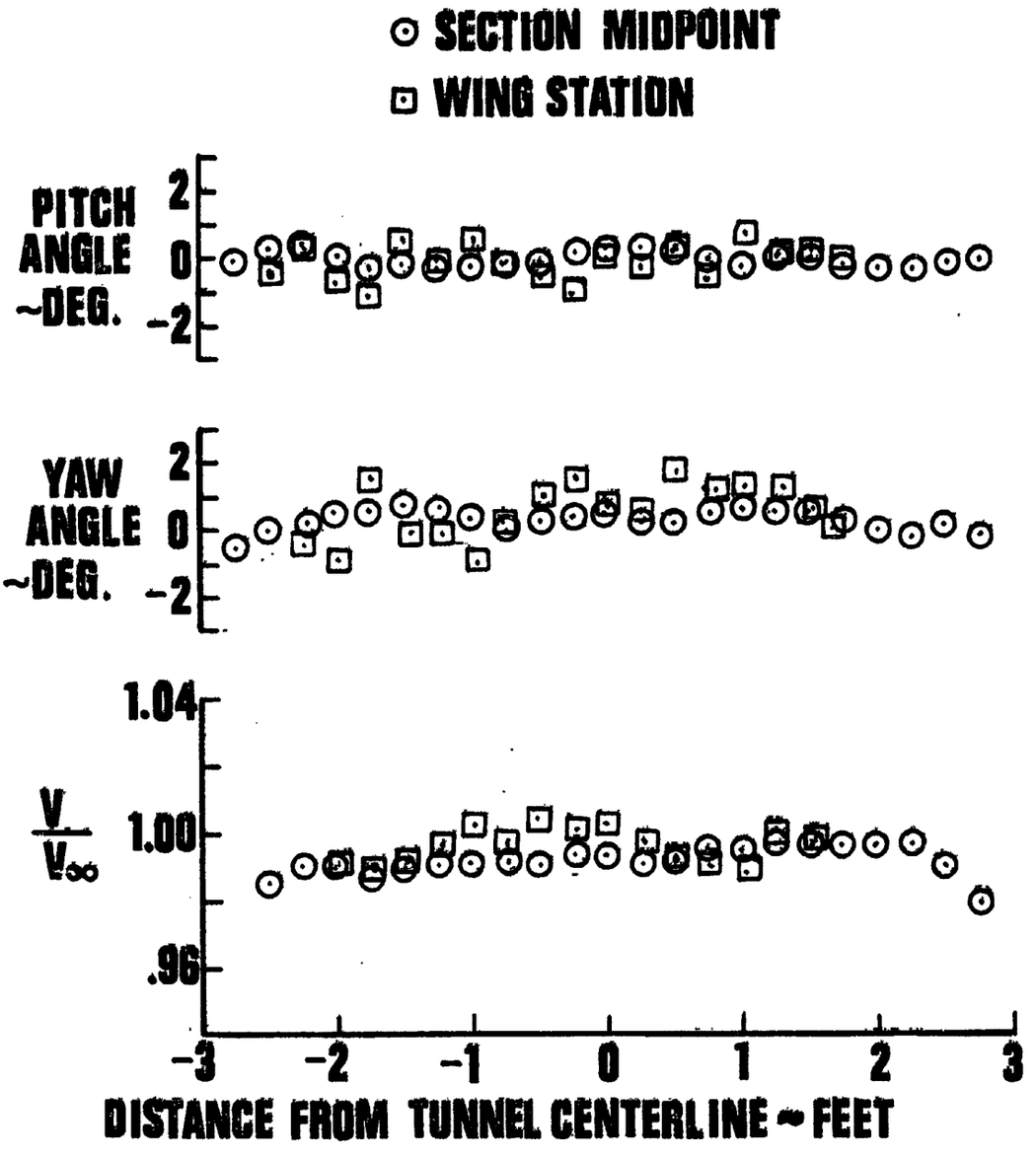

FIG. 2 CALIBRATION OF VIRGINIA TECH 6-FOOT SUBSONIC WIND TUNNEL V_∞ = 70 FPS

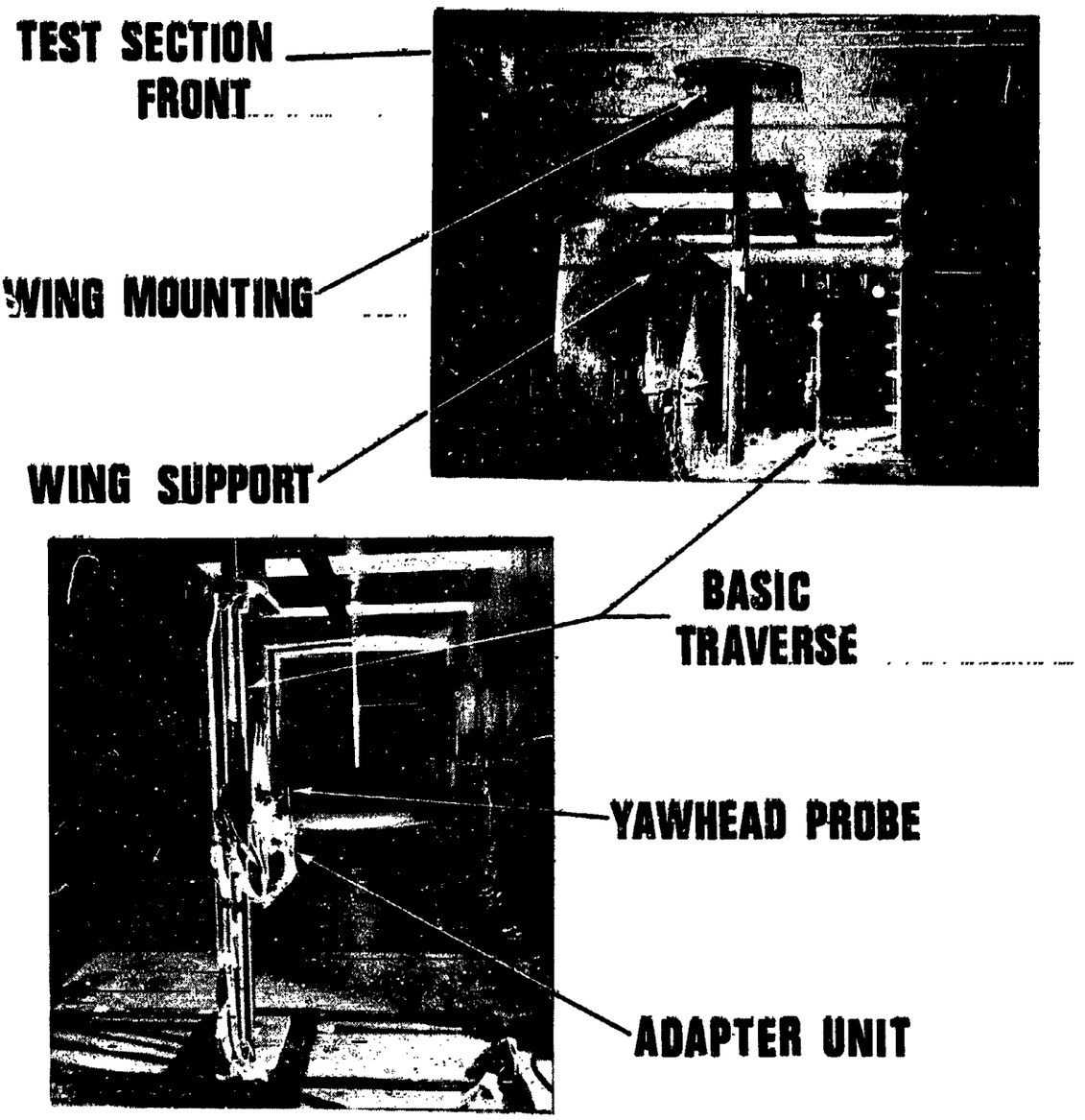

FIG.3 WIND TUNNEL TEST SET UP

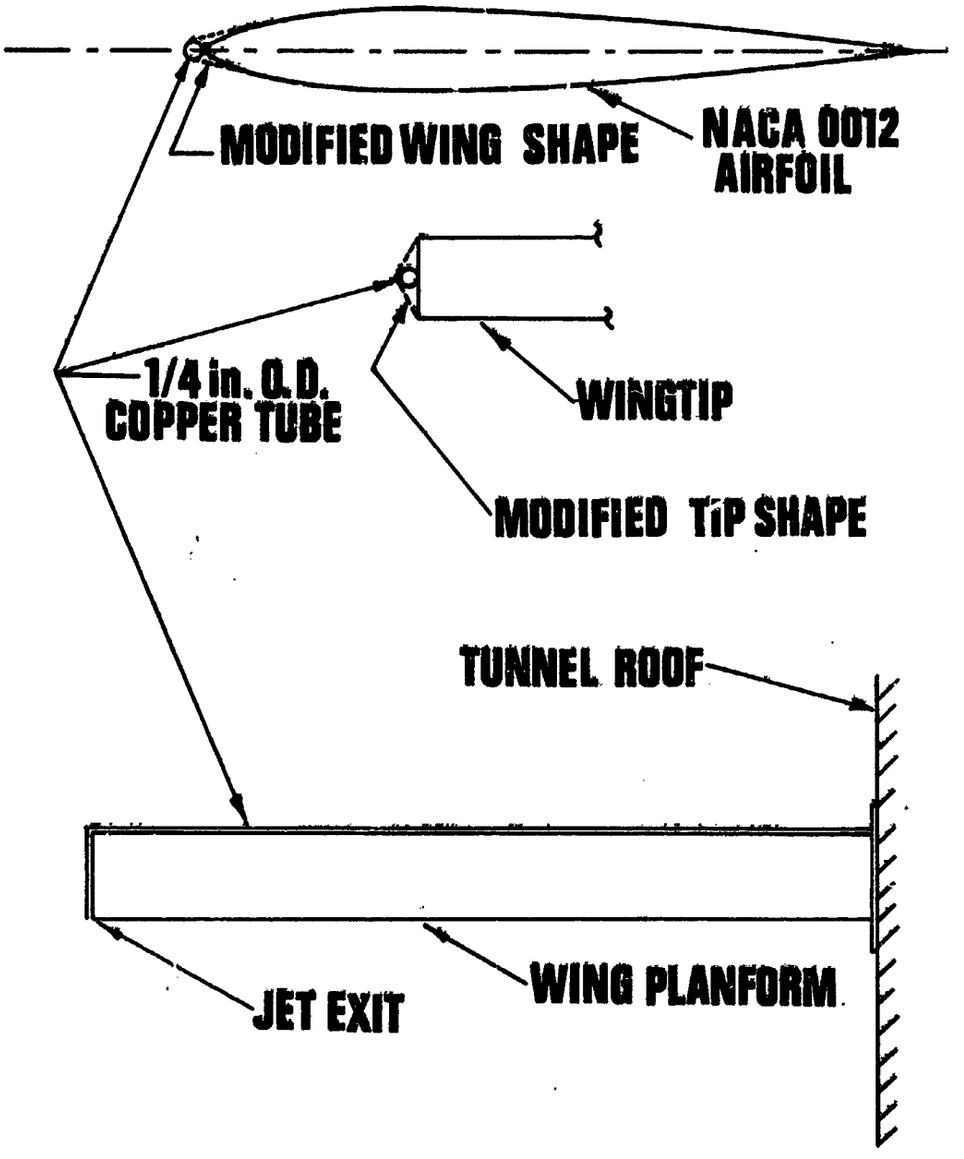

FIG. 4 WING AND MODIFICATION

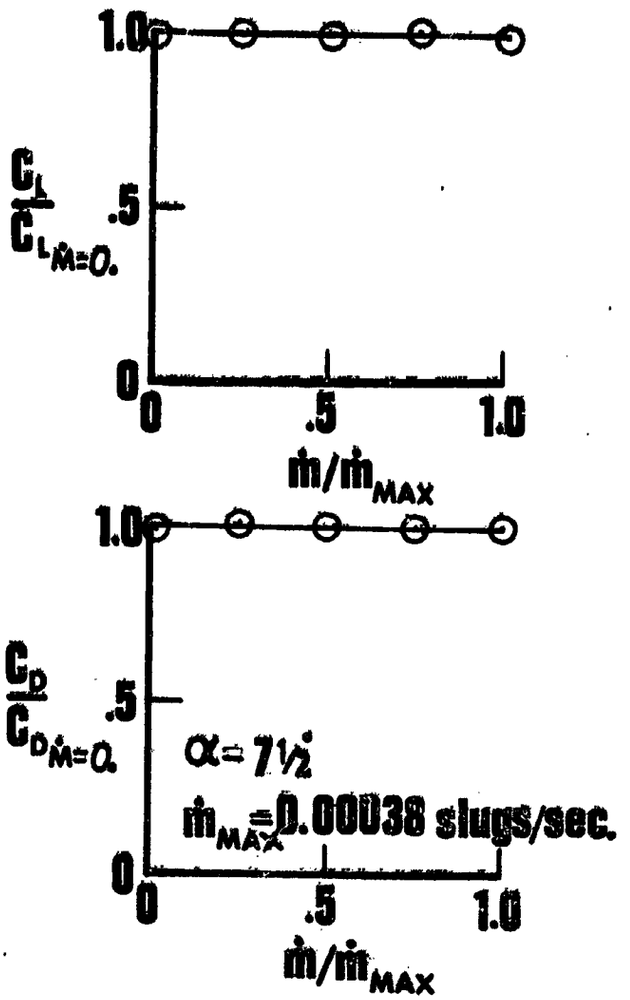

FIG.5 EFFECT OF MASS INJECTION ON WING FORCE COEFFICIENTS

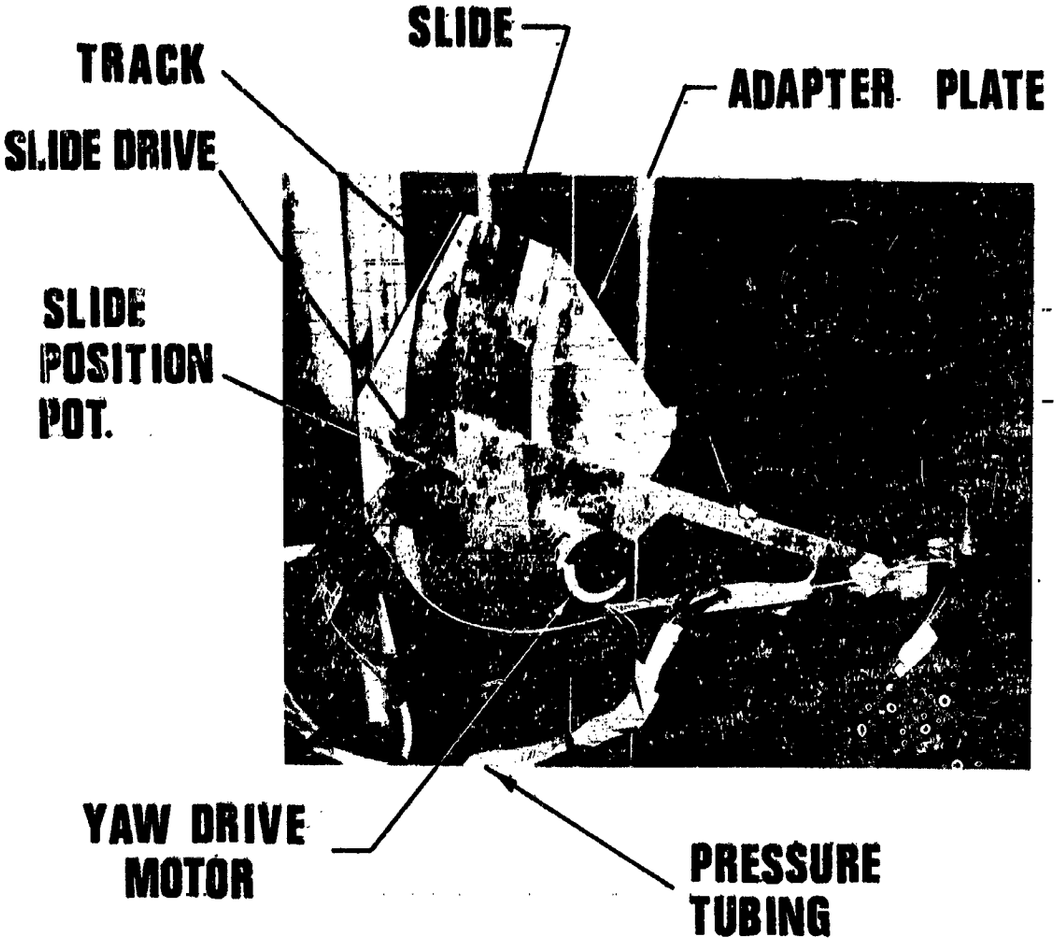

FIG.6 ADAPTER UNIT

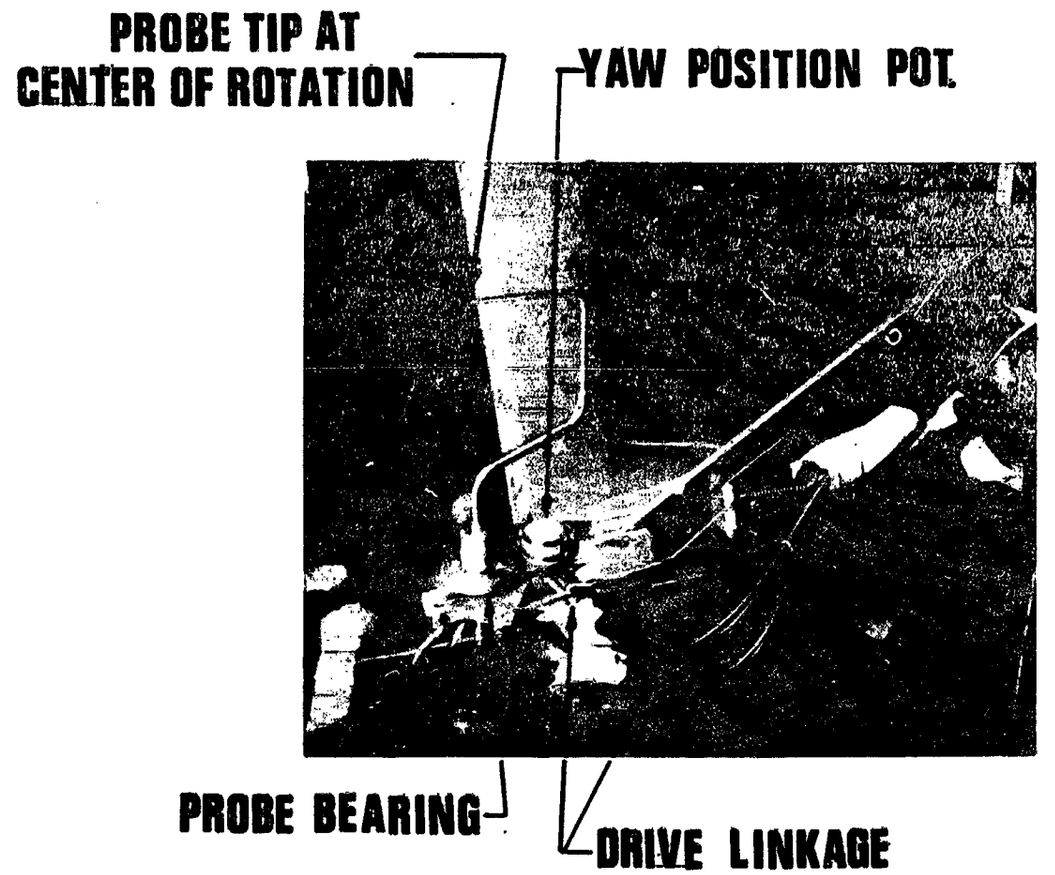

FIG. 7 DETAILS OF PROBE MOUNTING

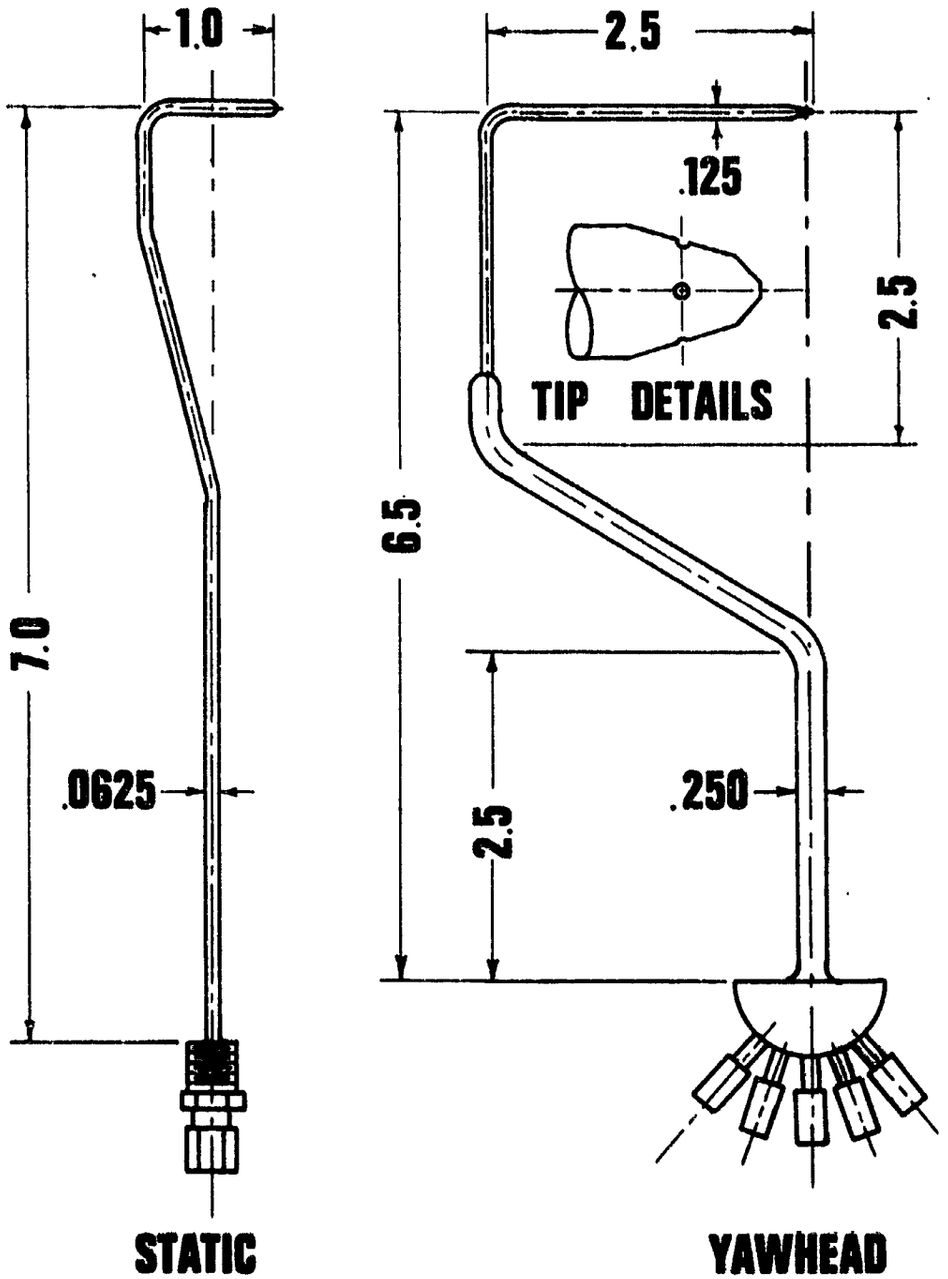

FIG. 8 YAWHEAD AND STATIC PROBES

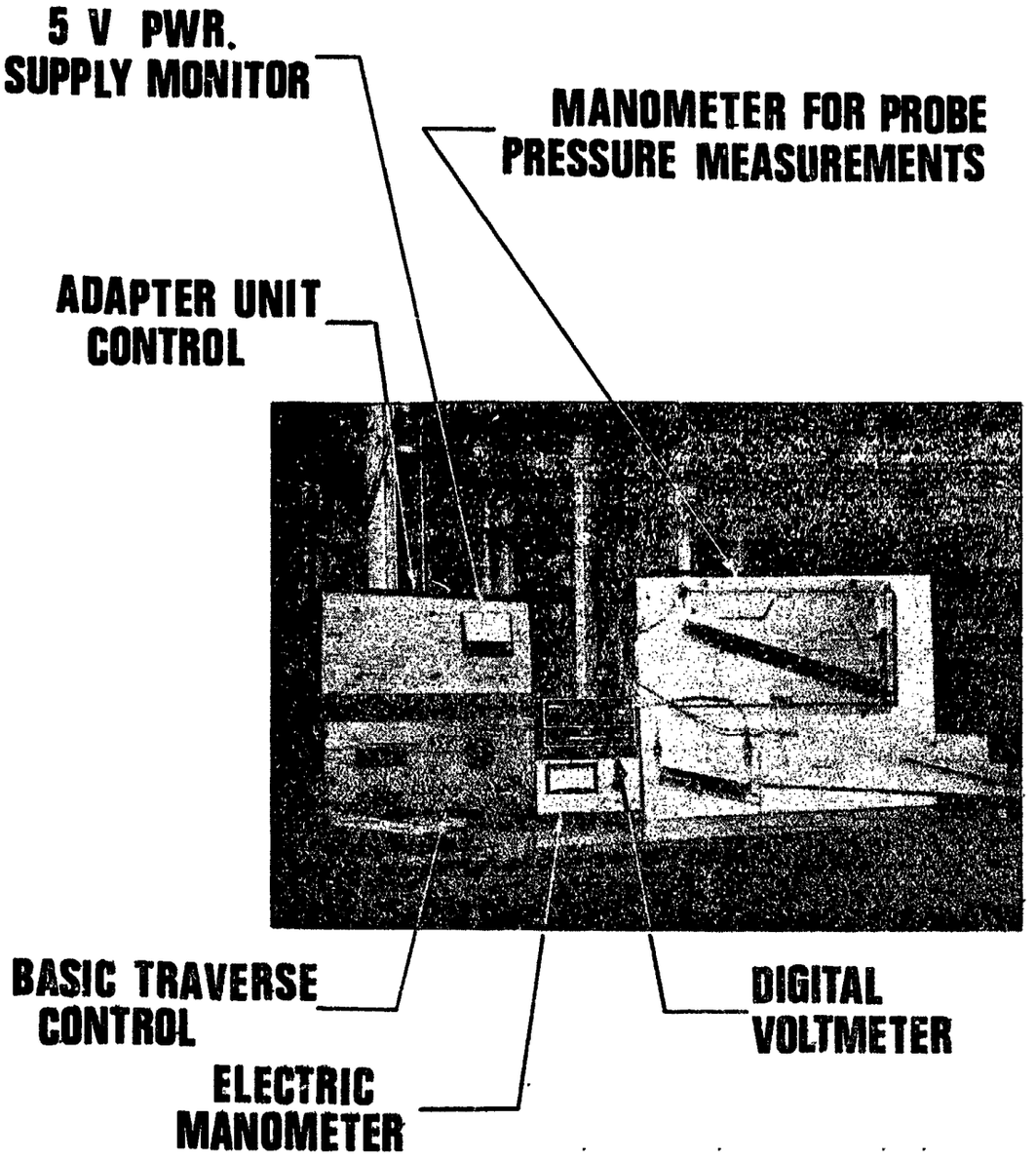

FIG. 9 SPECIAL CONTROL AND DATA RECORDING SET UP

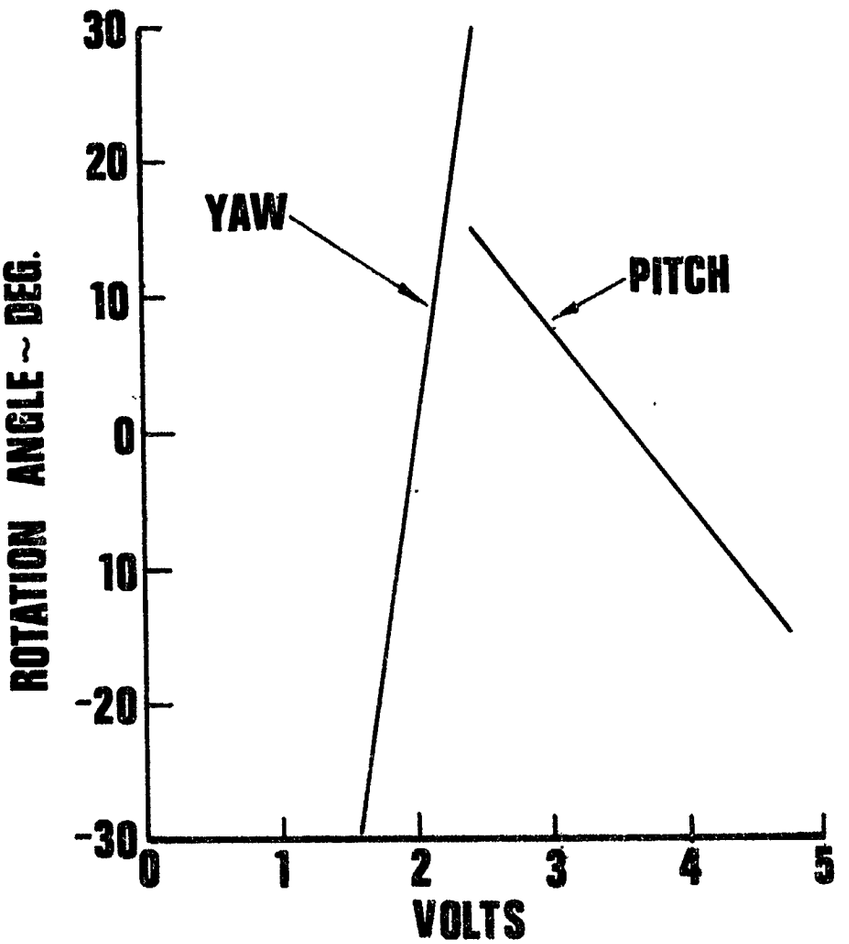

FIG. 10 TYPICAL PROBE POSITION CALIBRATION

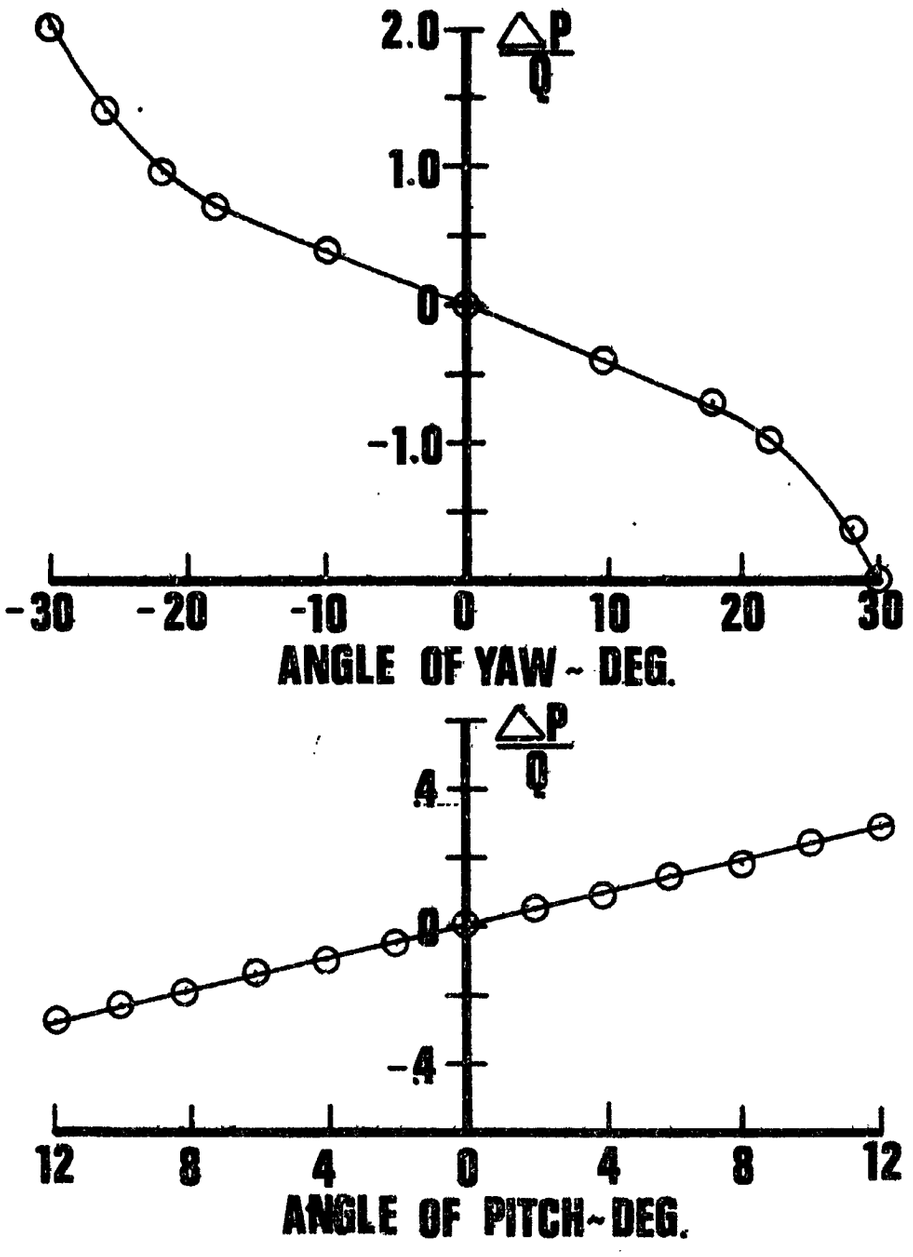

FIG. 11 FLOW ANGULARITY CALIBRATION

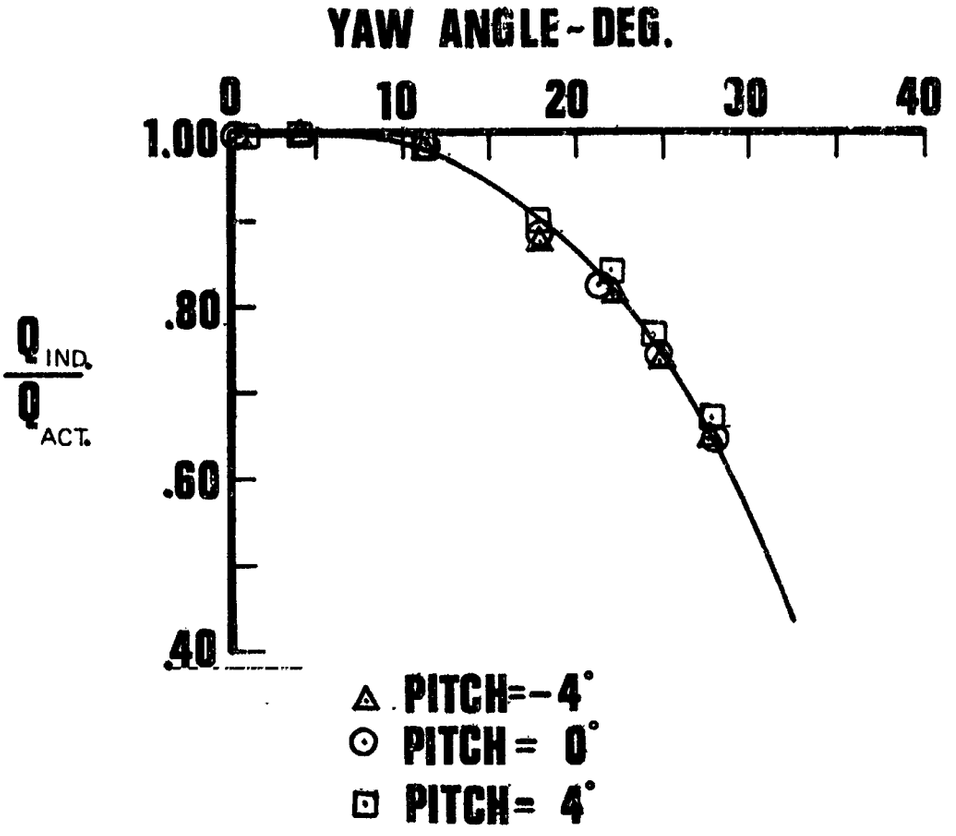

FIG 12 DYNAMIC PRESSURE CALIBRATION

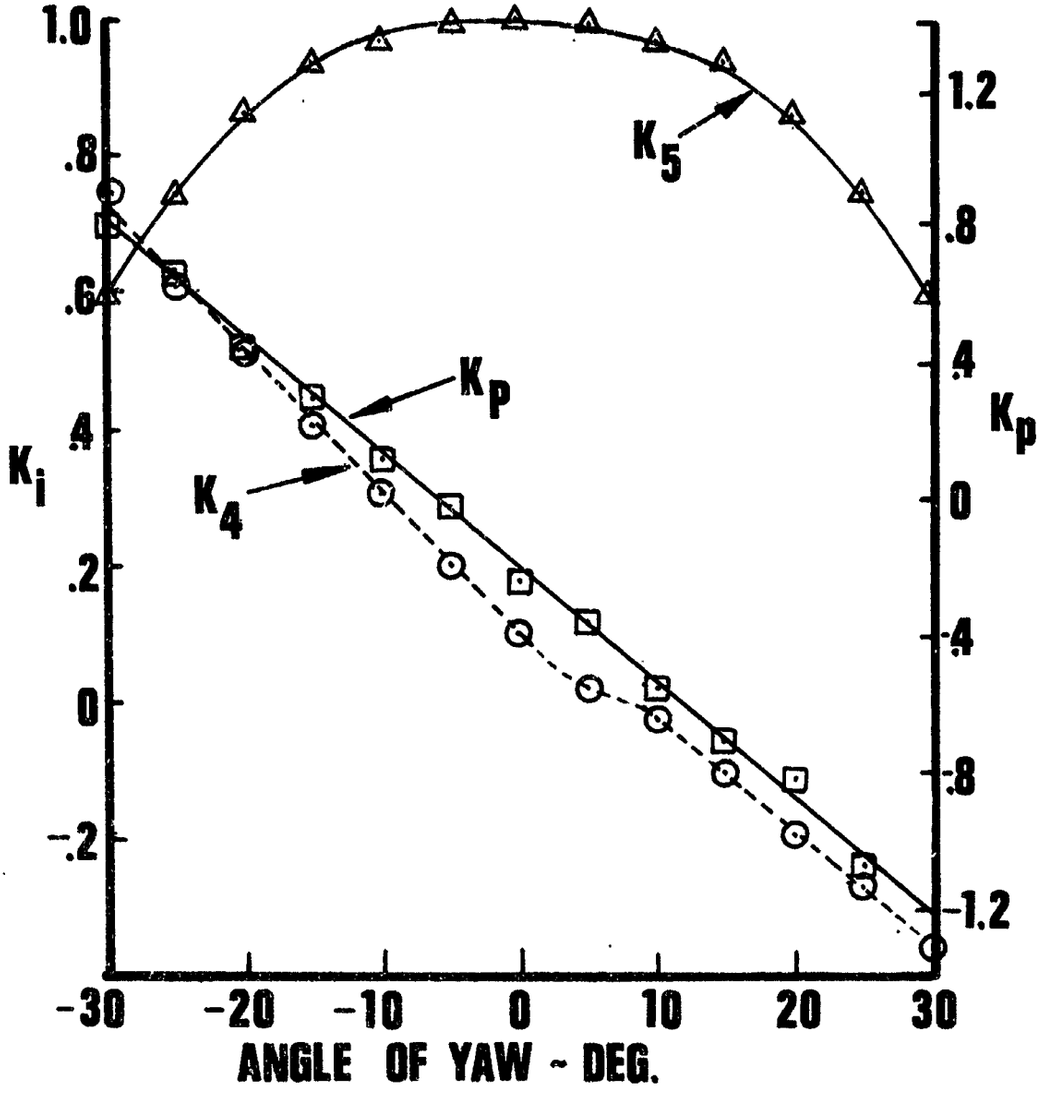

FIG 13 CALIBRATION FOR STATIC PRESSURE FROM YAWHEAD

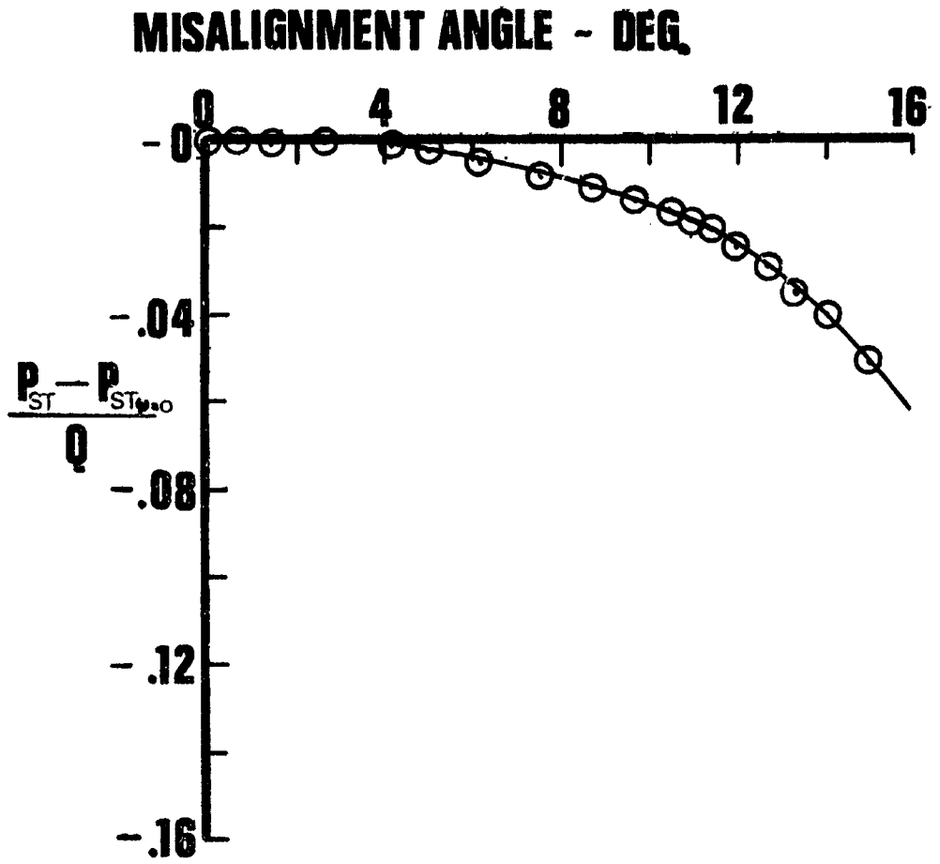

FIG 14 STATIC PROBE CALIBRATION

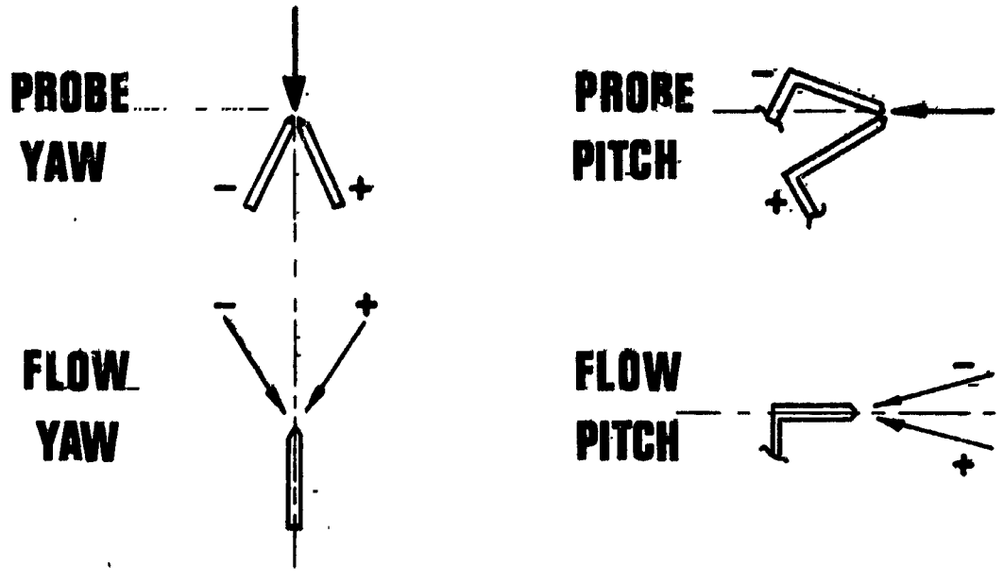

YAW ANGLE = PROBE YAW − FLOW YAW

PITCH ANGLE = PROBE PITCH − FLOW PITCH

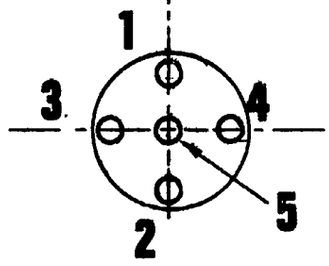

PROBE TIP

LOOKING DOWNSTREAM

FIG. 15 SIGN CONVENTIONS

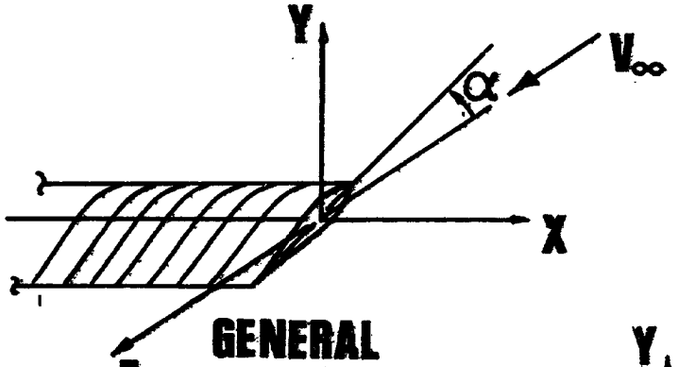

GENERAL DESCRIPTION

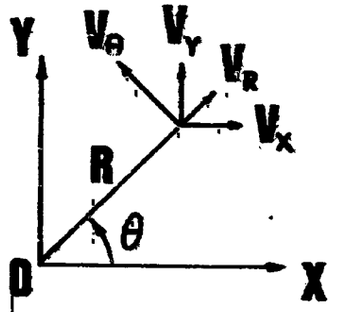

RELATION BETWEEN X, Y AND R, θ

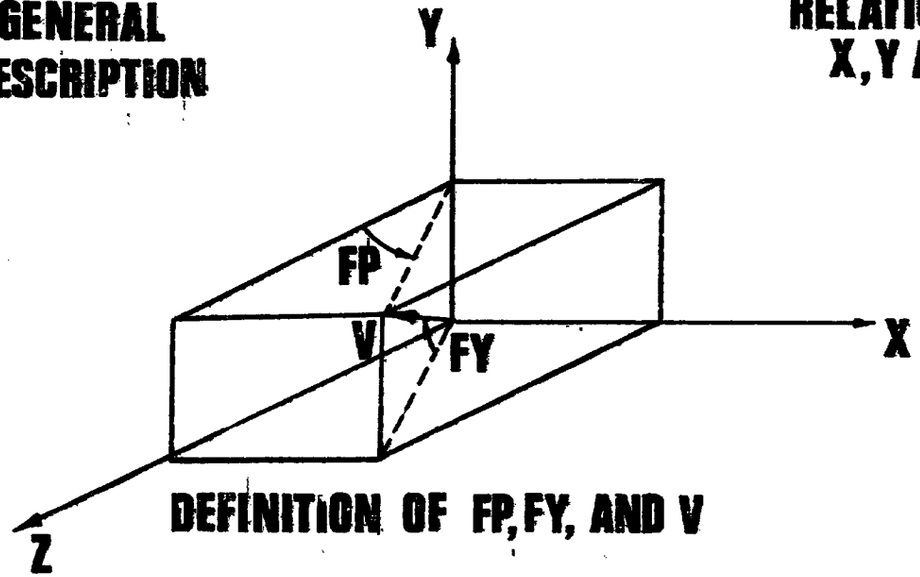

DEFINITION OF FP, FY, AND V

FIG. 16 COORDINATE SYSTEMS

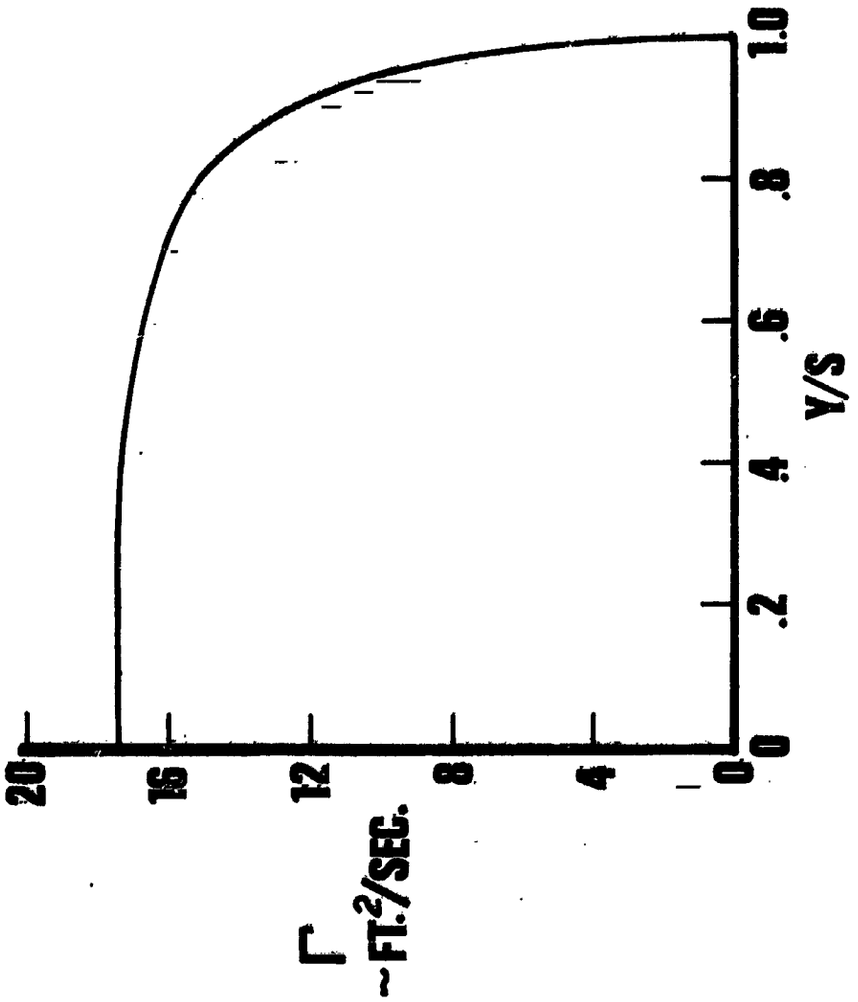

FIG. 17 CIRCULATION DISTRIBUTION ON WIND TUNNEL MODEL

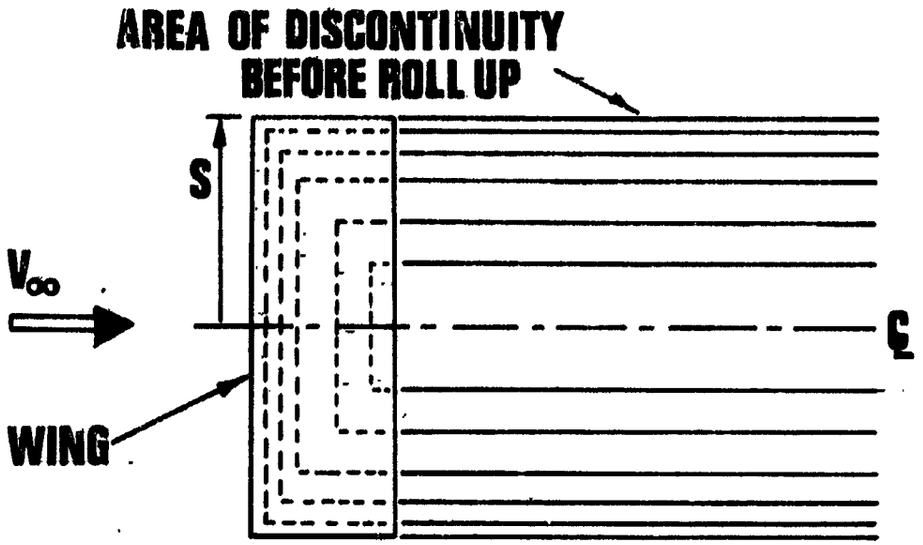

HORSESHOE VORTEX SUPERPOSITION

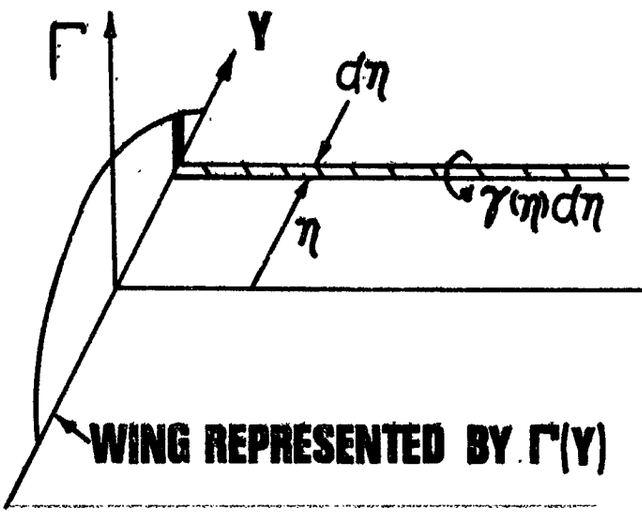

FIG. 18 CIRCULATION DISTRIBUTION CONCEPTS

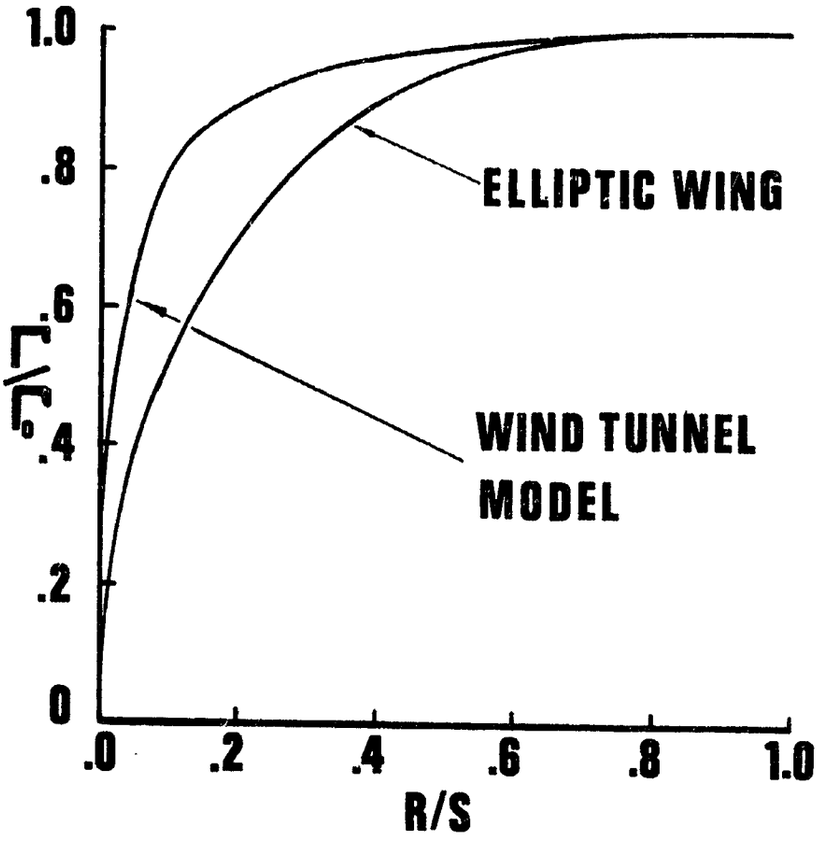

FIG. 19 GENERALIZED SOLUTION FOR THE ELLIPTIC WING CASE OF BETZ AND THE WIND TUNNEL MODEL

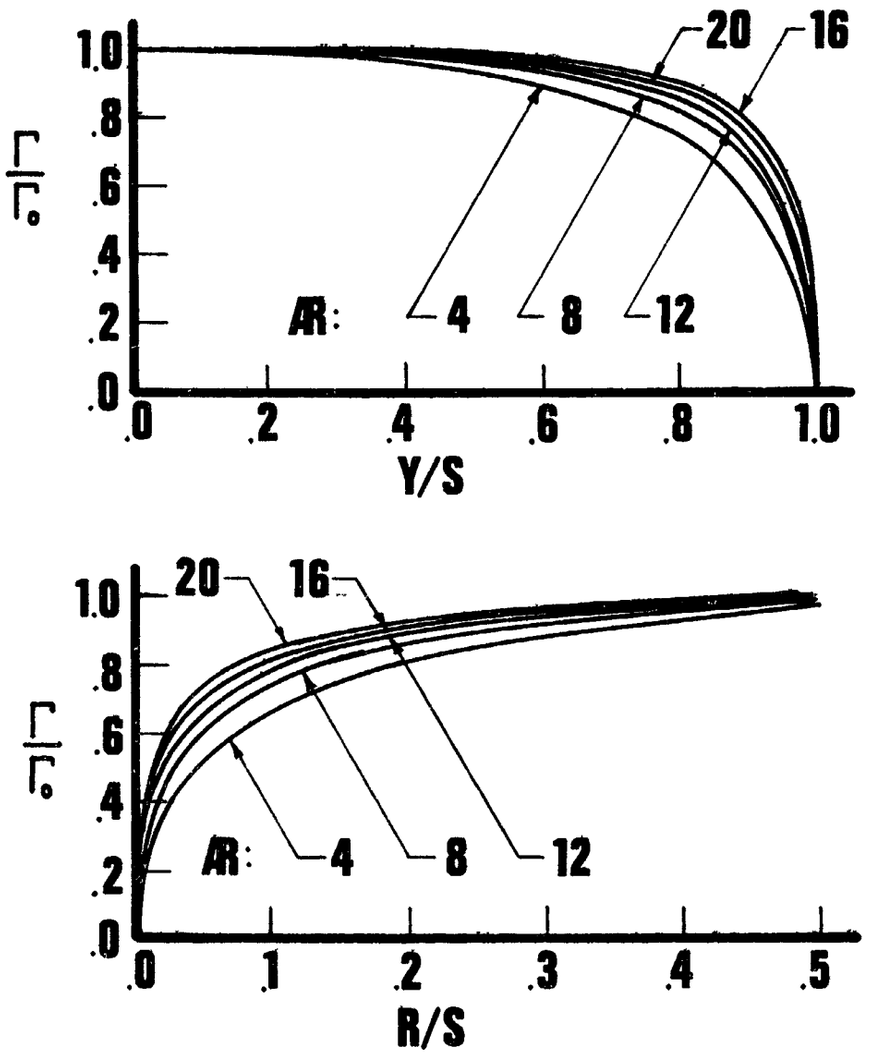

FIG. 20 RELATION OF RECTANGULAR WING AND VORTEX CIRCULATION DISTRIBUTION FOR VARIOUS ASPECT RATIOS

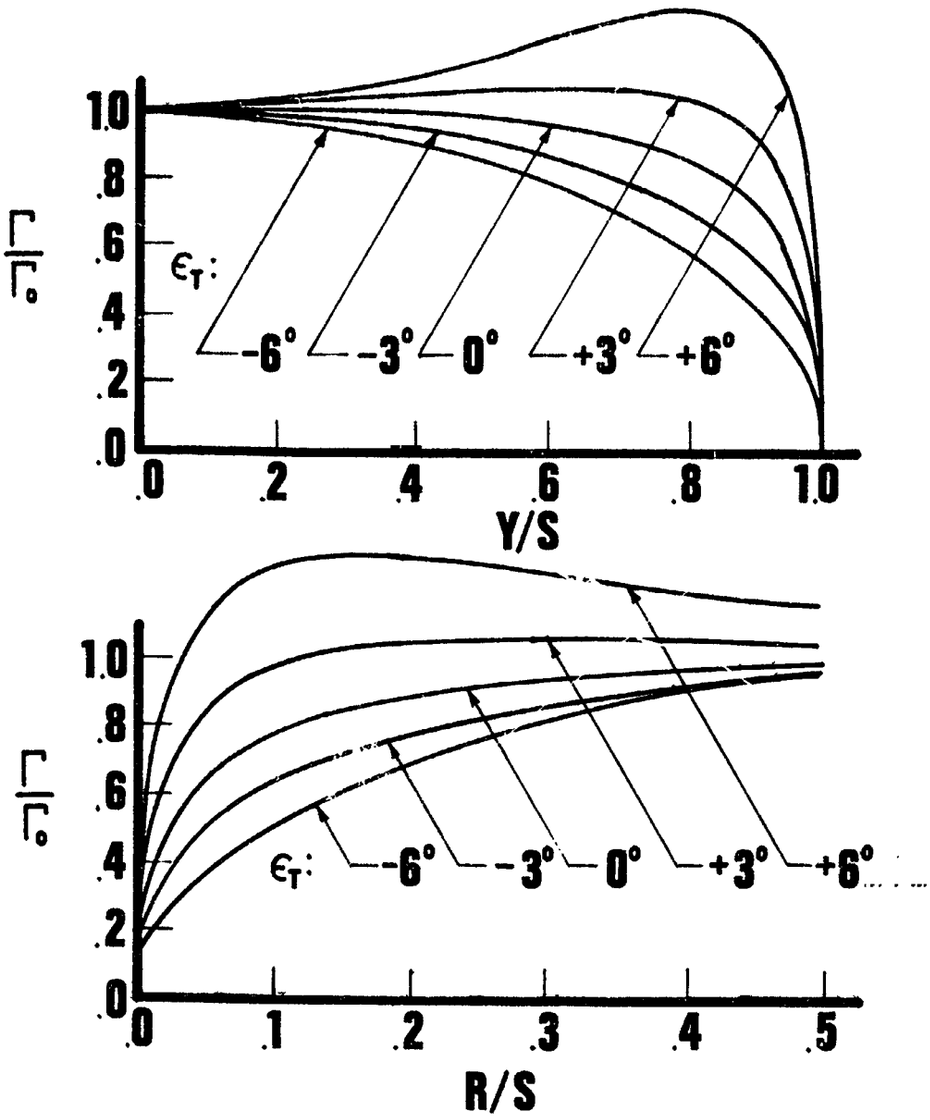

FIG. 21 RELATION OF RECTANGULAR WING AND VORTEX CIRCULATION DISTRIBUTION FOR VARIOUS WING TWIST ANGLES

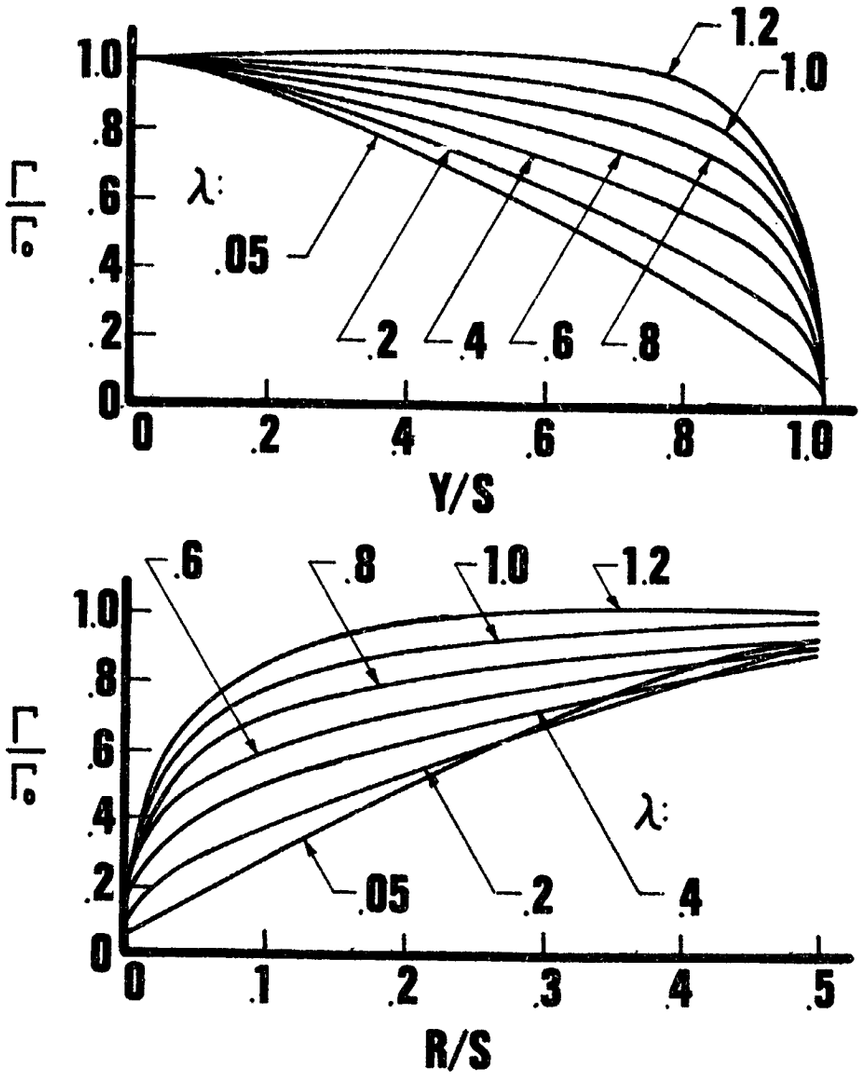

FIG 22 RELATION OF TAPERED WING AND VORTEX CIRCULATION DISTRIBUTION FOR VARIOUS TAPER RATIOS

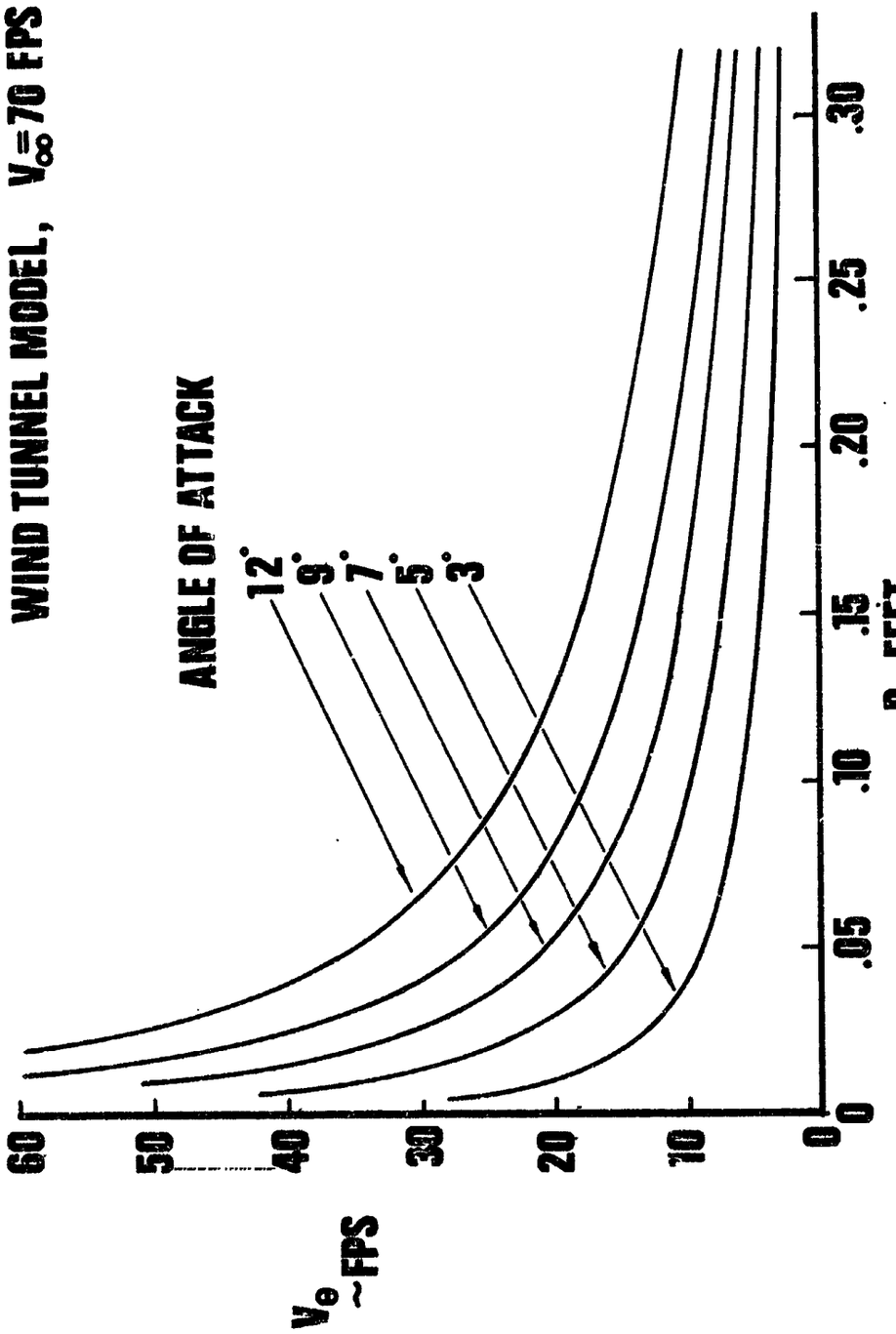

FIG. 23 CHANGE OF TANGENTIAL VELOCITY WITH ANGLE OF ATTACK

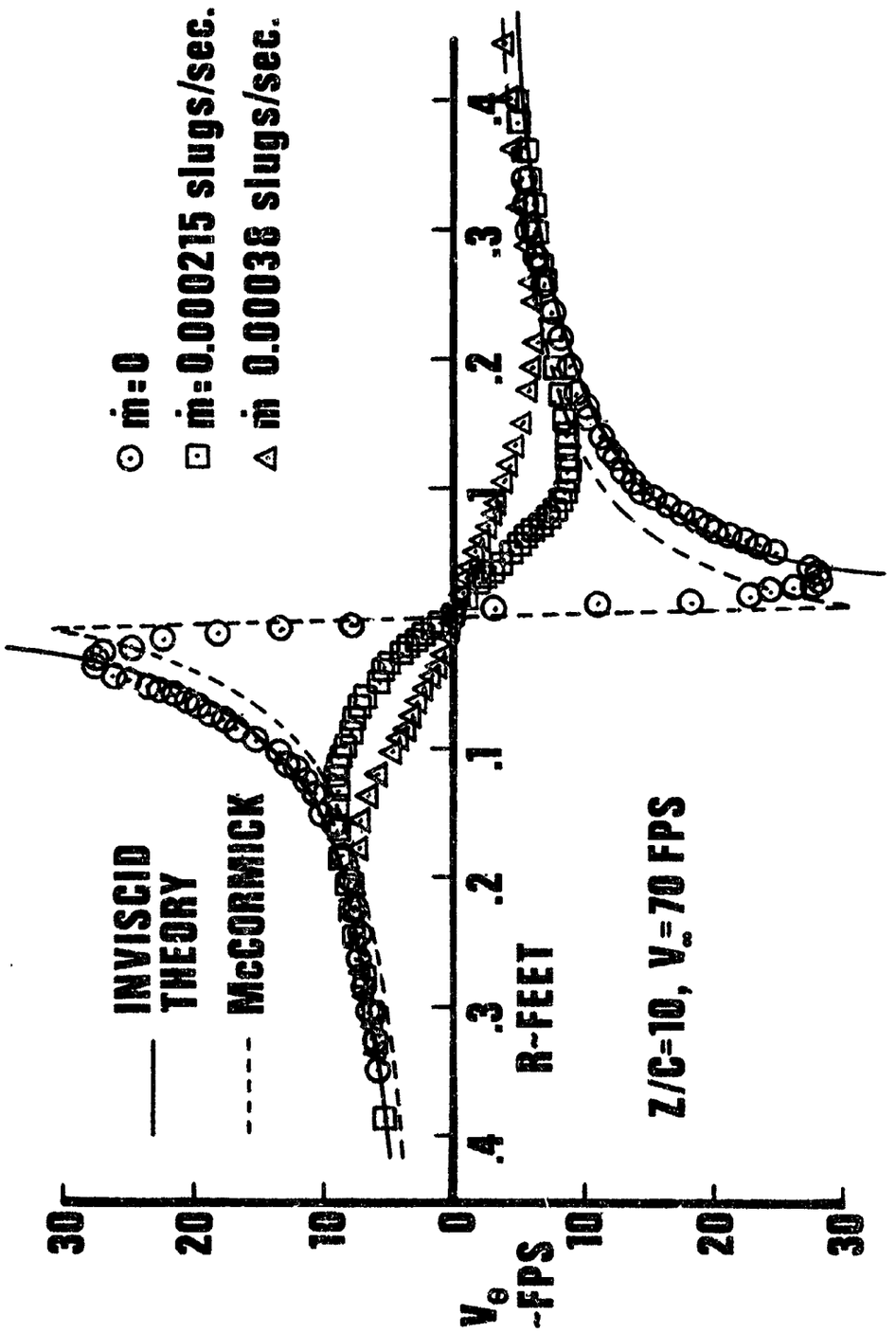

FIG. 24 TANGENTIAL VELOCITY PROFILES

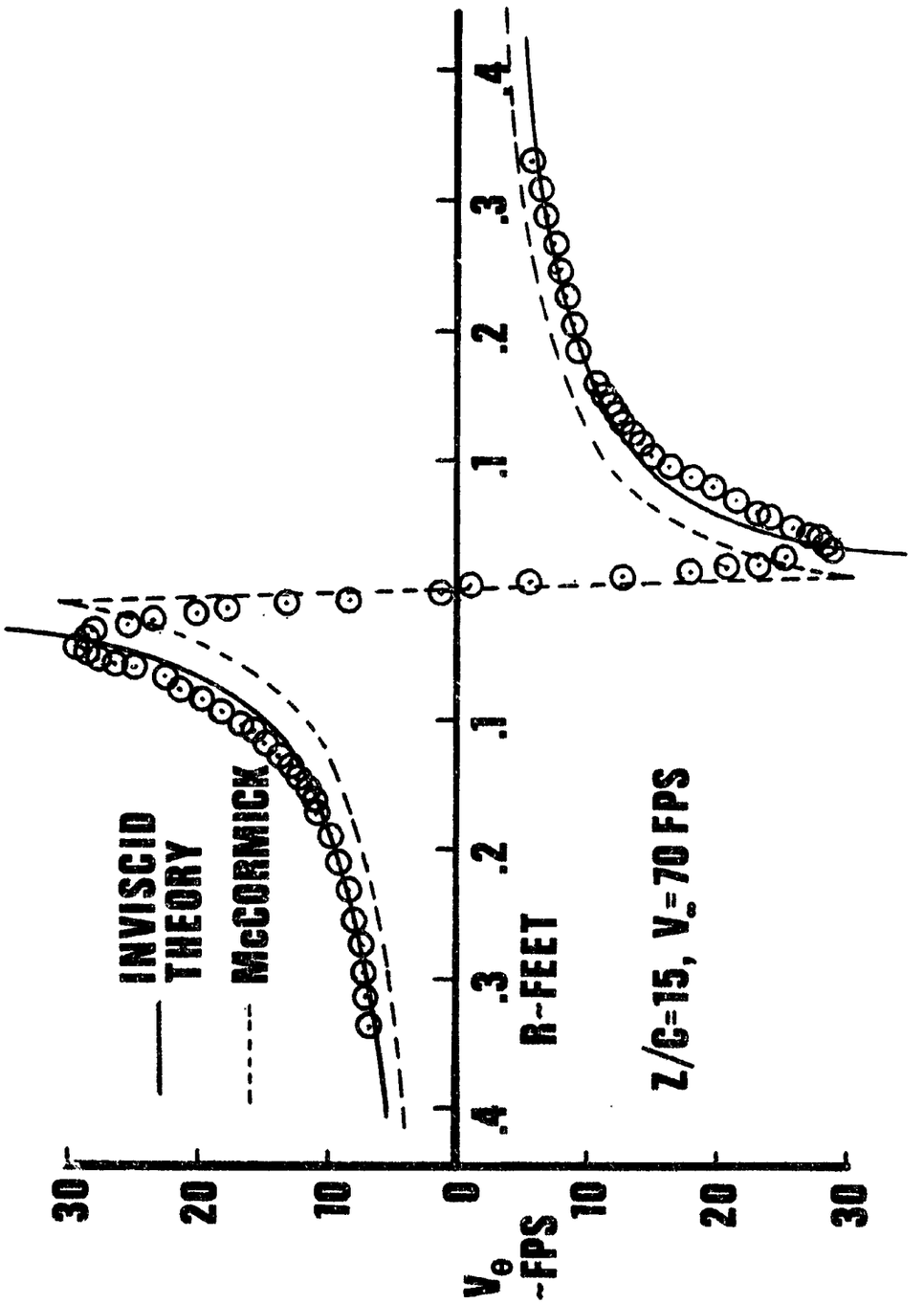

FIG. 25 TANGENTIAL VELOCITY PROFILES

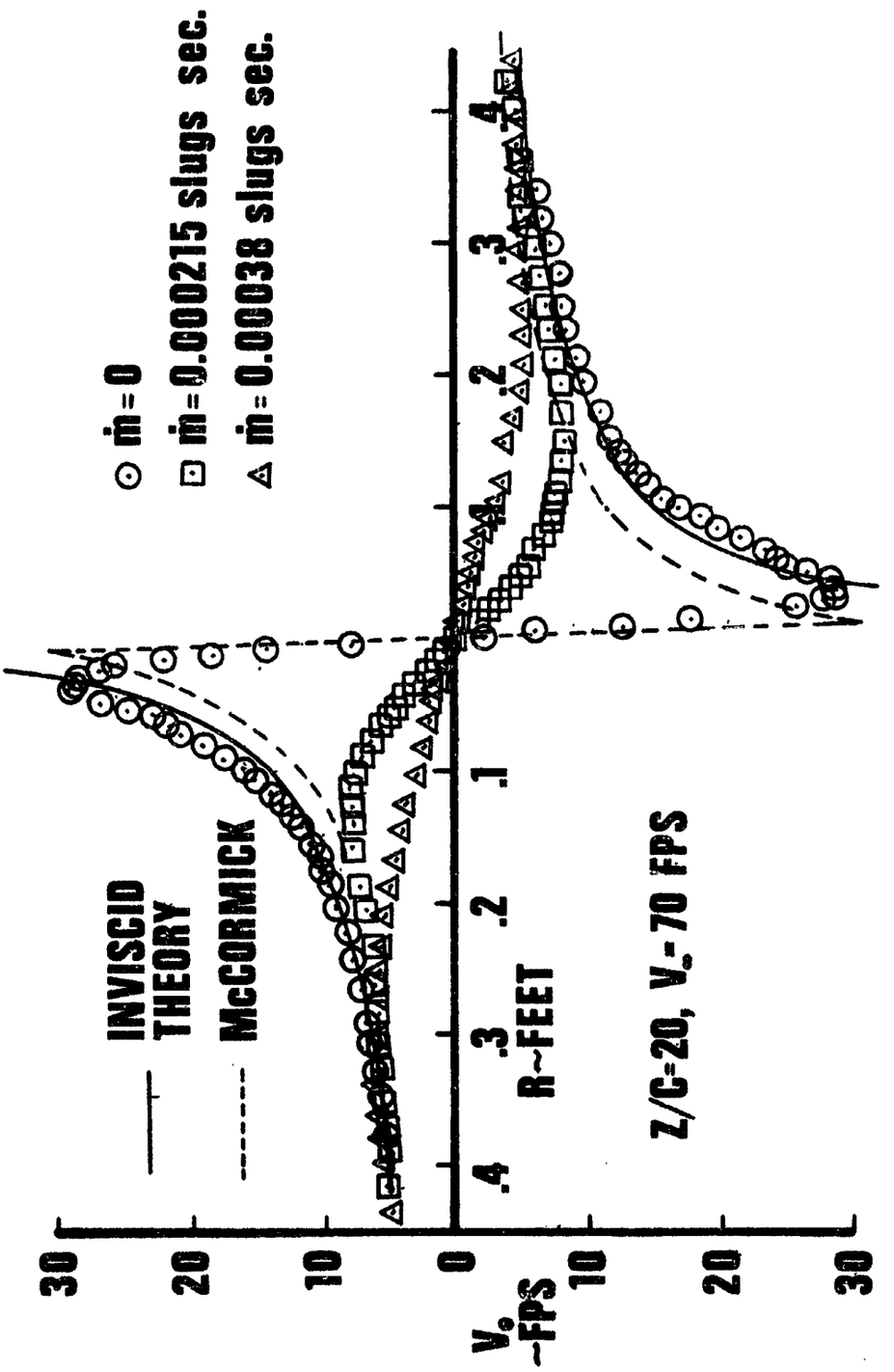

FIG. 26 TANGENTIAL VELOCITY PROFILES

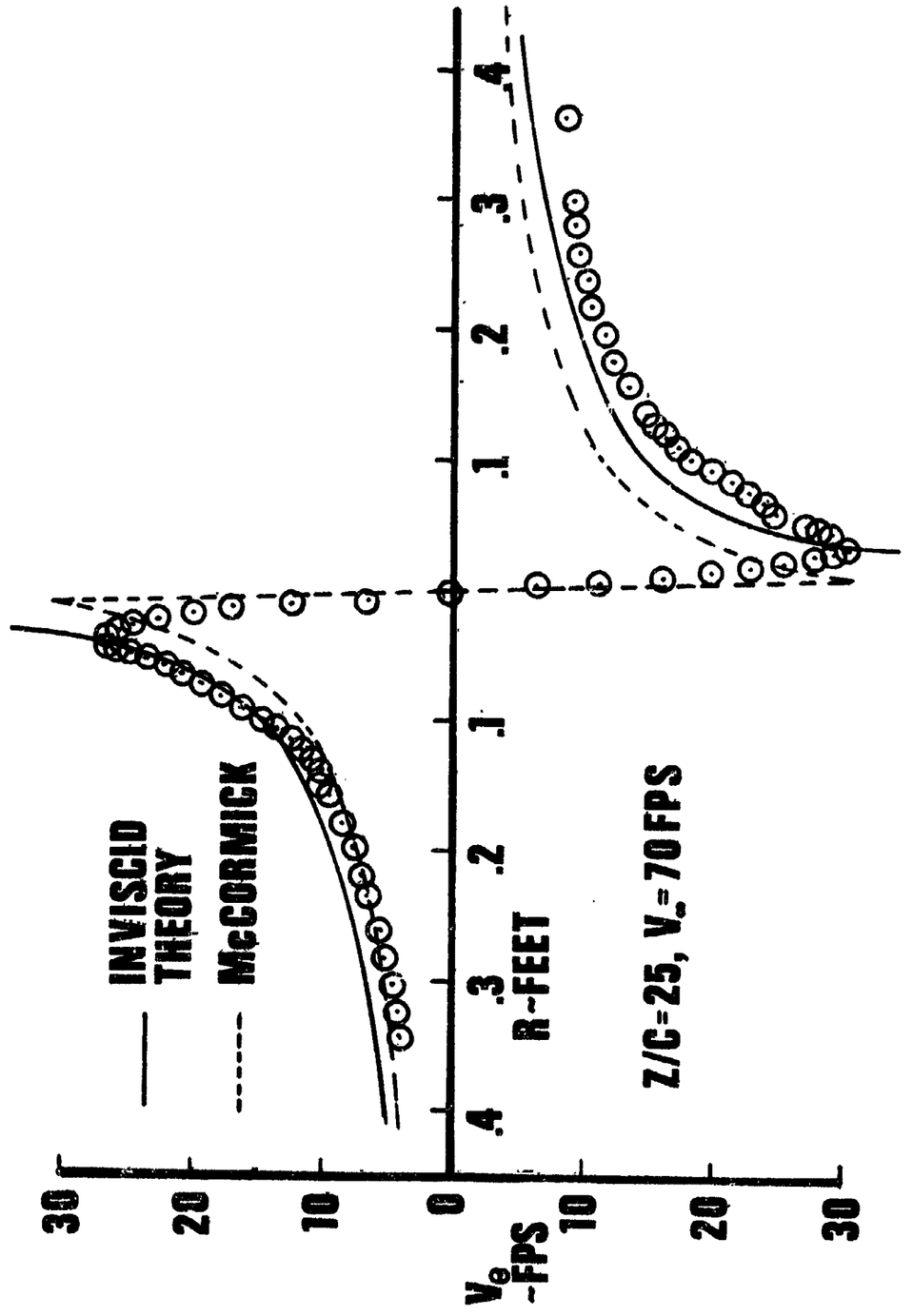

FIG. 27 TANGENTIAL VELOCITY PROFILES

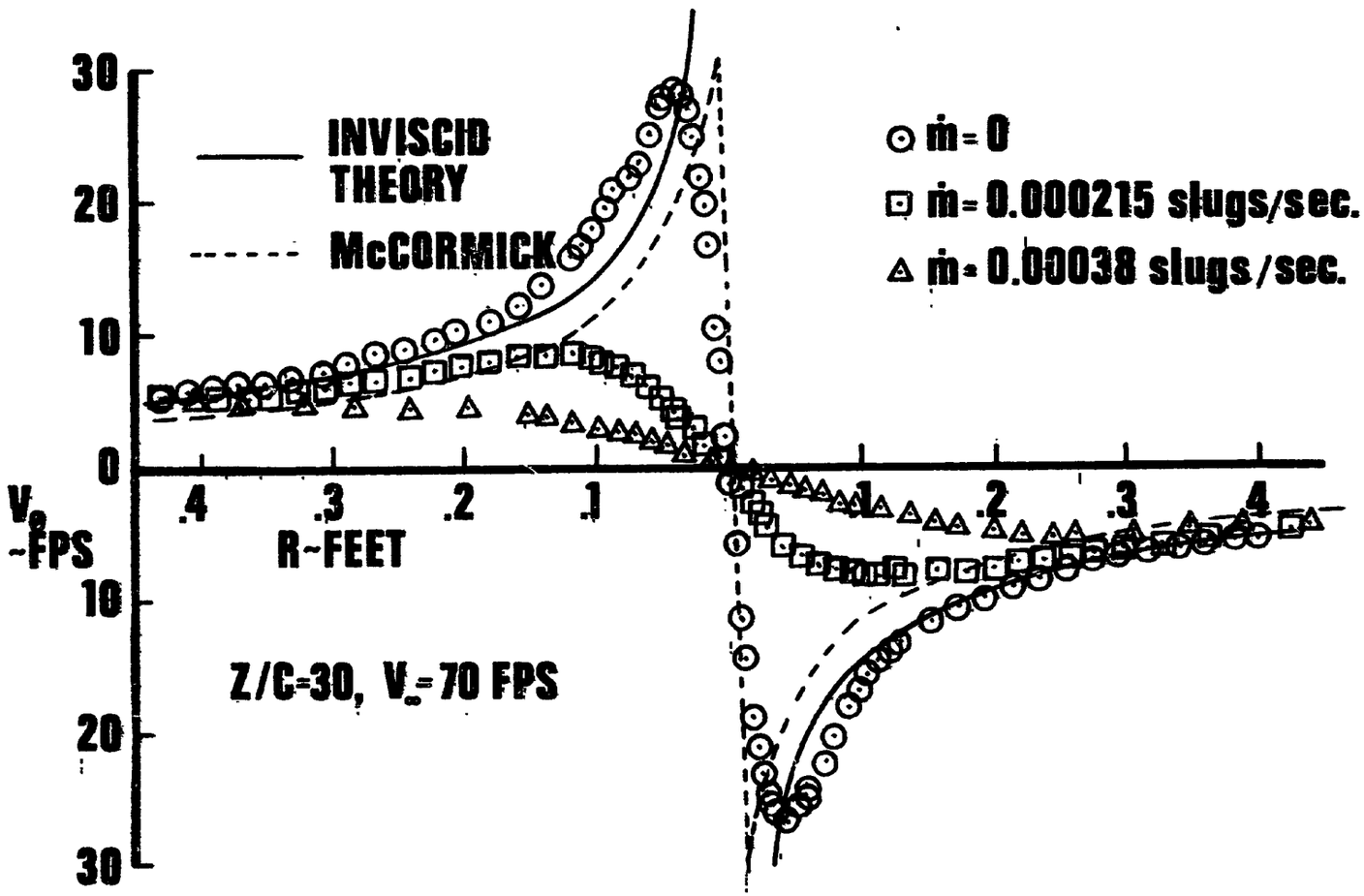

FIG. 28 TANGENTIAL VELOCITY PROFILES

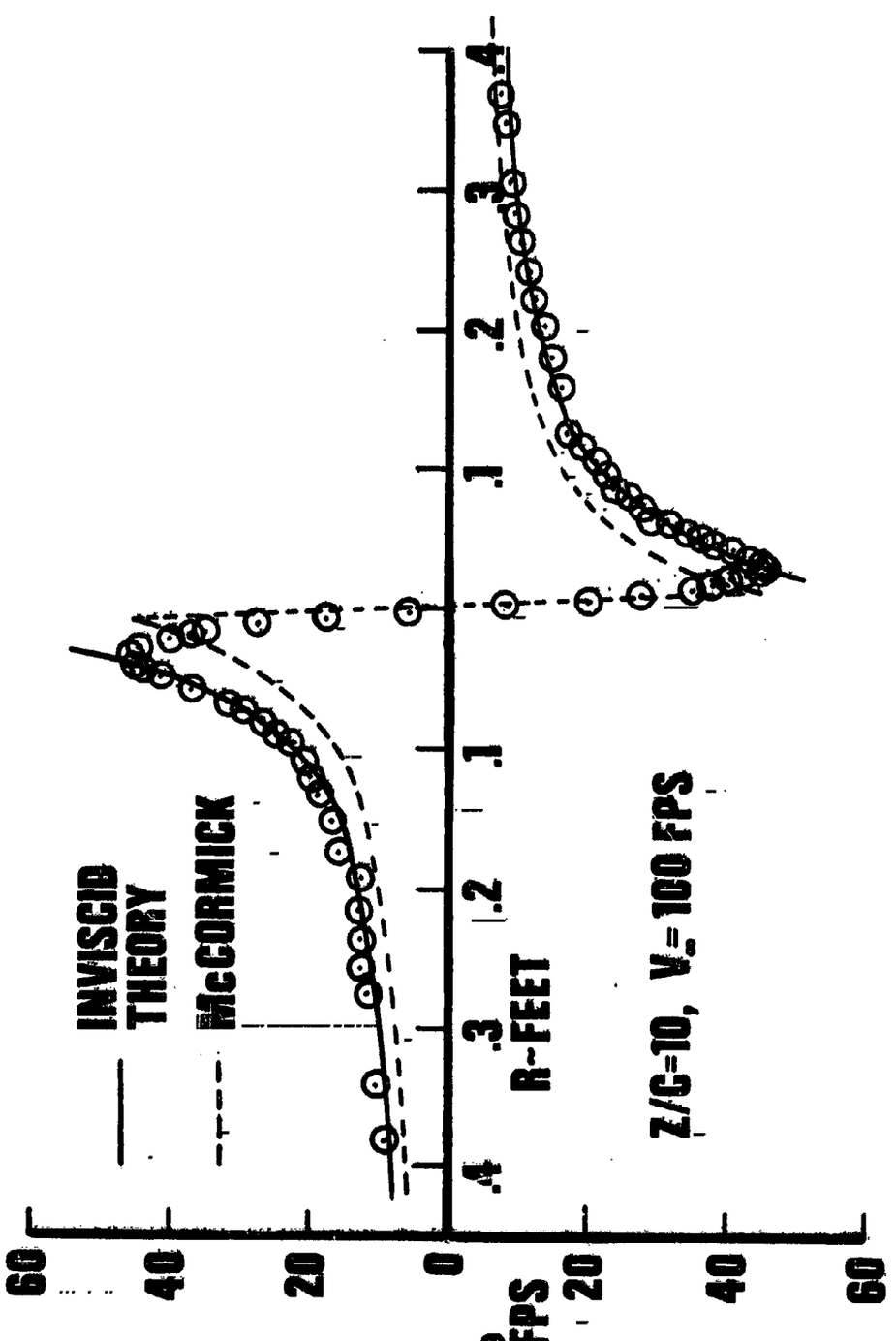

FIG. 29 TANGENTIAL VELOCITY PROFILES

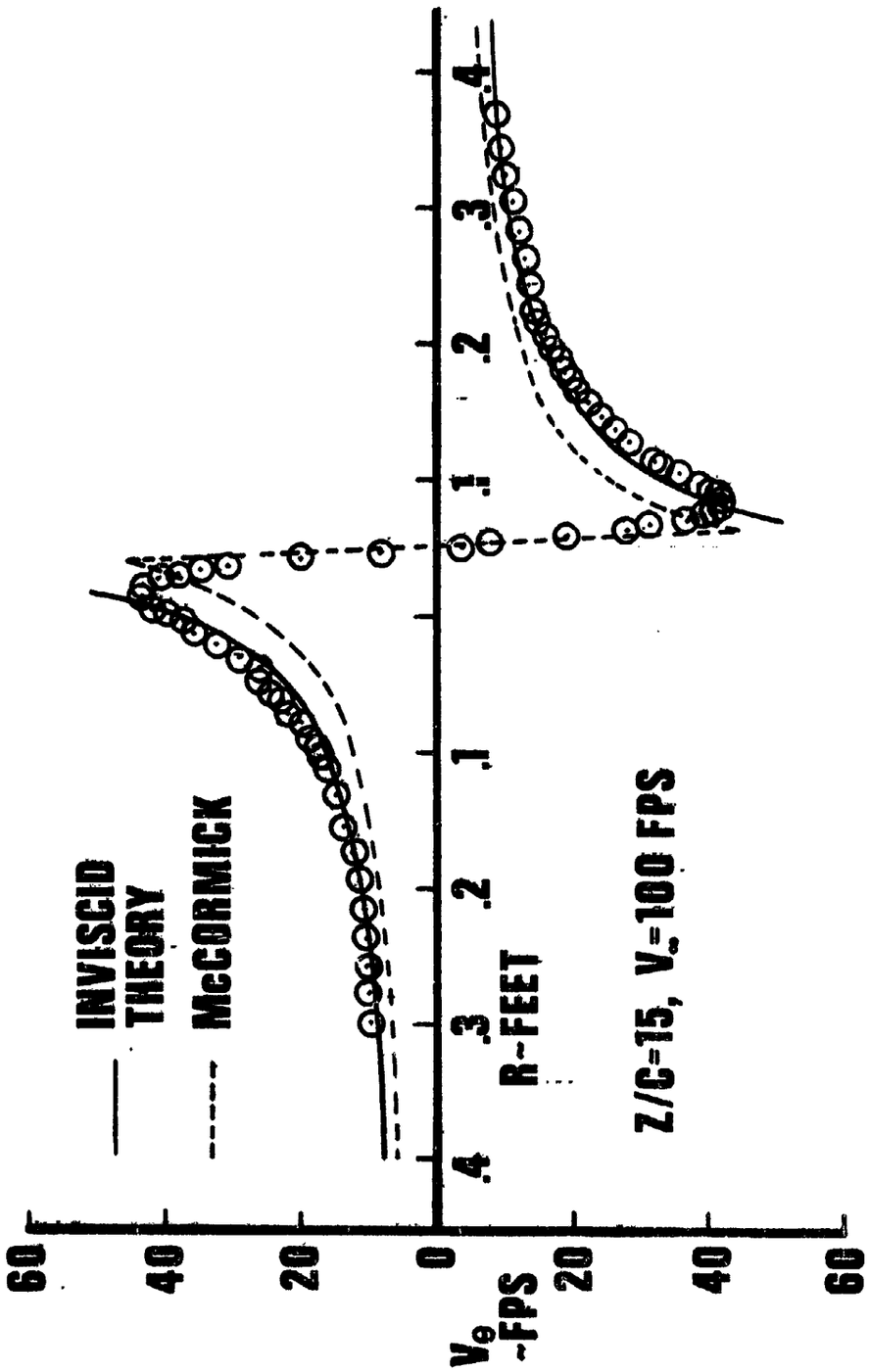

FIG. 30 TANGENTIAL VELOCITY PROFILES

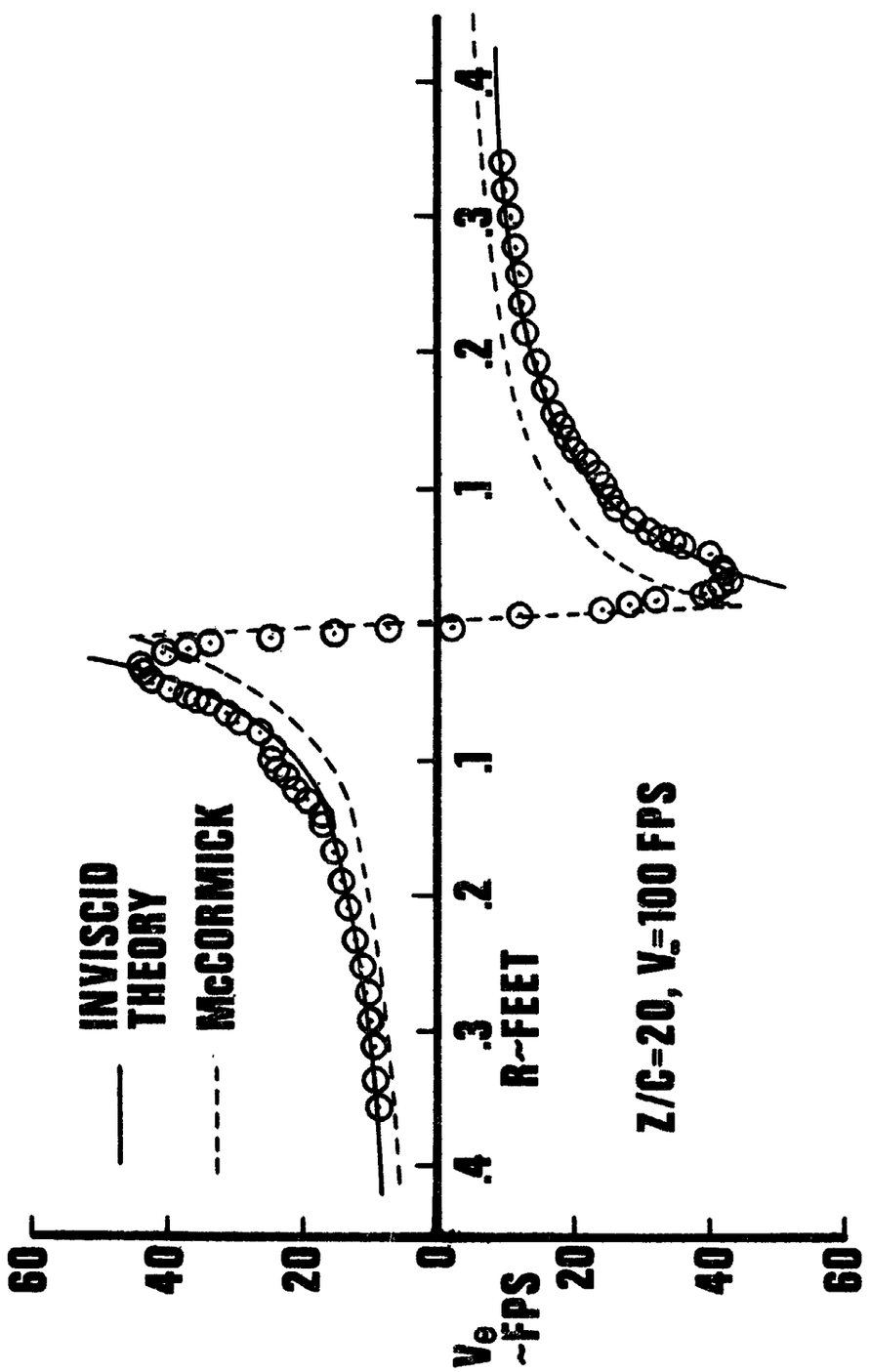

FIG. 31 TANGENTIAL VELOCITY PROFILES

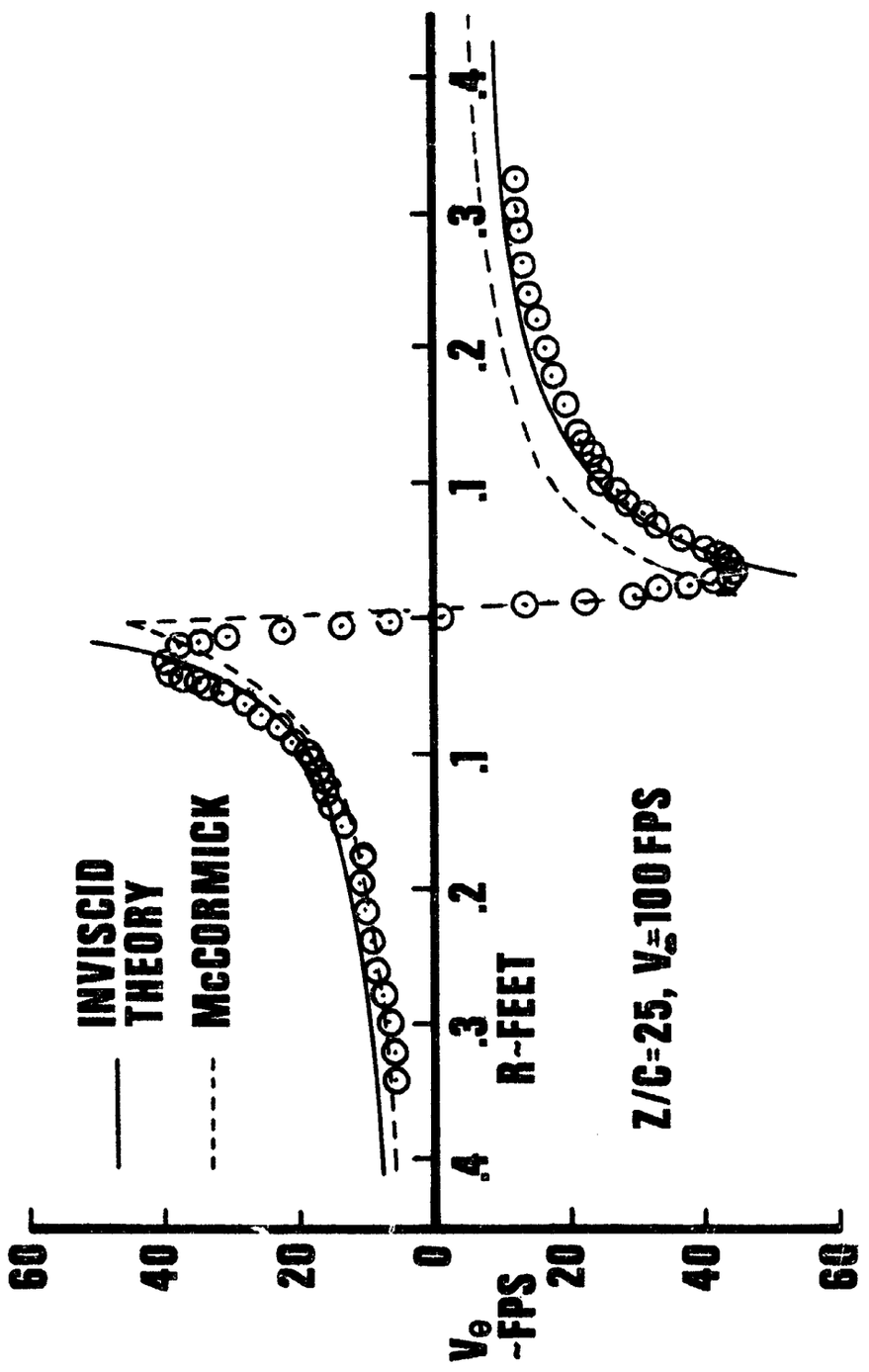

FIG. 32 TANGENTIAL VELOCITY PROFILES

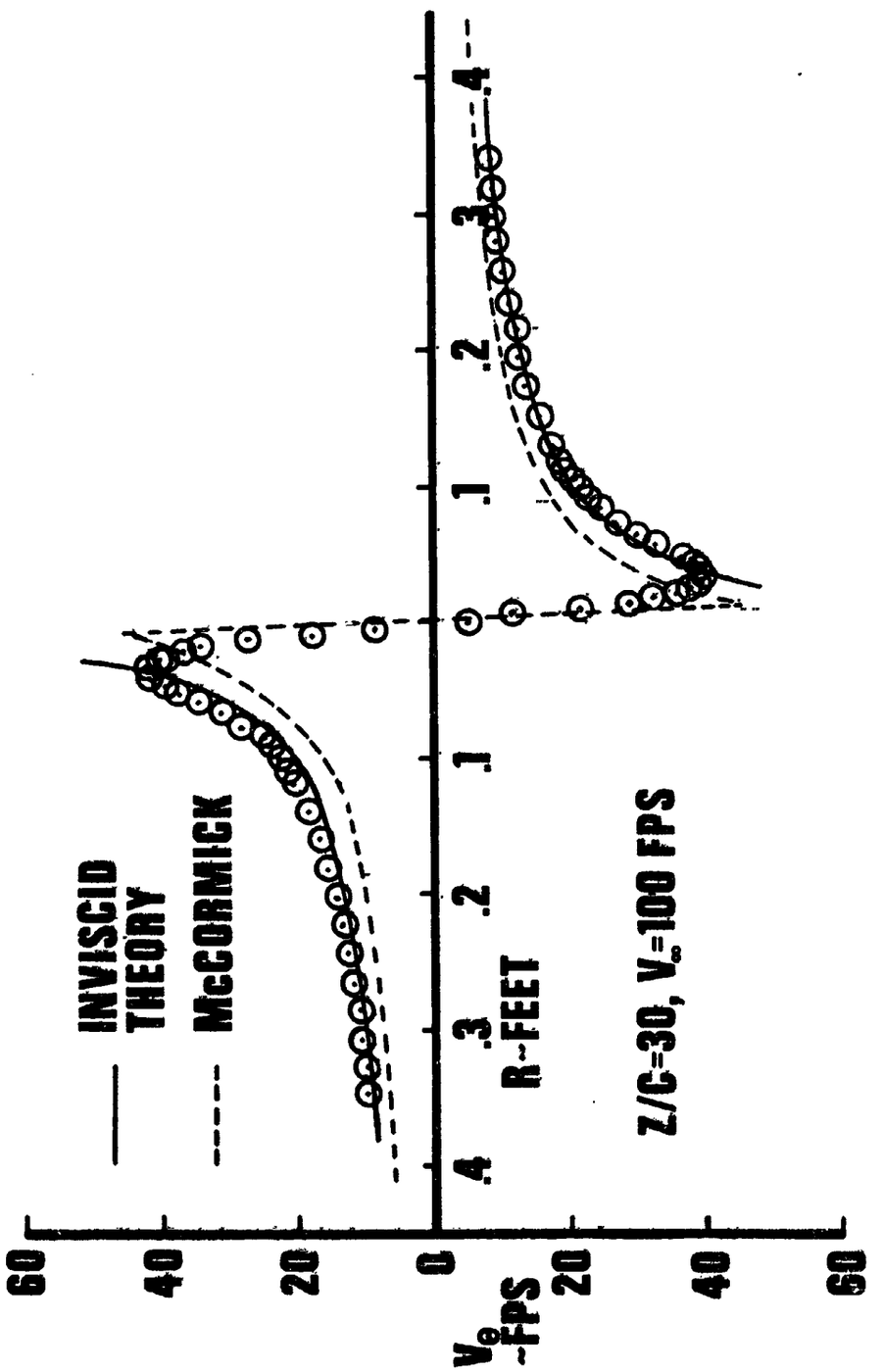

FIG. 33 TANGENTIAL VELOCITY PROFILES

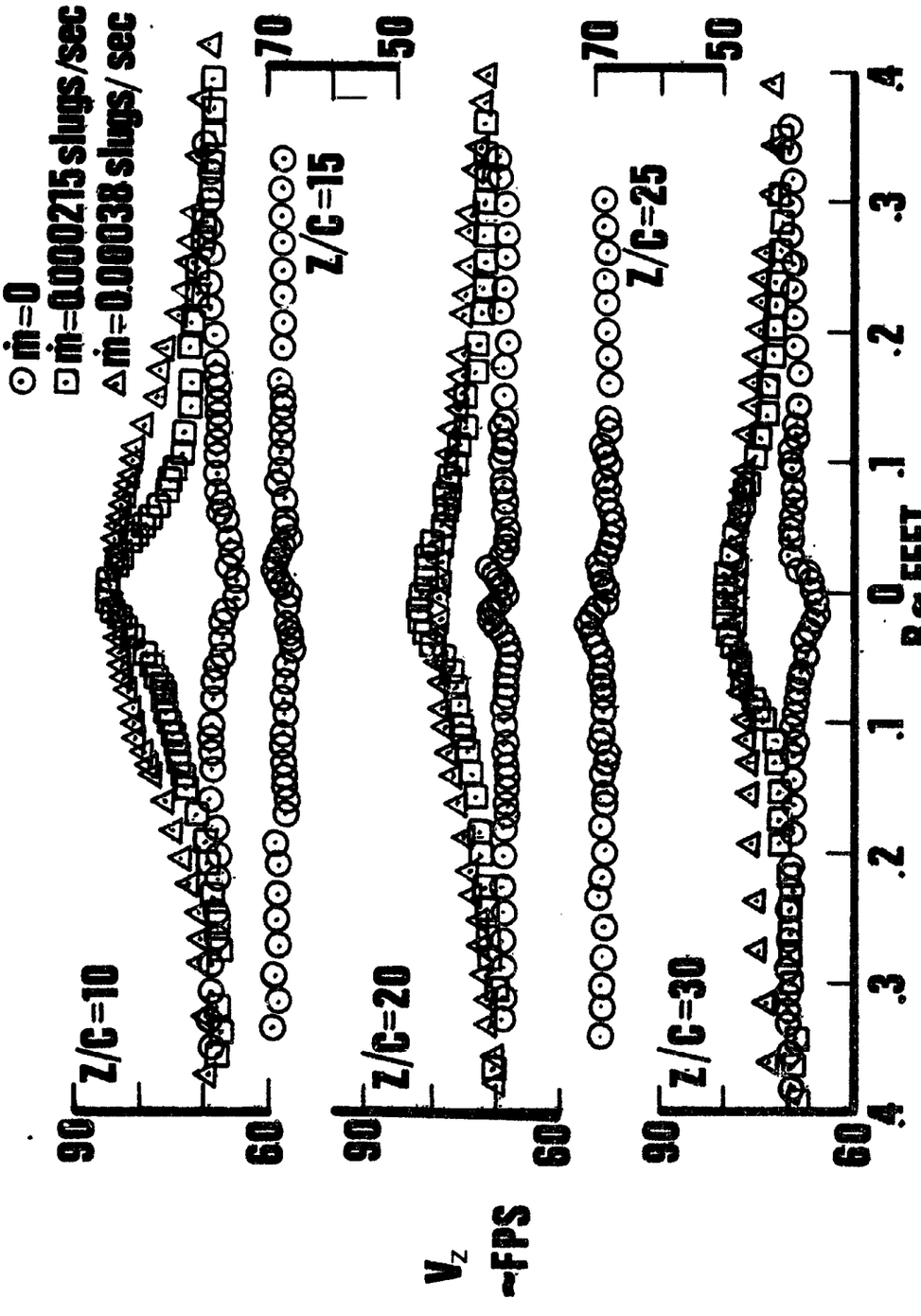

FIG. 34 AXIAL VELOCITY PROFILES FOR V_8=70 FPS

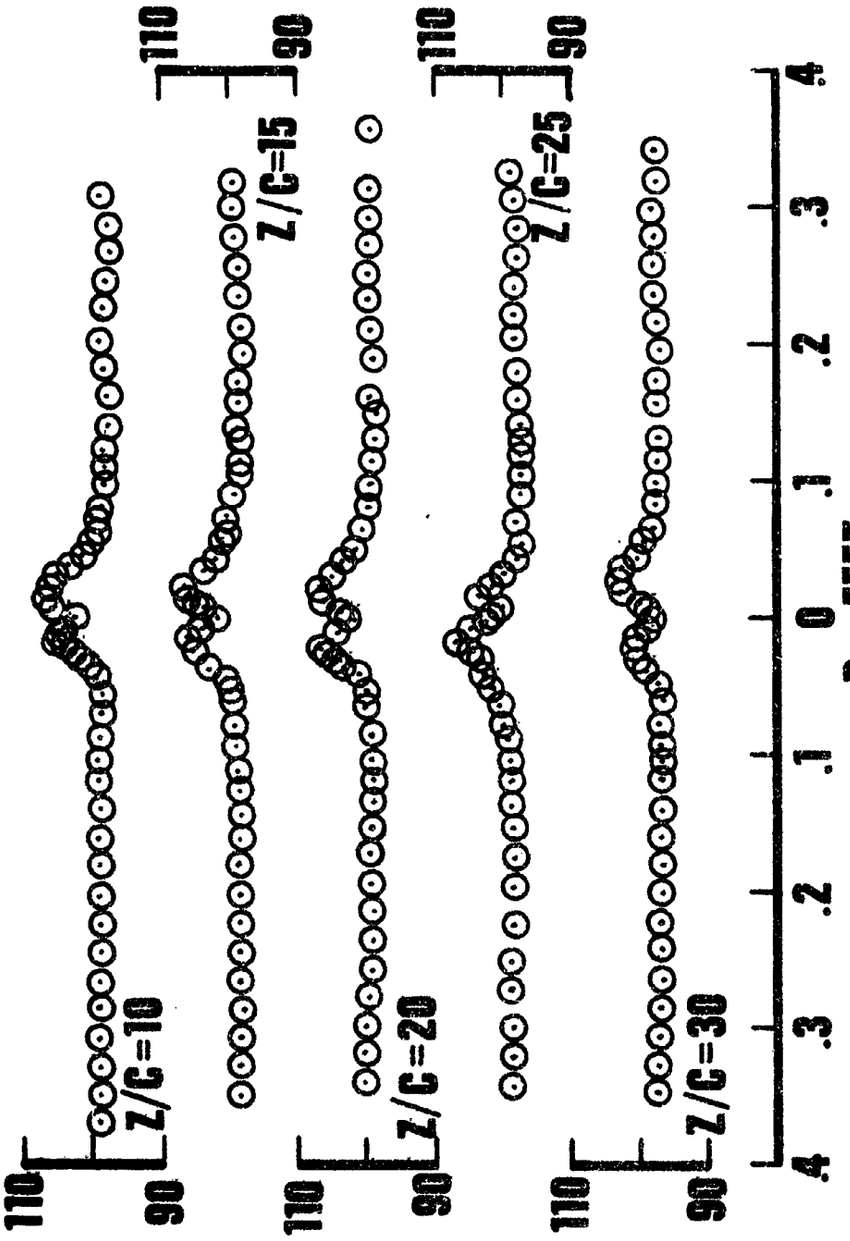

FIG. 35 AXIAL VELOCITY PROFILES FOR V=100 FPS

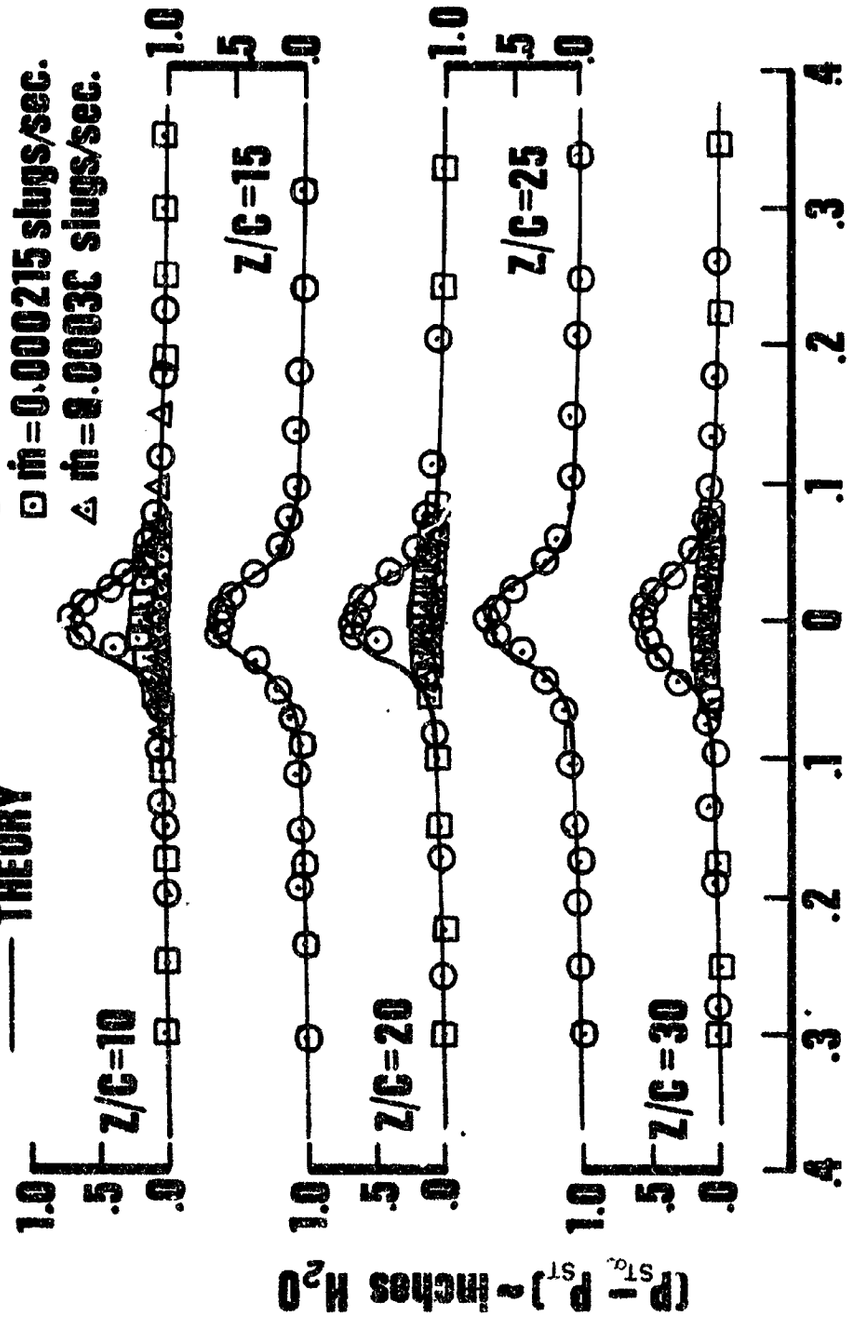

FIG 36 STATIC PRESSURE PROFILES FOR V_∞=70 FPS

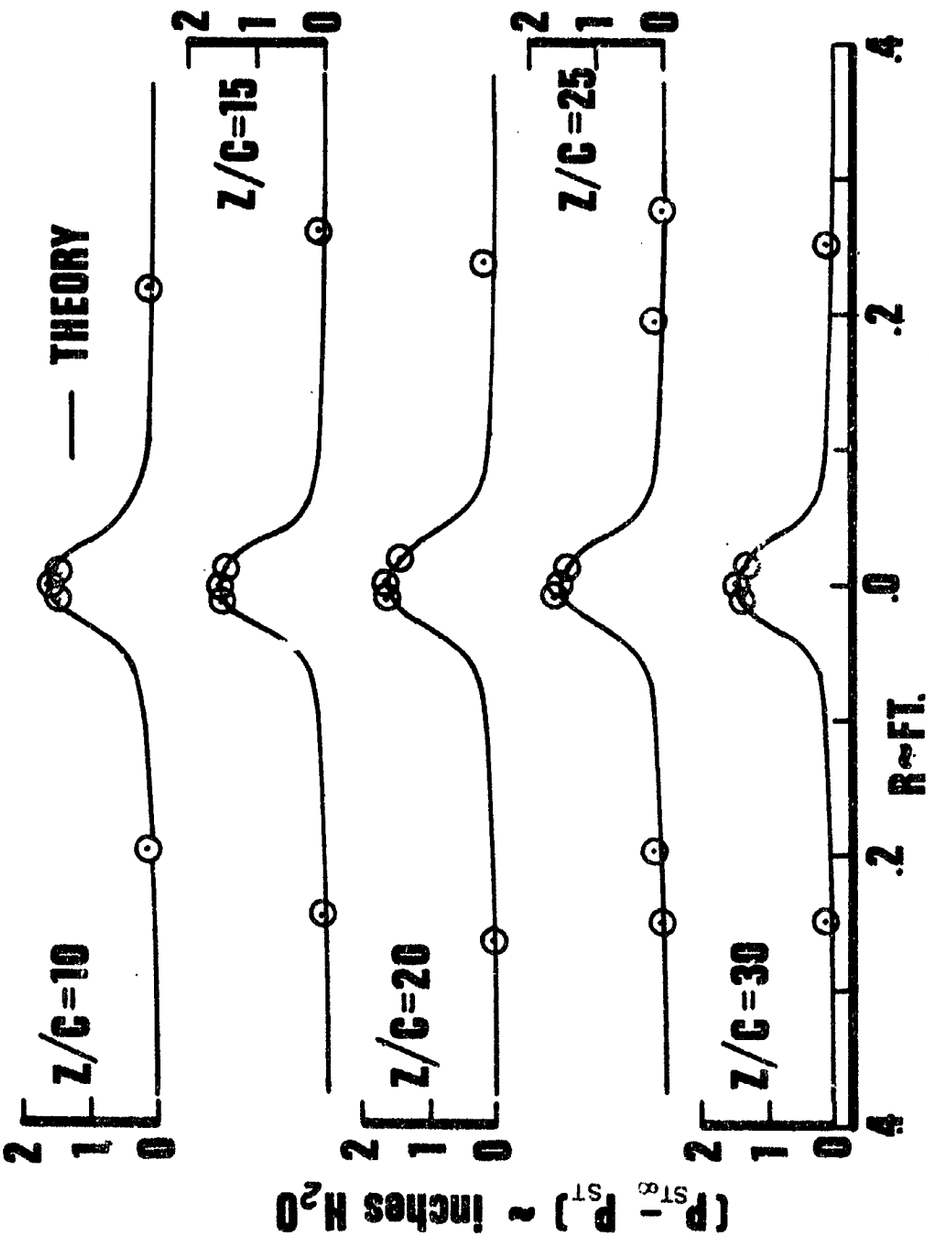

FIG. 37 STATIC PRESSURE PROFILES FOR V_∞=100 FPS

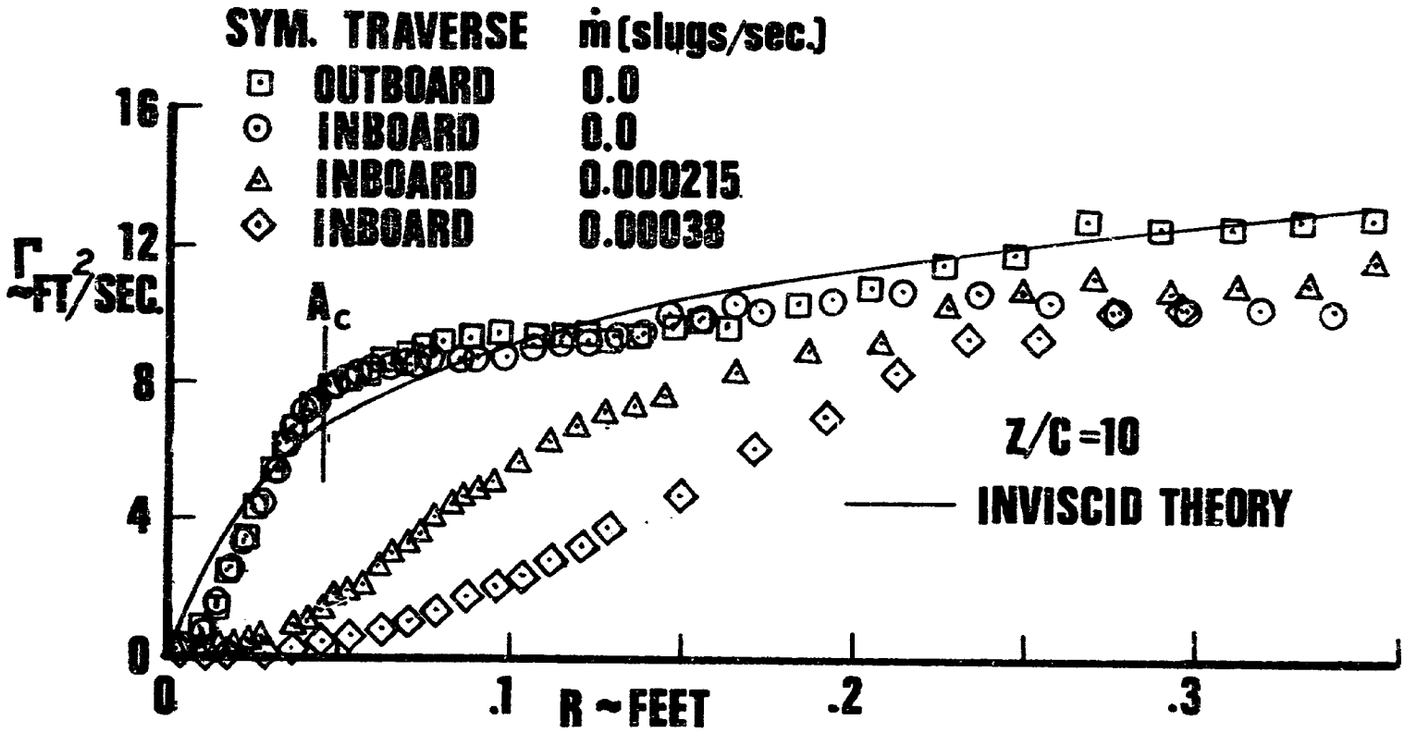

FIG. 38 TYPICAL CIRCULATION DISTRIBUTION FOR V_∞=70 FPS

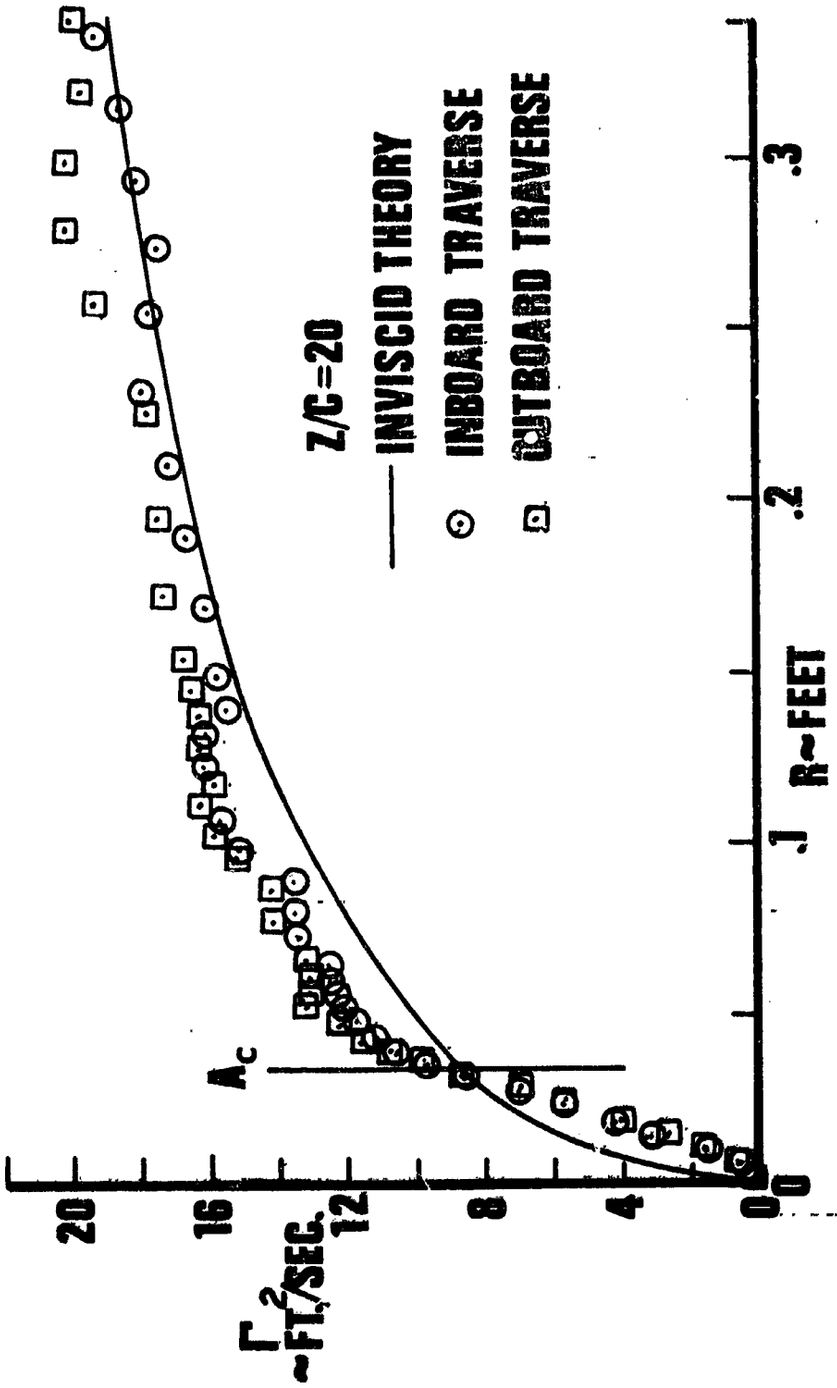

FIG 39 TYPICAL CIRCULATION DISTRIBUTION FOR V_{∞} = 100 FPS

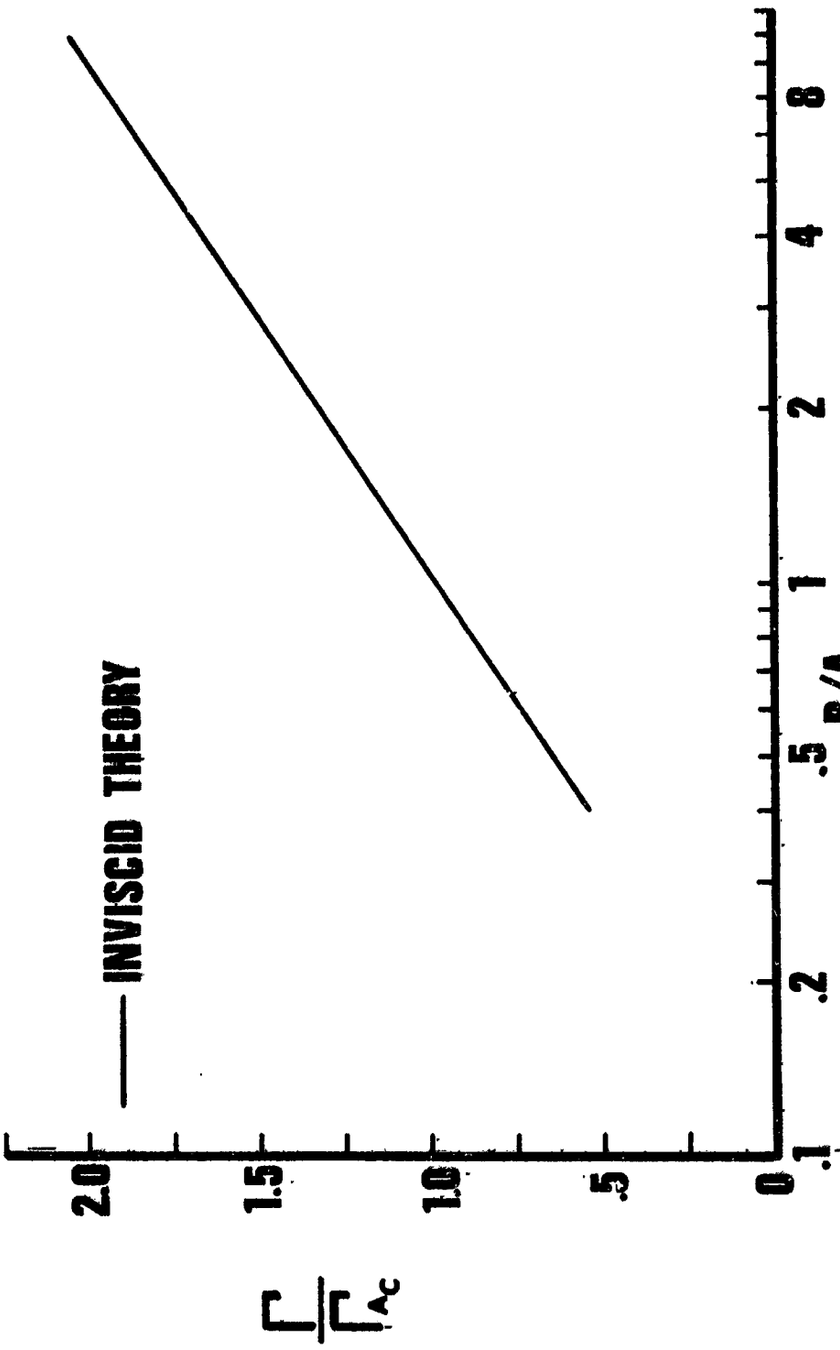

FIG. 40 LOG LAW OF CIRCULATION

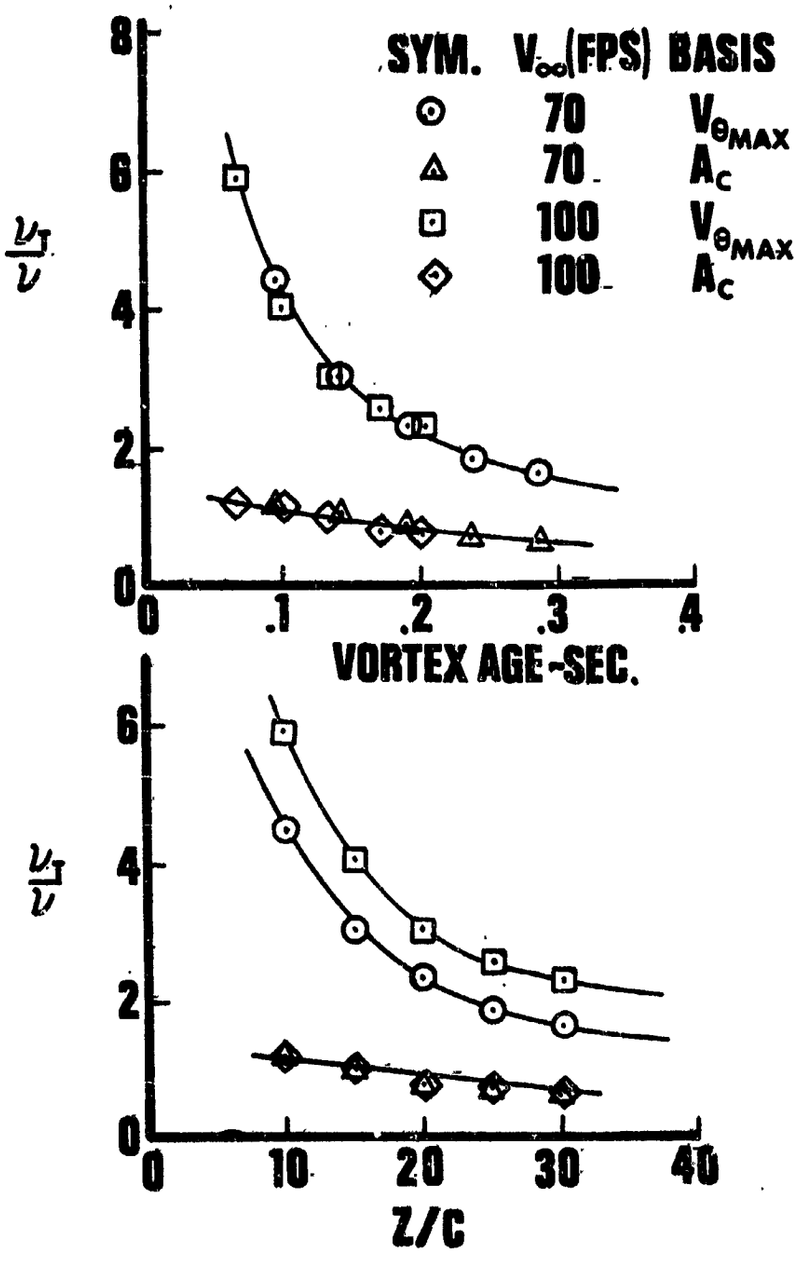

FIG.41 VARIATION OF EFFECTIVE VISCOSITY

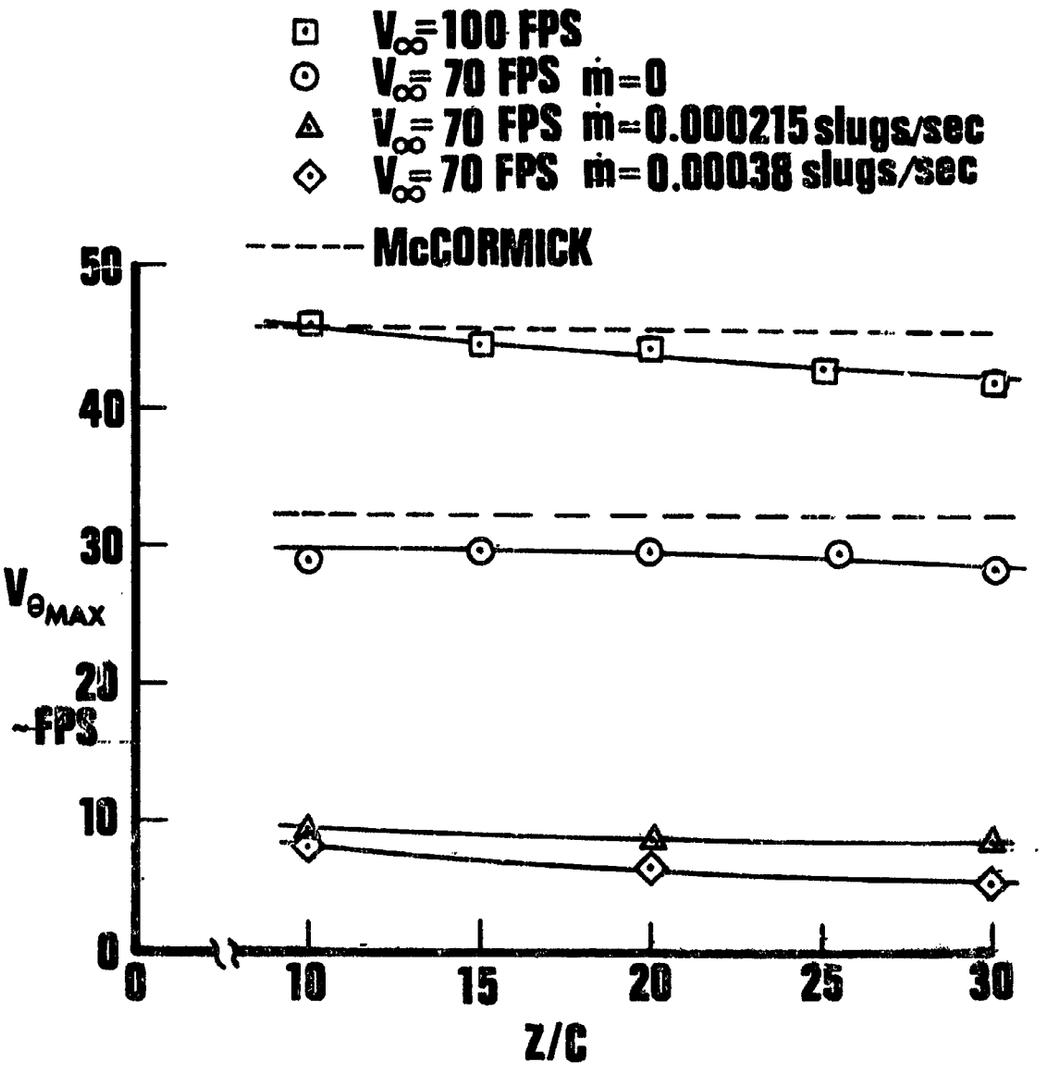

FIG. 42 DECAY OF $V_{\theta_{MAX}}$

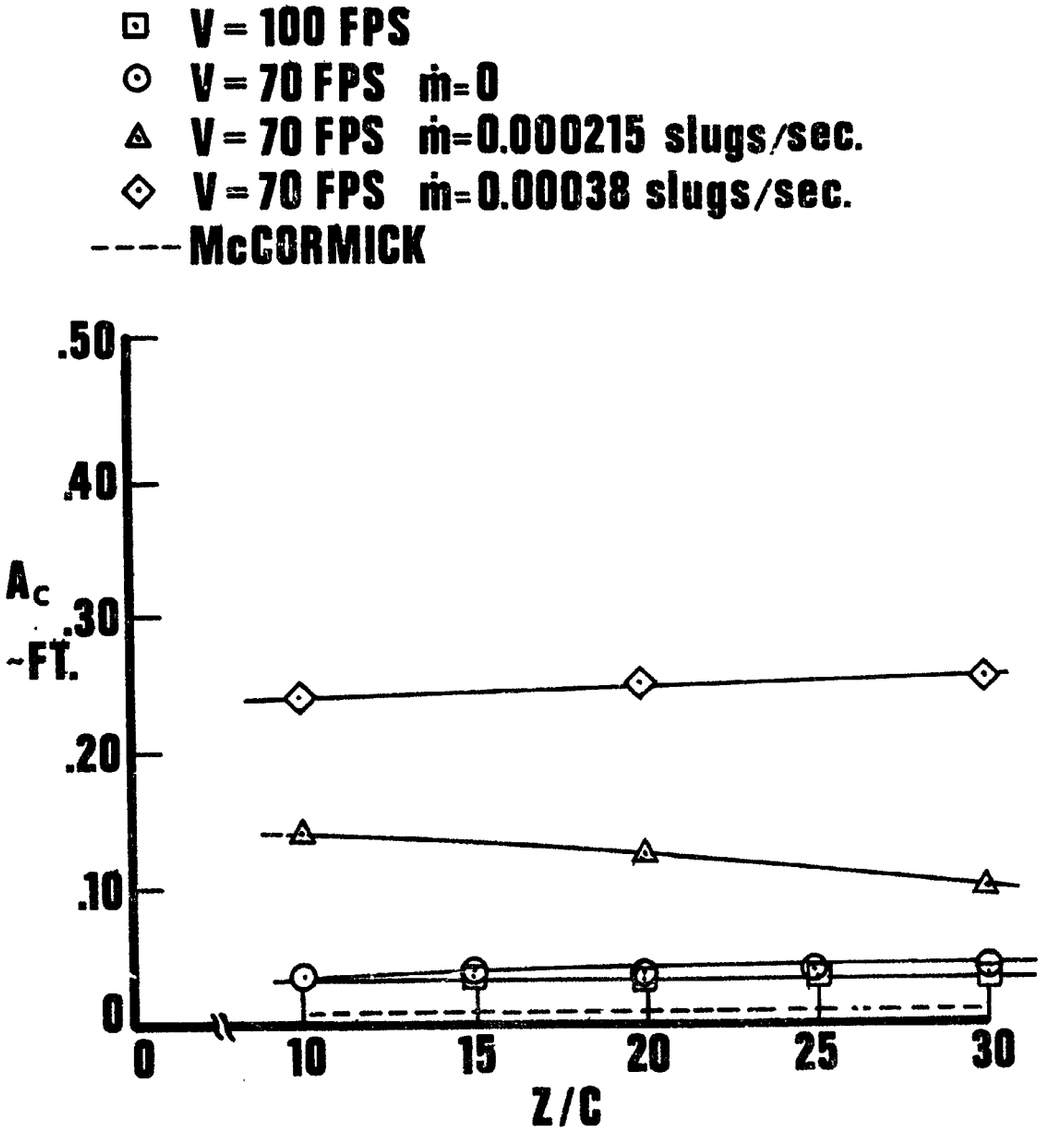

FIG. 43 CHANGE OF CORE RADIUS WITH Z/C

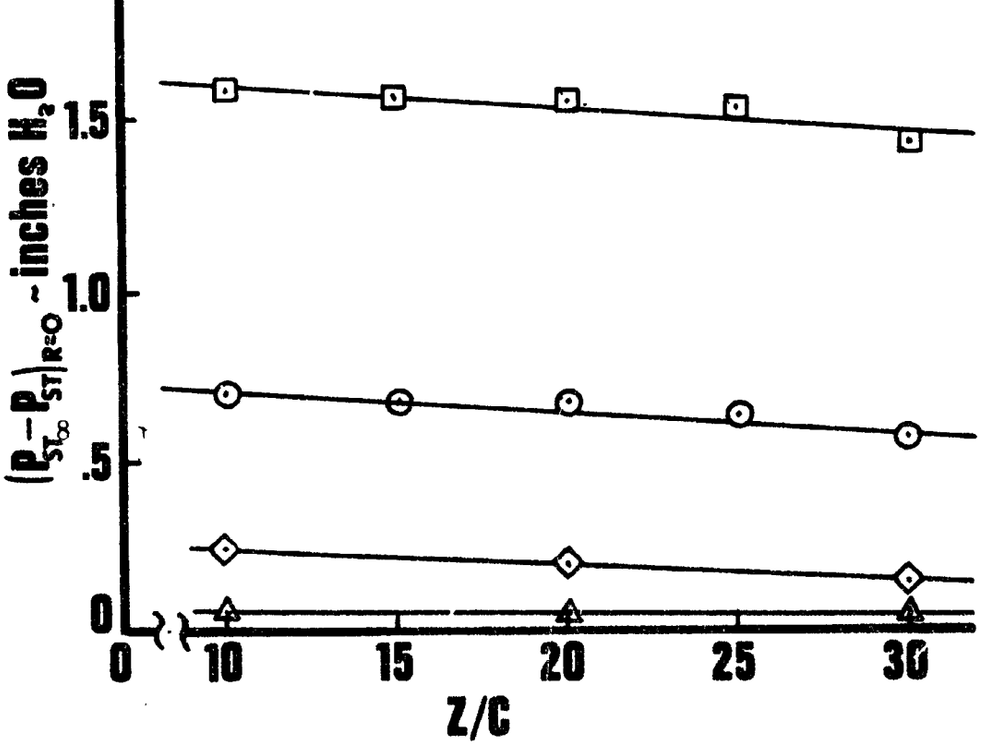

FIG.44 DECAY OF CENTERLINE STATIC PRESSURE DEFICIT

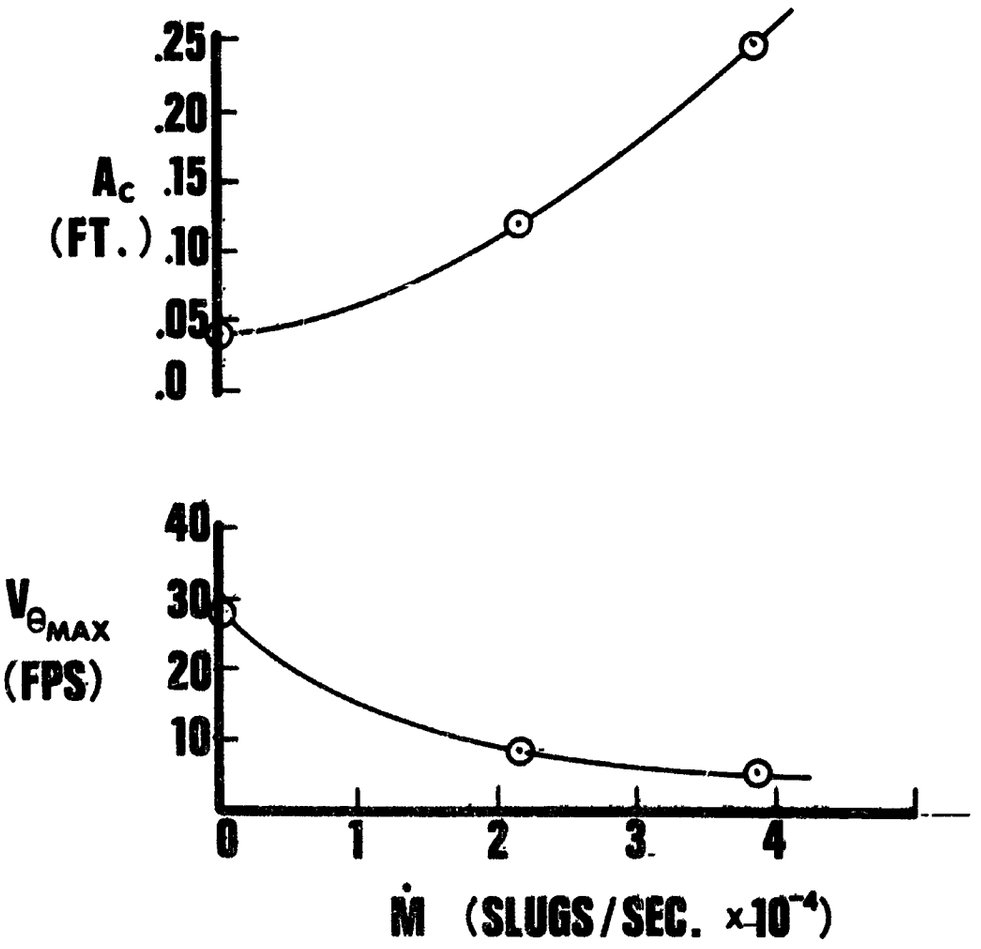

FIG. 45 TYPICAL CHANGE OF CHARACTERISTIC CORE PARAMETERS WITH MASS INJECTION, FOR Z/C = 30

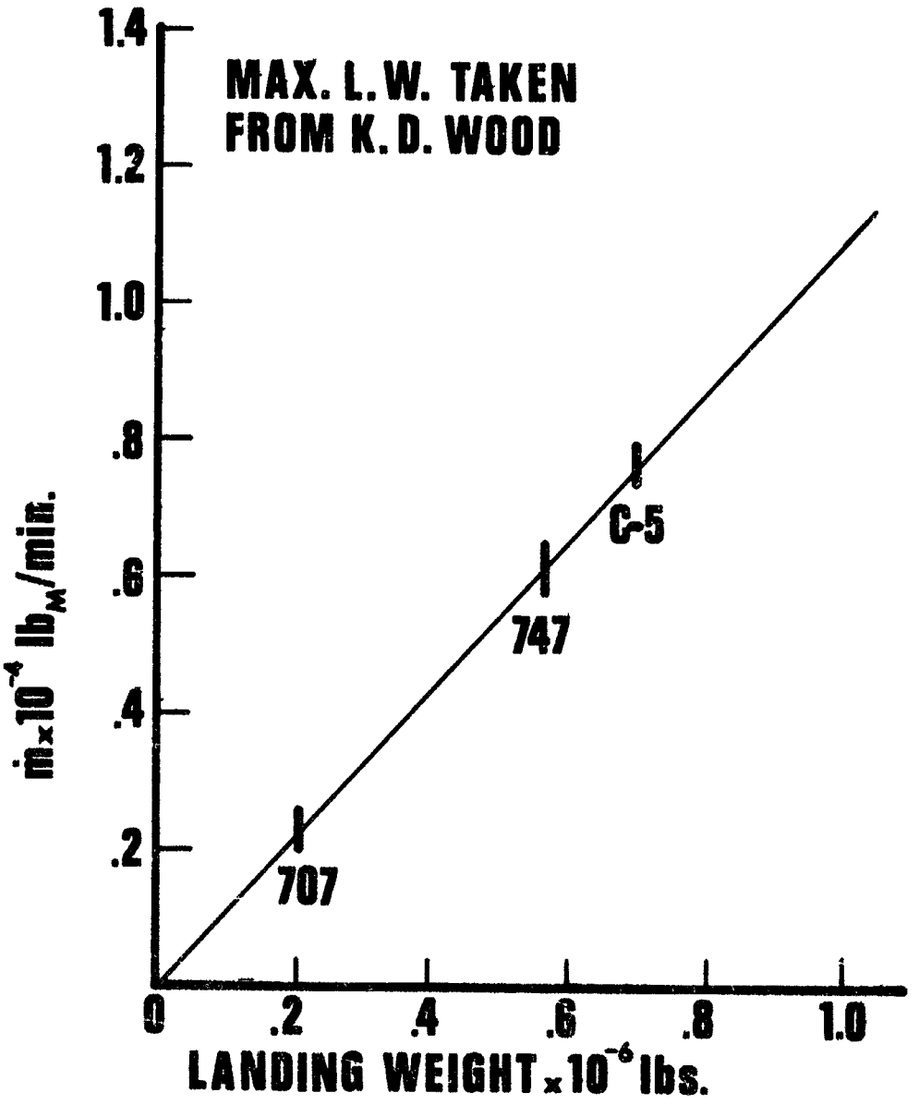

FIG. 46 ESTIMATED MASS INJECTION FOR VORTEX DISPERSION